Precise determination of variable density contrasts, position of contact surfaces and corrections to the possible errors for an intermediate layer in Gravity Inversion Modeling

A thesis submitted to the Department of Geophysics of the Faculty of Science in the partial fulfillment of the requirements of a Degree of the Doctor of Science (D.Sc.) of Kyoto University.

Ateya Ismail Lukandu

March 2003

"Commit yourself to quality from day one ...
its better to do nothing at all than to do something badly."

- Mark H. McCormick.

"The happiness and greatness, the rank and station, the pleasure and peace of an individual have never been consisted in his personal wealth, but rather in his excellent character, his high resolve, the breadth of his learning and his ability to solve the difficult problems."

- Abdu'l Baha.

Abstract

The *quantitative* determination of the variable density contrasts and position of contact surfaces for an *intermediate horizontal layer* in the sub-surface has been demonstrated. In particular a sub-surface dipping dike model with *apriori* depth-dependent density contrasts was adopted as a *forward model* to project synthetic *gravity anomaly effect* onto the Earth surface. The sub-surface *location* and *density contrasts* of the dipping dike in a series of the intermediate horizontal layers have been *recovered* by means of inversion analysis. Density contrasts errors of less than 8.0 percent were realized to a depth of 2.00 km in the sub-surface for a maximum gravity anomaly effect of 10.0 mGals, which is better comparison to sub-surface constant density models. Subsequently by the direct relationship of the *positions of contact surfaces* and disturbing masses in an intermediate horizontal layer the former have been determined simultaneously with the respective density contrasts.

Further, since geophysical fields observations are not error-free, the *possible height errors* and *the height error effects* in the determination of differential density contrasts and positions of contacts surface have too been investigated. *Height errors and error effects* in the disturbing masses considered were due to (1) *deviations* due to inaccurate average depth of layer, (2) *distortions* due to assigned layer thickness or assumed density, (3) top surface only being *identical to observations surface* and (4) layer being *approximated* as surface covered with a loaded mass. It has been clearly established that once errors and/or error effects are known the *exact or correct density contrasts* and/or *positions of contact surfaces* in a horizontal intermediate layer can be *obtained or reviewed* for a particular sub-surface.

For meaningful geological and/or geological interpretations the *height error limits* on height measurements for an intermediate horizontal layer were too considered based on the common geological materials of sub-surface dipping dike model. Finally to demonstrate the efficacy of the inverse modeling, the inversion analysis was successfully applied to a real case study. A *micro-gravimetry and/or localized structures* in the Central Ranges of Chubu District – Japan was chosen. In utilizing residual gravity anomaly, an arbitrary height error of +5.0 m on an intermediate horizontal layer of thickness 0.300 km had an average density contrasts error effect of 10.0 mg/cm^3 to a maximum depth of 0.700 km. The case of thickness of the layer being had a much less error effect compared to the other height errors. *Height error limits* depends mostly on the actual need or purpose of the resulting density contrasts in the horizontal layer.

Acknowledgements

I would like to express my sincere gratitude to *Prof. Shuzo Takemoto* and *Prof. Yoichi Fukuda* for their *supervision and guidance*; without which it would have been nigh impossible to come this far. Many thanks too to my colleagues in the Geodesy Laboratory of the Department of Geophysics for always having worked as a team; notably *Dr. Kumiko Nishi* of Geographical Survey Institute (GSI) (formerly of the Department of Geophysics - Kyoto University) for the numerous Perl Codes, Mr. Satoshi Okuyama for the optimization techniques, *M/s Leni S. Heliani* and *Dr.-Ing Joseph L. Awange* for the their deep insights and numerous suggestions in my research.

Further my esteemed thanks and regards to *Dr. Yuki Kuroishi* for his prior introduction to the challenging field of gravity research and the staff of the First Geodetic Division at *Geographical Survey Institute (GSI)* at Tsukuba City - Ibaraki Prefecture for extra Gravity and Leveling data for selected sections in Japan Alps. I would further like to extend my gratitude to *Mr. Hunja E. Waithaka* of the Institute of Seismology and Volcanology, Hokkaido University and *Dr. Victor S. Muhandiki* (formerly of the Department of Global Environment Engineering, Kyoto University) for their many candid discussions on various issues over the years.

I would also like to express my esteemed gratitude to *Geological Survey of Japan (GSJ)* for the bulk of gravity data utilized in this research, which was wholly provided on the *Gravity CD-ROM of Japan* dated 24th March 2000. And further GSI for the Digital Terrain Elevation Data (DTED) and extra gravity data for selected regions in the Japan Alps. Last but not least this research would not have been possible without the *Japanese Government Scholarship*. To all *many thanks* - your advice, support and encouragement will always be appreciated.

Dedication

To dedicate a Doctor Thesis is a difficult task; many people have supported me through times both bleak and wonderful. This thesis is first and foremost, dedicated to my Father *Mr. Herbert Lukandu Ateya* for his *unceasing support* and *confidence* over the years.

Second to the three special ladies who have affectionately chart my life; my mother *Mrs. Mwanaidi Ongasia* – though *excessively strict and possessive*, nurtured me well during childhood – those days of my unrivalled stubbornness; *Dr. Catherine Masitsa* for her *Love and Faith* - the mere thought of her patience despite the long period and distance made tasks of each passing day a top priority and to sweet little *Ayeshah Musungu* – the thought of whom often reminds me that when it is *too dark dawn* is near.

Last but not least to my siblings *Salim Shikuku*, *Dr. Mohammed Ochiba*, *Juma Barasa*, *Ramadhan Nyarotso*, *Saumu Munyolo* and *Rashid Wetoto* – for breaking the records and often reminding me, '*You lead and others follow*". This is yet one more.

Table of Contents

List of Figures

List of Tables

Chapter 1

A journey of thousand miles begins with the first step.
- Chinese Proverb.

Up to a point is better to let snags [bugs] be there
Than to spend such time in design that there are none (how many decades would this take?)
- A. N. Turing – Proposals for ACE (1945).

Any and every idea a person has is worthless as long as he keeps it in his brain.
It is like a piece of rock from which a diamond can be ground if it is put to a ground stone
... Such ground stones are the brains of other men.
- Thomas Bata (Czech Founder of Bata Shoe Company).

1 Introduction

1.1 Statement of the Problem

The sub-surface *density variation with respect to depth* is a well-recognized geophysical phenomenon. The cognizance of the density variations typically aids in the mapping of the local *lateral heterogeneities* in the Earth's *structure* and the *composition* for numerous geophysical, geological and exploration applications. Further, it aids in the understanding the processes-taking place within the Earth, which include such phenomena as sub-surface anticlines and synclines; presence of faults and dikes, lateral and/or vertical magma flows during Earthquakes and/or volcanoes etc. Almost all geophysical inferences about the Earth's structure and the physical processes going on inside the Earth, like, for example, core-mantle interaction, thermal convection, earthquake raptures to name but a few are carried out on the base of the surface made measurements.

The meaningful *geological and/or geophysical interpretation* for the above-mentioned purposes therefore depends on the ability to *distinctly differentiate the variable densities* of various sub-surface geological materials. Density variations are also useful in providing indirect clues to the presence of economically useful deposits e.g. minerals, petroleum and gas etc. Besides, the sub-surface lateral variations of density or *mass distributions* are associated with changes in the potential fields e.g. gravity perturbations including latitudinal variation of gravity of the Earth and Earth tides which have links to the Earth's interior. It is therefore vital to consider *variable density and/or density contrasts* rather than *constant density* when interpreting geophysical potential fields.

Problems utilizing *constant densities* have theoretically and practically been investigated, however the disturbing masses of *variable density distributions* for both theoretical and practical cases are still in the *process of development*. Studies on the two-dimensional gravity modeling with variable density contrasts have attracted a lot of interest for some time now. Rao [1986a; 1986b; 1990] has developed closed-form expressions for computing gravity from two-dimensional simple-shaped bodies such as rectangular cylinders, inclined faults and asymmetrical trapezoids, the densities of which follow quadratic polynomial functions of depth. Cordell [1973] shows an approximate

method to compute the gravity effect caused by a two-dimensional vertical prism with density contrast varying exponentially with depth, while Murthy and Rao [1979] studied gravity anomalies of two-dimensional arbitrary cross-section with *linear density variations* with depth.

Further, the problems of *inverse theory or downward continuation* of potential fields into arbitrary regions of the lower half-space on both two-dimensional (2D) and three-dimensional (3D) formulations have extensively been treated in geophysical literature. Research works of Savinsky et al., [1981] on downward continuation into the lower half-space to determine to the disturbing masses in a horizontal layer are particularly notable. In Savinsky [1984] the entire lower half-space is considered for the *determination of the disturbing masses* in an intermediate layer from observed potential fields i.e., gravity and magnetism. Closely linked are problems of structural or location interpretation of sub-surface features with sole objective of finding the lateral heterogeneities in the Earth for exploration or geological applications. Savinsky [1995] explores the determination of the location of contact surface (separating homogenous media) interface from gravitational and magnetic fields built upon the solution of the integral relating the fields with a density distribution of disturbing masses. The integral relationship developed in Savinsky [1995] enables (1) the solution of the problem to be found in the non-linearized variant and (2) calculated excessive density to be obtained for adjusting the occurrence depth and the oscillation amplitude of the contact surface.

In many cases geophysical formulae are homologous, that is, the structures of the formulae are identical and one equation can be obtained from the other by renaming the different variables and/or parameters. This concept has been extended to determine the possible *height error effects* on the disturbing masses in an intermediate horizontal layer. This determination of disturbing masses will *definitely be erroneous* if the horizontal layer heights are *inaccurately measured* mainly because the resulting disturbing masses do have a *physical meaning only* in the explicit intermediate horizontal layer. Following the works after Novoselitskii [1965; 1967] one could develop the possible height errors and their effects on the intermediate layer density and/or density contrasts by Fourier analysis and the convolution theorem. For most practical applications it seems possible to take advantage of the fast discrete Fourier transform and where necessary filter out the inherent distortion of the higher frequencies. It is essential to do this where the transfer function amplifies the high-frequency components of the spectrum as case of downward continuation [Cordell and Grauch, 1982].

The difficulties faced on seeking an inverse solution are primarily due to (i) the observed data belonging to real Earth whereas computed data belongs to a contrived Earth model (ii) the discrete nature of data and practically of a limited set and (iii) the presence of errors introduced by the measuring system, leading to the characteristic solution of inconsistency, non-uniqueness and instability. The three features imply that geophysical inverse problems are in general 'ill-posed' i.e., in a strict sense the solution would not exist or would be non-unique. Inverse modeling allows for the quantitative prediction and establishment of relations to measurements of real objects in such situations. With this background the study aims to answer the following questions: -

- Can one determine quantitatively the *depth-dependent density variations* in a sub-surface horizontal layer or for sub-surface structures?

- What are the possible *height errors* on the determination of *density variations* and the position of the contact surfaces in a horizontal layer? Do the height errors have a significant effect on the resultant density variations and contact surface positions?

- What are the *height error limits* for a given intermediate horizontal layer for *meaningful* geophysical and/or geological *interpretations*? At what accuracy does the errors on height measurements cease to have a significant effect on a geological and/or geophysical interpretation?

To answer the above-posed questions the present study simulates a gravity anomaly effect of synthetic sub-surface dipping dike model with depth-dependent variable density contrasts in a series of horizontal layers with respect to depth. Each of the horizontal layers has its possible maximum value of depth-dependent variable density contrast known *apriori*. Subsequently, variable *density contrasts* are *recovered* for a series of horizontal layers of varying layer heights i.e., thicknesses of layers in the dipping dike used in the inverse analysis. Similar inversion analysis for an actual case study in an investigation site in Central Ranges of Chubu District, Japan is attempted to demonstrate the efficacy of the *inversion modeling* with actual geophysical data.

In an attempt to answer the above-posed questions, the objectives of the present study are therefore formulated as:

(1) The first task is to determine the depth-dependent variable density contrasts by inversion analysis in the series of horizontal layers i.e., the maximum layer density contrasts. It is directly related to the recovery of the causative structure as enunciated by the contours of the density contrasts and effectively the disturbing masses in an intermediate layer. More so, the positions of the contact surfaces are possible due to their direct relationship to the disturbing masses.

(2) By cognizance that height measurements are (1) prone to errors and/or blunders and (2) rounded off heights of horizontal layers as often seen in geophysical literature e.g. Bear et al. [1995]; Nagihara and Hall [2000], the second task then is to determine the possible *height error effects* on the density variations (disturbing masses) and the positions of the contact surfaces.

(3) The third task is to determine for a given horizontal intermediate layer the *maximum error limits* on heights for meaningful geological and/or geological interpretation? At what accuracy does the errors on height measurements cease to have a *significant effect* on the interpretations?

(4) Utilize the above procedure i.e., (1), (2) and (3) to the project by inversion analyses on a real case study in a part of Central Ranges in Chubu District, Japan utilizing actual geophysical data (i.e., gravity data and common geological materials) supplied by Geological Survey of Japan [GSJ, 2000].

1.2 Solution of the Problem

Modern inversion analysis presumes that geophysical data are *inaccurate* i.e., they have both measurement errors and noise; *incomplete* i.e., the relevant physical properties cannot be completely determined and yet *redundant* and thus probably inconsistent [Sleep and Fujita, 1997]. The geological and/or geophysical applications of any geophysical method requires consideration of the target that the technique is actually measuring and which results are conclusive and which depend strongly on interpretations, that is, the limitations of the method. For any geophysical method to be useful, we must be able to relate the data it generates to some physical properties within the Earth. The mathematical interpretation of geophysical data or geophysical potential fields anomalies can be carried out directly by *forward modeling*. The physical properties might be a mathematical relationship between *density and gravity variations, density and rock types* or location parameters of a sub-surface structure.

In geophysical literature, the quantitative determination of sub-surface density variations with respect to depth from *inversion analysis* has *not been explicitly investigated*. There have been various attempts to model the sub-surface using forward methods, which include linear functions e.g. Murthy and Rao [1979], linear operators e.g. Bear et al. [1995], quadratic or polynomial functions e.g. Rao [1986a; 1986b; 1990], Martin-Atienza and Garcia-Abdeslem [1988], exponential functions e.g. Cordell [1973], Chai and Hinze [1998] among others. In Damiata and Lee [2002] solids of revolution have been used to determine the *radial variable density* in the sub-surface. In all these cases the *density variations* of the resulting structures were *directly inferred from the forward models*. It is also possible with density gradients to obtain realistic solutions for the causative geometry including depth of the gravity and to locate *density changes* in the horizontal plane while the use of gravity itself can be used to accomplish the latter. High quality gradients either horizontal or vertical are effective in the density prediction *consistent with measured near surface densities* [Butler, 1984].

The determination of the density of the intermediate layer from gravimetric data is based on the dependence of the observed gravity values on the form of the surface of the local relief [Tkachenko, 1975]. The problem is to derive the greatest possible amount of information on the position and the structure of the field sources from measurements of the gravitational field anomalies observed on the Earth's surface [Glasko et al., 1973]. The disturbing mass in a horizontal layer ultimately makes it possible to compute the differential *density contrasts* and the *positions of the contact surfaces*. Data inversion for a contact surface has been a key problem of gravimetric studies and the analysis of the properties of this problem in some cases requires complicated and long mathematical derivations [Starostenko et al., 1992]. It is well known that in a general case the problem

of determining a contact surface does not have the stability property and it is necessary to impose some *restrictions* on the solution in order to attain it i.e., the contact surface position [Starostenko et al., 1994]. In order for stability of the inverse problem to be direct corollary of the uniqueness theorem it is necessary and adequate that the uniqueness class be compact [Tikhonov, 1943].

In both *forward* and *inverse analysis*, it makes little sense to create or fit models to levels exceeding the *accuracy* of the data and to attempt to obtain detail that lies beyond the resolution of the method. Conversely, it is usually impractical to include all known geological facts in a geological model. For example, it is unwise to worry about the precise value of a single physical parameter that varies several percentage points when another important property in the formula under evaluation is unknown to an order of magnitude. Therefore the geological information of geologic materials in an area is important for any meaningful geological and/or geophysical interpretations. The source of such data could either be seismic, borehole data etc. that have explicit values for particular sub-surface locations.

In this study we consider a *quantitative determination* of the disturbing masses (i.e., variable density contrasts and position of contact surfaces) for an intermediate horizontal layer. Closely related to disturbing masses we investigate the possible *height errors* and their *effects* on the both density contrasts and the positions of the contact surfaces for the same intermediate layer. In a nutshell then Chapter 2 commences with a theoretical background for the entire study, which includes the *density variations*, *inversion analysis* and by *downward continuation* techniques, the development of *possible height errors* utilizing Fourier analysis and convolution theorem. The background theory covers gradients and density variations in Section 2.2 (i.e., geophysical gradients in Section 2.2.1 and sub-surface density variations in Section 2.2.2), the disturbing masses of an intermediate horizontal layer in Section 2.3 (i.e., variable density contrasts in Section 2.3.1 and positions of contacts surfaces in Section 2.3.2).

Further the height *error effects* on the disturbing masses due to possible height errors on intermediate horizontal layer are considered in Section 2.4. It includes *deviations* due to inaccurate average depth of horizontal layer in Section 2.4.1, *distortions* due to assigned layer thickness or assumed density in Section 2.4.2, top surface being *identical* to *observations surface* in Section 2.4.3 and layer being *approximated* as surface covered with a mass in Section 2.4.4. By the direct relationship between the disturbing masses and position of contact surfaces, the error effects on the positions of contact surfaces are determined simultaneously with determination of the error effects on density contrasts in Section 2.4. Finally Chapter 2 concludes with *height error limits* for a meaningful geological and/or geological interpretation in Section 2.5 for an intermediate layer.

Chapter 3 delves into the *forward modeling* of synthetic gravity anomaly effect of sub-surface dipping dike model in Section 3.2 (i.e., *location* and *parameters* in Section 3.2.1, *geological materials* in Section 3.2.2, *synthetic* density contrasts in Section 3.2.3,

synthetic *gravity anomaly effects* in Section 3.2.4 and the *final* gravity anomaly effect in Section 3.2.5). Section 3.2.4 follows the *synthetic modeling* of the dipping dike model similar to works of Ateya and Takemoto [2002a; 2002b] and Ateya et al., [2003]. Inversion analysis based on the gravity anomaly effects of the dipping dike is covered in Section 3.3, in which Section 3.3.1 has the determination of the intermediate horizontal layer density contrasts and position of contact surfaces while Section 3.3.2 has the possible *height error effects* on the density contrasts and positions of contact surfaces as outlined in background theory in Section 2.4. Finally Chapter 3 concludes with Section 3.3.3 that investigates on the basis of the synthetic gravity anomaly effects, the height error limits for meaningful *geological and/or geophysical interpretations*.

The inversion analysis is then *applied* to a real case study utilizing actual regional geophysical data in Chapter 4 to test its efficacy. It is a *microgravimetry investigation site* situated in the Central Ranges of Chubu District, Japan. The location of entire region and different data sets for the inversion analysis are shown in the Chapter 4 too. *Geological data* is outlined in Section 4.1.2 while *digital terrain data* (topography) and *gravity* data are given in Section 4.2 (i.e. digital terrain model (DEM) provided by Geographical Survey Institute (GSI) in Section 4.2.1 and gravity data provided on CD-ROM supplied by Geological Survey of Japan (GSJ) in Section 4.2.2), with due acknowledgements. The inversion analysis in Chapter 4 for the microgravimetry investigation site follows a pattern similar to that in Chapter 3 including investigations on the height error limits. Finally, Chapter 5 *summarizes* and *concludes* the study.

Chapter 2

We are dwarves sitting on the shoulders of giants.
We see things that are deeper or further, not by the penetration of our own vision
or by our own height, but because they support us and lend us their height.
- Bernard de Chartres (12th Century).

One cannot escape the feeling that these mathematical formulae
have an independent existence and intelligence of there own, that they are wiser than we are,
wiser even than their discoverers, that we get out of them more than was originally put into them.
– Heinrich Hertz (From Nicholson & Eric Weinstein's).

2 Theory

2.1 Introduction

Mapping of the Earth's heterogeneities in two or three dimensions is increasingly being addressed using various methods including *inversion analysis* and *downward-continuation,* which are the useful eyes of geophysicists and geologists to the invisible underground structures. *Inversion* is an important tool when interpreting geophysical data as it attempts to *reconstruct rock property distribution from measurements of their physical properties their responses.* The inherent non-uniqueness underlying all geophysical inverse problems requires additional information to select a single (viable) solution among the ensemble of infinite rock-property distributions able to fit the data. Such information may be provided in the form of (1) a specific starting model for the inverse run, (2) a specific parameterization restricting the search for predetermined geometrical shapes, or (3) an extra mathematical requirement for the solution.

The goal of gravity inversion is to estimate the *parameters* (*densities, geometry*) of a postulated underground model from a set of given gravity observations. In three-dimensional gravity inversion, the model can be defined by surfaces [Barbosa et al. 1999], topographic variations [Oldenburg, 1974] or grid of prismatic cells. Mostly inverse methods are preferred to forward methods as they offer quantitative solutions that can be determined more efficiently than the trial-and-error approach of the forward modeling. For example, inversion of gravity data constitutes an important step in the quantitative interpretation since construction of density contrasts models remarkably increases the amount of information that can be extracted from the gravity data. The present tendency is to collect different kinds of geophysical data, which includes *seismic, gravity, and magnetic data*, in order to learn about the Earth's interior. However, in geosciences rarely do measurements of data provide sufficient constraints on a problem to allow for a unique and stable solution from inversion analysis.

The magnitude of gravity depends on five factors: latitude, elevation, topography of the surrounding terrain, Earth tides and the density variations in the subsurface while the density of sub-surface rocks e.g. sedimentary rocks varies with depth and horizontal location because of the effects of stratigraphic layering, facies variations, diagenesis,

tectonic history, cementation and compaction from geostatic pressure. Improper field measurement intervals, separation of high frequency effects from low frequency ones and the shortage of *apriori* information about the densities for elevations corrections, are also part of the problems that commonly affect the practical geophysical data interpretations. Any data that has not been measured precisely or processed using the appropriate techniques cannot give a very good result irrespective of the type of modeling procedures used or vice versa. The main problem in gravity processing and interpretation is the separation of the anomalies resulting from the *body of interest* and the Bouguer anomalies.

2.2 Data gradients and Density Variations

2.2.1 Geophysical Data Gradients

Conventional gravimetry is applied mostly to delineate very shallow structures or cavities where interfering sources are the major obstacle to a reliable interpretation. Considerable attention has been directed recently to applications of gravity gradients e.g. Stanley and Green [1976], Butler [1979] and Butler et al., [1982]. Gravity-gradient interpretive procedures are developed from properties of true or differential gradients, while density gradients are determined in an interval of finite difference sense from field gravity data. A generalized approach to structural interpretation from gravity data consists of (1) determining vertical and horizontal gradient profiles perpendicular to the strike of a two-dimensional anomaly, (2) determining the structural geometry from the gradient space plot and (3) locating profile positions of structural corners from vertical gradient profile. Further the importance and usefulness of the gravity gradients of tensor especially the vertical and horizontal gradients of vertical gravity in locating subsurface objects have long been noted e.g., Evjen [1936]; Hammer and Anzoleaga [1975] and Butler [1983].

Recent developments in aerial gradiometry systems e.g., Jekely, [1988], Vasco [1989], Bell et al., [1997] have resulted in renewed interest in gravity gradient measurements especially in the delineation of salt intrusions [Bell, 1998]. Because derivatives of vertical gravity have greater spatial resolution, delineate lateral boundaries of bodies better and can provide more depth information that vertical gravity alone, numerous investigations (e.g., Evjen [1936]; Hammer and Anzoleaga [1975]; Butler [1983], Blakely and Simpson [1986], Grauch and Cordell, [1987], Butler, [1995]) have derived theoretical expressions for the horizontal and vertical derivatives of the vertical gravity field resulting from simple geometries (spheres, horizontal cylinders, plates truncated plates). Nevertheless, there has not been a complete analysis of all the components of the gravity gradient tensor [Mickus and Hinojosa, 2001]. In Mickus and Hinojosa [2001], derivation of the gravity gradient tensor components as functions of the vertical component of gravity in the Fourier transform domain is studied.

Application of this generalized gravity gradient inversion procedure to high quality gravity data results in an effective density prediction consistent with measured near-surface densities and the known increase in density with depth in deep sedimentary

basins [Butler, 1995]. The geoid undulations, gravity anomalies and the gravity gradient changes themselves are different measures but all reflect the density variations of the Earth [Li and Gotze, 2001]. Vertical and horizontal intervals must be selected properly relative to the depths of interest. For horizontal gradient determinations, there is virtually complete freedom in the selection of any desired horizontal interval, while for vertical gradient determinations; the vertical interval is limited by practical considerations [Butler, 1984].

And the vertical gravity gradient being more sensitive than gravity itself to the geologic structures and neighboring disturbing bodies having fewer influences in its interpretation, it can be ideal for interpretation. The utilization of the vertical gradient of gravity, even when computed from the gravity field, has definite advantages. It is possible to obtain realistic solutions for the geometry including depth of the causative (gravity) and to locate density changes in the horizontal plane while the use of gravity itself can be effective to accomplish the latter. However, in case of interfering anomalies, the resolving power of the gravity field is smaller than that of the vertical gradient.

2.2.2 Sub-surface Density Variations

The sub-surface or lower half-space consists of the position below the Earth surface i.e. $z > 0$ with the z-axis being directed downwards. It is recognized that the sub-surface density of sedimentary rocks varies with depth and hence any anomalous body surrounded by them shows a decrease in its density contrasts with depth while its density remains unchanged throughout its volume [Murthy and Rao, 1979]. In this respect, it is vital to consider variable density rather than constant density when interpreting or in the recovery of sub-surfaces structures. Various approximate and closed form expressions that describe the gravitational attraction of a vertical cylinder or horizontal circular disk with constant density are reported in geophysical literature e.g. Nettleton [1976] and [Damiata and Lee, 2002]. Further the use of vertical cylinders although a gross simplification is educationally instructive in the forward modeling of various geological features of interest e.g., salt dome, volcanic plug and igneous intrusions.

Several authors have studied two-dimensional gravity modeling with variable density contrasts e.g. Cordell [1973]; Murthy and Rao [1979]; Rao [1986, [1986a, 1990]; Martin-Atienza and Garcia-Abdeslem, [1988]. These different works have elaborately been presented in Chapter 1. On the other hand, Damiata and Lee [2002] derived integral expressions for the vertical component of gravitational attraction arising from vertical circular cylinders and horizontal circular disks with radial variation of density. Further, the density of the sub-surface structures have been investigated where some authors assume a known *density contrasts* and design nonlinear operators to determine the geometry of the source. Other investigators use an approach of solving the unknown *density distribution* by applying a linear operator to the data e.g., Butler [1995] or the generalization of Parasnis' [1961] approach to include the variable density in a cylinder [Moon, 1981]. Boulanger and Chouteau [2001] and Chasseriau and Chouteau [2003], adopt the parameterization of the sub-surface into regular rectangular prisms and they

utilized geological constraints to recover the geometry (depth and size) and density distribution of the original dipping dike model.

2.3 Disturbing Masses Distribution in Layer

The main problems connected with the theory of continuation of the potential fields into arbitrary regions of the lower half-space in a two-dimensional formulation have been studied thoroughly [Savinsky et al., 1981] and their possibility of extension to a three-dimensional cases have too been demonstrated. The problem is to derive the greatest possible amount of information on the position, location and the structure of the *causative sources* from measurements of the gravitational field anomalies observed on the Earth's surface [Glasko et al., 1973]. The determination of the disturbing masses in a horizontal layer ultimately makes it possible to compute the differential density contrasts and the positions of the contact surfaces.

The two-dimensional (2-D) or three-dimensional (3-D) determination of the density contrasts in a sub-surface layer is a geophysical ill-posed problem. Ill-posed problems can be dealt with satisfactorily by using some kind of regularization [Glasko et al., 1987], which means restricting the solution to a subset of parameter space. Tikhonov's regularization method is useful in investigations of real structures under the actual conditions of the experiments and the data processing. The stable solution of the three-dimensional case is possible, thanks to regularization techniques on the basis of the general principles enunciated by Tikhonov and Glasko [1965] and Tikhonov and Arsenin [1974]. Nevertheless, since Tikhonov's method should be considered as a means to automating the interpretation process in the case of considerable, *apriori* unknown total errors of input data, a minimum of additional information on the structure is desirable [Glasko et al., 1973].

2.3.1 Variable Layer Density

When the *density or density contrasts* vary in the lower half-space or in a sub-surface structure then have what is called *variable density* in a horizontal layer. Consider a system of rectangular co-ordinates with z-axis directed downwards, the *disturbing or gravitating masses* in the lower half-space i.e., $z > 0$ are reflected in the potential field observed on the Earth's surface. The problem is to derive the greatest possible amount of information on the positions, locations and the sub-surface structures of the causative sources from these measurements of the gravitational field anomalies $\Delta g(x_j, y_j, z_j)$ observed. A possible location in the horizontal layer can be placed at a depth from $h = H_0$ to $h = H_0 + \Delta H$, where ΔH is the thickness of the horizontal layer and $Q(x, y, h)$ as the disturbing masses that represent the density distributions within it.

For convenience, we briefly mention the initial algorithm for the *downward continuation* of the potential field [Savinsky, 1967a]. Let $Q(x_j, y_j, z_j)$ be the measured or

observed values of the field, x_j, y_j be horizontal co-ordinates and z_j the elevation of the points of the measurements above some underlying plane h. In order to find the field $Q(x,y,h)$ on the plane at height h, the following system can be constructed:

$$\int_{-\infty}^{\infty}\int_{-\infty}^{\infty} K(x-x_j, y-y_j, z_j+h)Q(x,y,h)dxdy = Q(x_j,y_j,z_j), j = 1,2,...,N.$$
$$K(x-x_j, y-y_j, z_j+h) = \frac{z_j}{2\pi[(x-x_j)^2+(y-y_j)^2+(z_j+h)^2]^{3/2}} \quad (2\text{-}1)$$

As a result of the approximation:

$$Q(x,y,h) = \sum_{j=1}^{N} \alpha_j K(x-x_j, y-y_j, z_j+h) \quad (2\text{-}2)$$

and by substitution of (2-2) into (2-1) the problem reduces itself to the determination of the coefficients α_j of the polynomial from the linear algebraic equations with the Grams matrix. Figure 2.1 shows the schematic representation of the disturbing masses in an intermediate horizontal layer.

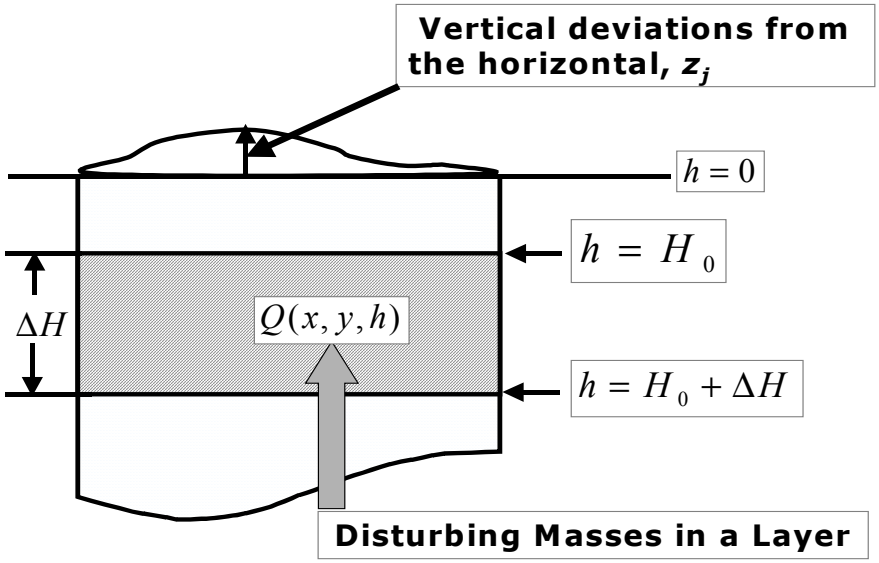

Figure 2-1: A schematic diagram for a sub-surface horizontal layer and its disturbing masses (density distributions).

If one assumes that there are values of the gravity field $\Delta g(x_j, y_j, z_j)$, j = 1, 2… N, where z_j are deviations in the vertical distance from the horizontal measurement level $h = 0$, the solution of the problem can be achieved analytically through:

$$f\int_{-\infty}^{+\infty}\int_{-\infty}^{+\infty}\int_{H_0}^{H_0+\Delta H}\frac{(z_j+h)Q(x,y,h)dxdydh}{\left[(x-x_j)^2+(y-y_j)^2+(z_j+h)^2\right]^{3/2}} = \Delta g(x_j,y_j,z_j), j = 1,2,...,N. \quad (2\text{-}3)$$

where f is the gravitational constant, the x_j and y_j are the x - axis and y - axis coordinate values. In this case we seek to obtain the density distribution $Q(x,y,h)$ *within the horizontal layer* in the polynomial form, the terms of which are formed by the functions of the kernel of the integral equation [Savinsky, 1963; Savinsky et al., 1981]:

$$Q(x,y,h) = f\sum_{j=1}^{N}\frac{\alpha_j(z_j+h)}{\left[(x-x_j)^2+(y-y_j)^2+(z_j+h)^2\right]^{3/2}} = \sum_{j=1}^{N}\alpha_j K_j(x,y,h). \quad (2\text{-}4)$$

On substitution of (2-4) into (2-3) the problem of determining the polynomial coefficients α_j is reduced to solution of the set of equations (2-5) with the index i represents same number of points on the (x,y) plane as index j:

$$\sum_{j=1}^{N} a_{ji}\alpha_j = \Delta g(x_j,y_j,z_j), j = 1,2,...,N, \quad (2\text{-}5)$$

where a_{ji} is given by:

$$a_{ji} = f^2\int_{H_0}^{H_0+\Delta H}\left\{\int_{-\infty}^{+\infty}\int_{-\infty}^{+\infty}\frac{(z_j+h)(z_i+h)dxdy}{\left[(x-x_j)^2+(y-y_j)^2+(z_j+h)^2\right]^{3/2}\left[(x-x_i)^2+(y-y_i)^2+(z_i+h)^2\right]^{3/2}}\right\}dh$$

$$= 2\pi f^2\int_{H_0}^{H_0+\Delta H}\frac{(z_j+z_i+2h)dh}{\left[(x_j-x_i)^2+(y_j-y_i)^2+(z_j+z_i+2h)^2\right]^{3/2}}$$

$$= \pi f^2\left\{\frac{1}{\left[(x_j-x_i)^2+(y_j-y_i)^2+(z_j+z_i+2H_0)^2\right]^{1/2}} - \frac{1}{\left[(x_j-x_i)^2+(y_j-y_i)^2+(z_j+z_i+2(H_0+\Delta H))^2\right]^{1/2}}\right\} \quad (2\text{-}6)$$

Equations (2-6) has the Grams ortho-normalization matrix, its elements being the products K_j, K_i which determines the *existence and uniqueness* of the analytic solution at

linearly independent $K_j, j = 1,2,...,N$ and enables us to use the convenient method of ortho-normalization of K_j given by Savinsky [1967b]. This allows the polynomial coefficients α_j to be computed at N that are practically as great as one can wish [Savinsky, 1985] and it is possible by use of a regular grid discrete points to determine the density or density contrasts of the disturbing masses. The resulting expression $Q(x, y, h)$ is the normal solution of the set (2-6) possessing the property [Savinsky, 1963; Sen & Stoffa, 1995]:

$$\|QR\|_{L_2}^2 = \|Q\|_{L_2}^2 + \|Q_0\|_{L_2}^2 \tag{2-7}$$

where QR is any of the set of possible solutions of (2-3) and Q_0 is orthogonal to the subspace with the basis $K_j, j = 1,2,...,N$. Hence it follows that the found Q has the minimal norm in L_2 and is the best smoothly varying solution.

The point-to-point spacing adopted allows for the solution to be obtained analytically along the entire surface as given by equation (2-3). The problem of finding the different densities in the entire lower half-space below $h = H_0$ was previously considered in Savinsky [1984] where the limit for integration in (2-3) was ∞ instead of $H_0 + \Delta H$. The resulting density distribution or disturbing masses $Q(x, y, h)$ in (2-5) have physical meaning only at $H_0 < h < H_0 + \Delta H$. Since the result has a physical meaning only between the range $H_0 < h < H_0 + \Delta H$, a series of different heights of the horizontal layers can be chosen to cover a whole entire sub-surface structure or the entire lower half-space.

When the inequality $0.65dr \leq H_0 \leq 1.55dr$ (where dr is the average distance between the measurement points i.e., the grid spacing of the field points) holds, the resulting Q usually can be used for geological interpretations. The set (2-6) becomes poorly defined at increasing H_0 as the influence of errors in field measurements sharply rises [Savinsky et al., 1967]. Since geophysical inversions result in non-unique solutions, the objective of inversion is first to find a solution (or solutions) and represent the degree of non-uniqueness of the solution in a quantitative manner.

In this case the regularization method can be applied to the solution with use of a discrepancy based on the general principles proposed by Tikhonov [Tikhonov and Arsenin, 1974]. Such inverse problems that do not possess uniqueness and stability are ill posed; otherwise the inverse problem is well posed problem. Regularization techniques can be applied to ill-posed problems to restore well posedness [Koch, 1990].

2.3.2 Methods of Regularizing the Solutions

The approximation of the solution with aid of the polynomial (2-2) enable the obtaining a convenient method of its regularization on the basis of the general principles

enunciated by Tikhonov and Arsenin [1974]. Let a_{ji} be the coefficient of the system of linear algebraic equations used for finding a_{ji} and a

$$\Delta U_j = \sum_{i=1}^{\infty} a_{ji}\alpha_i - \Delta g(x_j, y_j, z_j) \tag{2-7}$$

be deviations at the *j*-th point of the measurement, assumed for finding the field on the underlying plane. Using the method of residual, we have $|| Q^{reg}(x,y,z) ||^2_{L_2} = \min_{\Delta U_j} || Q(x,y,z) ||_{L_2}$ in the conditions

$$\frac{1}{N}\sum_{j=1}^{N} \Delta U_j^2 = \beta^2, \sum_{j=1}^{N} \Delta U_j = 0 \tag{2-8}$$

where β is chosen is such a way that it is proportional to the root-mean-square error σ of the measurements. The procedure of ortho-normalization of K_j and the representation of the solution enables as to obtain an expression for its norm (in assumption that

$$|| Q^{reg}(x,y,z) ||^2_{L_2} = \sum_{i=1}^{N} \overline{\alpha}_i^2 \tag{2-9}$$

which in turn facilitates reduction of the problem to the finding of the conditional extremum of the function (2-9) of *N* variables for the conditions (2-8)

$$\begin{aligned} &\frac{\partial \Phi}{\partial \Delta U_j} = 0, j = 1,2,...,N. \\ &\Phi = \sum_{i=1}^{N} \overline{\alpha}_i^2 + \lambda_i \left(\frac{1}{N} \sum_{j=1}^{N} \Delta U_j^2 - \beta^2 \right) + \lambda_2 \sum_{j=1}^{N} \Delta U_j \end{aligned} \tag{2-10}$$

By virtue of $\alpha_j = \sum_{j=1}^{N} b_{ij}\overline{\alpha}_i$ [Savinsky et al., 1981], we have

$$\begin{aligned} \frac{\partial \sum_{i=1}^{N} \overline{\alpha}_i^2}{\partial \Delta U_j} &= \frac{2\sum_{i=1}^{N} \overline{\alpha}_i \partial \sum_{j=1}^{N} b_{ij}[Q(x_j, y_j, z_j) + \Delta U_j]}{\partial \Delta U_j} \\ &= 2\sum_{i=1}^{N} \overline{\alpha}_i b_{ij} = 2\alpha_j \end{aligned} \tag{2-11}$$

Solving

$$\frac{\partial \Phi}{\partial \Delta U_j} = 2\alpha_j + \frac{2\lambda_i \Delta U_j}{N} = 0, j = 1,2,...,N. \tag{2-12}$$

and together with equations (2-8), we have

$$\Delta U_j = -\frac{\sqrt{N}\beta \left(\alpha_j - \frac{1}{N}\sum_{j=1}^{N} \alpha_j \right)}{\sqrt{\sum_{j=1}^{N} \alpha_j^2 - \frac{1}{N}\left(\sum_{j=1}^{N} \alpha_j \right)^2}}, j = 1,2,...,N. \tag{2-13}$$

Regularization of the solution can be reduced to the finding of $Q(x, y, z)$ for the initial values of $Q(x_j, y_j, z_j) + \Delta U_j$ with the aid of the algorithm. In equation (2-13) α_j should correspond to $Q(x_j, y_j, z_j) + \Delta U_j$, however for values of β not high in equation (2-13) α_j can be substituted for $Q(x_j, y_j, z_j)$ which in many cases enables us to obtain a satisfactory solution of the problem. When the interference (noise) is significant, the procedure is successively repeated k times for a given small values of β less σ. This permits the regularized solution to be found with complete formalization of the algorithm.

2.3.3 Position of the Contact Surfaces

A *contact surface* is a delineating surface (i.e., distinct separator surface) between two or more densities in the lower half-space or a sub-surface causative structure. Data inversion for *determination of a position of the contact surface* is a key problem in gravimetric studies. Analysis of the properties of this problem in some cases requires complicated and long mathematical derivations, which can sometimes distract the geophysical essence of the material [Starostenko et al., 1992]. There are three basic statements of the problem of the gravity data inversion for a *contact surfaces positions*, two of which we mention here. For two-dimensional contact surface position cases, two statements are schematized in Figure 2.2 and Figure 2.3 respectively.

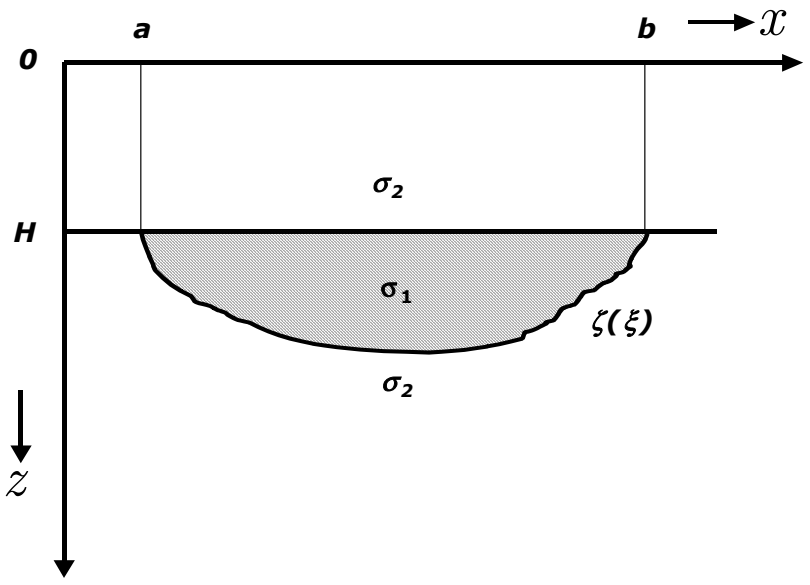

Figure 2-2: A localized body with a constant density σ_1 surrounded by homogenous material of density σ_2

The regions occupied by the anomalous (disturbing) masses that create corresponding fields are hatched. The objective is to determine the position of contact surfaces given the potential field $\Delta g(x, y, z)$ and relief $z = h(x)$. The substantive difference between the models of Figure 2.2 and Figure 2.3 are: (1) Figure 2.2 the sought-for contact surface position $\zeta(\xi)$ is assumed to be finite and in the describable finite interval [a, b], besides it belongs to a localized body structure and (2) Figure 2.3 stretches infinitely along the axis $z = 0$ and the anomalous mass situated between axis $z = 0$ surface and contact surface $\zeta(\xi)$ can be conveniently divided into two parts: a horizontal plane-parallel layer of thickness h and the region between the plane $z = h$ and the contact surface $\zeta(\xi)$.

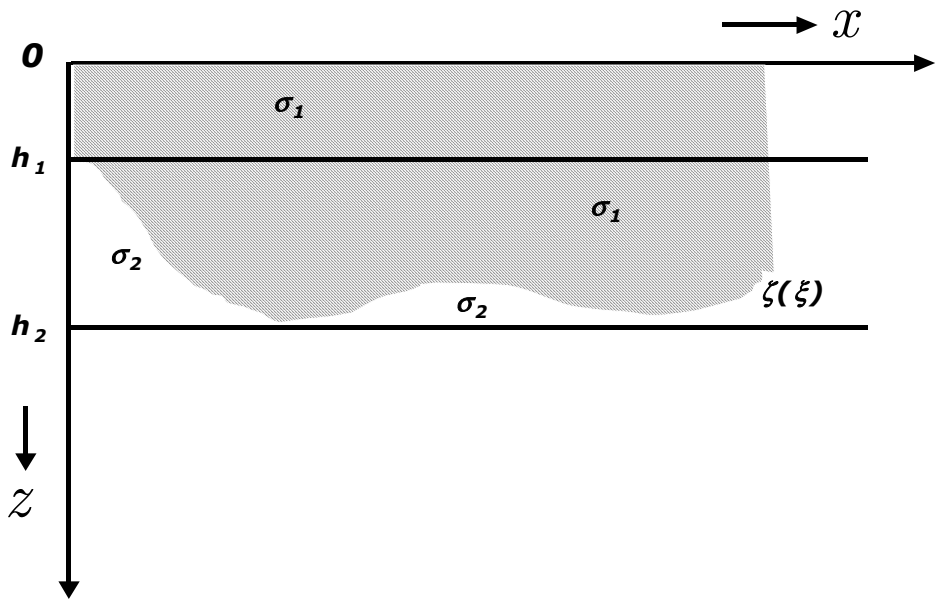

Figure 2-3: A body of an infinite extension with constant density σ_1 in a contact interface with a homogenous material of density σ_2

Therefore after Starostenko et al., [1992], we can define the positive constant of mass density according to the rule $\sigma = \sigma_2 - \sigma_1$ while for localized bodies we usually assume $\sigma = \sigma_1 - \sigma_2$, which is more natural, for both cases given in Figure 2.2 and Figure 2.3. Among the parameters of a contact surface are: the depth H, the effective density $\sigma = \sigma_2 - \sigma_1$ or $\sigma = \sigma_1 - \sigma_2$, the co-ordinates of the ends of the interval e.g. a and b, the shape of the separation boundary $\zeta(\xi)$ in the interval $[a, b]$. Algorithm for

solving the linear inverse problem for a contact surface on the basis of the method of normalization was proposed by Tikhonov and Glasko [1964] and for the non-linear problem in Tikhonov and Glasko [1965].

Further we refer to the works of Tikhonov and Glasko [1965] and Tikhonov and Arsenin [1974], which allowed the solution of the problem in the nonlinear statement to be found and the methods for simultaneous determination of shape and form of the contact surface to be developed [Glasko et al., 1970; 1973]. If the layer densities are known, the position of uppermost or lowest contact surface is known, and the positions of other contact surfaces are to be reconstructed thereby, then it is a nonlinear problem. On the other hand, the problem is linear if the position of the contact surfaces is given and the different densities of the layers bounded above and below the contact surface are to be found [Starostenko et al., 1982].

There are several methods in geophysical practice for the determination of the position of contact surfaces. For example, the contact surface separating two homogenous layers can be found by recalculating the measured gravity field $\Delta g(x,y,0)$ to the underlying horizontal plane $h = H_{av}$ occurring at the proposed average depth of the contact surface [Mironov, 1980]. The actual deviations of the contact surface from this plane are then computed from the formula [Savinsky, 1995]:

$$\Delta S(x,y) = \frac{1}{2\pi f D}\Delta g(x,y,H_{av}) \tag{2-14}$$

where D is the difference between densities of the upper and lower layers, H_{av} is average their height and f is the gravitational constant. In the case of a horizontal intermediate layer the integration of $Q(x,y,h)$ in the indicated layer with respect to h gives the function $Q_s(x,y)$ i.e., the average density referred to the unit area of the horizontal intermediate layer [Savinsky, 1995]:

$$Q_s(x,y) = \int_{H_0}^{H_0+\Delta H} Q(x,y,h)dh \tag{2-15}$$

$$= f\sum_{j=1}^{N}\alpha_j * \left\{ \frac{1}{\left[(x-x_j)^2+(y-y_j)^2+(z_j+H_0)^2\right]^{1/2}} - \frac{1}{\left[(x-x_j)^2+(y-y_j)^2+(z_j+H_0+\Delta H)^2\right]^{1/2}} \right\} \tag{2-16}$$

In the case of the two homogenous media one could use the function $Q_s(x,y)$ to find the height of the contact surface $S(x,y)$ measured from the lower boundary $H_0 + \Delta H$ upwards given as:

$$S(x,y) = Q_s(x,y) / D \tag{2-17}$$

where D is the given excess density of the lower layer. The division of the maximal (positive) value of $Q_s(x,y)$ by the layer thickness ΔH one finds the excessive density D_c corresponding to the case when the depths H_0 and $H_0 + \Delta H$ are the limits of deviations of the contact surface. We thus obtain:

$$S(x,y) = Q_s(x,y) / D_c \tag{2-18}$$

The *advantage* of the method is the possibility of obtaining the *calculated excessive density* D_c and to *control*, on this basis, the given depth of layer H_0 and its thickness ΔH. This feature of the method is due to the solution integral equation (2-3) relating the field $\Delta g(x_j, y_j, z_j)$ directly with the density distributions of the disturbing masses $Q(x,y,h)$. Effectively this relationship allows for the determination of the density contrasts of the disturbing masses in a series of horizontal intermediate layers.

2.4 Possible Errors in the Variable Density in a Layer

Having treated the theory of determination of a variable density in a horizontal layer by means of *gravitational anomalies* in the previous sections, we show that it is possible to compute the *possible deviations* from the actual *differential density contrasts* determined. This arises when the intermediate layer parameters are given inaccurately or simplified by rounding off the layer height values. In a classic paper after Peters [1949], it is shown how a potential field (magnetic or gravitational) measured at the Earth's surface can be analytically projected upward or downward i.e., mathematically transformed to what it would be if it could be measured either above the Earth's surface or along a horizontal plane inside the Earth.

Downward continuation is essentially the mathematical process for finding the appearance of the surface anomaly at a specific depth. It is possible by downward continuation to compute the field at the actual depth of the sub-surface structure. For potential fields the function is to convert the observed gravity or magnetic fields to what it would be *if the features of the major interest were much shallower*. With actual data, the process of downward continuation is usually unstable in a *mathematical sense with very short-wavelengths components – including those associated with errors in the data – become infinite during downward continuation* [Sleep and Fujita, 1997, p. 100]. Thus downward-continued anomaly changes greatly as small changes occur in data. Viewed another way, downward continuation represents an attempt to determine a simplified mass distribution at some depth that would satisfy the data. Certain possible mass distributions at that depth, including those with very short-wavelength variations, have essentially no effect on the observed data.

Following the works by Novoselitskii [1965, 1967], one can develop the possible errors due to *inaccurate heights* on *horizontal layer* and their effects on the resultant density and/or density contrasts for a sub-surface structure or a horizontal layer by utilization of both Fourier analysis and convolution theorem. The Fourier series assumes that the gravity anomaly and the masses in Earth are periodic, thus when the data are upward or downward continued, the process behaves as if the two ends of the region are being tied together [Sleep and Fujita, 1997, p. 100]. If data is available for only a small area, it is better to remove the *average anomaly* and the *linear trend of the gravity anomaly* across the region before beginning the Fourier analysis. For most practical applications it seems best to take advantage of the fast discrete Fourier transform and where necessary filter out the inherent distortion of the higher frequencies. It is essential to do this where the transfer function amplifies the high-frequency components of the spectrum as case of downward continuation [Cordell and Grauch, 1982].

2.4.1 Deviations due to inaccurate average depth of horizontal layer

Inaccurate height measurements result in distortions of differential densities. To investigate the effect of the distortion, let the potential and geophysical field be related by $V_z(x)/2\pi fh = U(x)$ while keeping the thickness h of the intermediate layer constant, we can write two integral equations referring to the density for a two-dimensional distribution:

$$U(x) = \frac{1}{2\pi h}\int_{-\infty}^{+\infty} \sigma(\xi)\ln\frac{(x-\xi)^2 + H_2^2}{(x-\xi)^2 + H_1^2}d\xi\,, \tag{2-19}$$

$$U(x) = \frac{1}{2\pi h}\int_{-\infty}^{+\infty} \overline{\sigma}(\xi)\ln\frac{(x-\xi)^2 + \overline{H}_2^2}{(x-\xi)^2 + \overline{H}_1^2}d\xi \tag{2-20}$$

In equation (2-20), the depth of the top, $\overline{H_2}$, of the layer is given with a certain error; however, the height is maintained i.e., $\overline{H_2} - \overline{H_1} = H_2 - H_1 = h$. Assuming that the Fourier transforms for $\sigma(x), \overline{\sigma}(x)$ and potential $U(x)$ exists, we can obtain by the convolution theorem:

$$S(\omega) = U(\omega)\left\{\frac{e^{-(H-h/2)|\omega|} - e^{-(H+h/2)|\omega|}}{h\mid\omega\mid}\right\}^{-1} = U(\omega)\frac{h\mid\omega\mid}{e^{-H|\omega|}}\frac{1}{e^{h/2|\omega|} - e^{-h/2|\omega|}}. \tag{2-21}$$

$$\overline{S}(\omega) = U(\omega)\left\{\frac{e^{-(\overline{H}-h/2)|\omega|} - e^{-(\overline{H}+h/2)|\omega|}}{h\mid\omega\mid}\right\}^{-1} = U(\omega)\frac{h\mid\omega\mid}{e^{-\overline{H}|\omega|}}\frac{1}{e^{h/2|\omega|} - e^{-h/2|\omega|}}. \tag{2-22}$$

Here we have $\overline{H} = (\overline{H_2} + \overline{H_1})/2$. Subtracting equation (2-22) from equation (2-21) leads to equation (2-23) below:

$$\begin{aligned}
&\Delta S(\omega) = S(\omega) - \overline{S}(\omega) \\
&= U(\omega)\frac{h \mid \omega \mid}{e^{h/2|\omega|} - e^{-h/2|\omega|}}\left(\frac{1}{e^{-H|\omega|}} - \frac{1}{e^{-\overline{H}|\omega|}}\right) \\
&= U(\omega)\frac{h \mid \omega \mid}{e^{-H_1|\omega|} - e^{-H_2|\omega|}}\left(1 - \frac{1}{e^{-(\overline{H}-H)|\omega|}}\right).
\end{aligned} \tag{2-23}$$

Denoting $\overline{H} - H$ by ΔH, we arrive at the equation (2-24) below or later equation (2-25):

$$\Delta S(\omega) = S(\omega) - \overline{S}(\omega) = S(\omega)\left\{1 - \frac{1}{e^{-\Delta H|\omega|}}\right\} \tag{2-24}$$

$$\overline{S}(\omega) = \frac{S(\omega)}{e^{-\Delta H|\omega|}}. \tag{2-25}$$

For positive $(\overline{H} > H)$ and for negative $(\overline{H} < H)$ the ΔH values, we obtain following relations respectively.

$$S(\omega) = \overline{S}(\omega)e^{-\Delta H|\omega|}, \tag{2-26}$$

$$\overline{S}(\omega) = S(\omega)e^{-\Delta H|\omega|} \tag{2-27}$$

Transition from the Fourier transforms to the original functions leads to the well-known integrals with Poisson kernels:

$$\sigma(x) = \frac{1}{\pi}\int_{-\infty}^{+\infty} \overline{\sigma}(\xi)\frac{\Delta H}{(x-\xi)^2 + \Delta H^2}\, d\xi, (\overline{H} > H) \tag{2-28}$$

$$\overline{\sigma}(x) = \frac{1}{\pi}\int_{-\infty}^{+\infty} \sigma(x)\frac{\Delta H}{(x-\xi)^2 + \Delta H^2} d\xi, (\overline{H} < H). \tag{2-29}$$

Similar operations are feasible for a three-dimensional distribution. To this end, we apply the convolution theorem for a two-fold Fourier transformation to the equations:

$$W(x,y)=\frac{1}{2\pi h}\int_{-\infty}^{+\infty}\int_{-\infty}^{+\infty}\sigma(\xi,\eta)\left[\begin{array}{c}\dfrac{1}{\sqrt{(x-\xi)^2+(y-\eta)^2+H_1^2}}\\ -\dfrac{1}{\sqrt{(x-\xi)+(y-\eta)+H_2^2}}\end{array}\right]d\xi d\eta \tag{2-30}$$

$$W(x,y)=\frac{1}{2\pi h}\int_{-\infty}^{+\infty}\int_{-\infty}^{+\infty}\overline{\sigma}(\xi,\eta)\left[\begin{array}{c}\dfrac{1}{\sqrt{(x-\xi)^2+(y-\eta)^2+\overline{H_1^2}}}\\ -\dfrac{1}{\sqrt{(x-\xi)^2+(y-\eta)^2+\overline{H_2^2}}}\end{array}\right]d\xi d\eta \tag{2-31}$$

Given the three-dimensional case, the depth of the top, $\overline{H_2}$, of the layer is given with a certain error; however, the height is maintained i.e., $\overline{H_2}-\overline{H_1}=H_2-H_1=h.$ and $\overline{H}=(\overline{H_2}+\overline{H_1})/2$. Once again denoting $\overline{H}-H$ by ΔH, the convolution theorem has the form (cf. Equations 2-21; 2-22 and 2-23):

$$S(u,v)=W(u,v)\frac{h\rho}{e^{-H\rho}}\frac{1}{e^{h\rho/2}-e^{-h\rho/2}} \tag{2-32}$$

$$\overline{S}(u,v)=W(u,v)\frac{h\rho}{e^{-\overline{H}\rho}}\frac{1}{e^{h\rho/2}-e^{-h\rho/2}},(\rho=\sqrt{u^2+v^2}) \tag{2-33}$$

For the difference between equations (2-32) and 2-33), we obtain:

$$\begin{aligned}\Delta S(u,v)&=S(u,v)-\overline{S}(u,v)\\&=W(u,v)\frac{h\rho}{e^{-H_1\rho}-e^{-H_2\rho}}\left(1-\frac{1}{e^{-(\overline{H}-H)\rho}}\right)\end{aligned} \tag{2-34}$$

$$\text{or since } W(u,v)\frac{h\rho}{e^{-H_1\rho}-e^{-H_2\rho}}=S(u,v) \tag{2-35}$$

$$\text{we have } \overline{S}(u,v)=\frac{S(u,v)}{e^{-\Delta H\rho}}. \tag{2-36}$$

From equation (2-36), two equations follow:

$$S(u,v)=\overline{S}(u,v)e^{-\Delta H\rho},(\overline{H}>H), \tag{2-37}$$

$$\text{and } \overline{S}(u,v)=S(u,v)e^{-\Delta H\rho},(\overline{H}<H). \tag{2-38}$$

Since the pair of Fourier transforms is unique, we obtain the integral formulas:

$$\sigma(x,y)=\frac{1}{2\pi}\int_{-\infty}^{+\infty}\int_{-\infty}^{+\infty}\overline{\sigma}(\xi,\eta)\frac{\Delta H}{\left[(x-\xi)^2+(y-\eta)^2+\Delta H^2\right]^{3/2}}d\xi d\eta,(\overline{H}>H). \tag{2-39}$$

$$\overline{\sigma}(x,y)=\frac{1}{2\pi}\int_{-\infty}^{+\infty}\int_{-\infty}^{+\infty}\sigma(\xi,\eta)\frac{\Delta H}{\left[(x-\xi)^2+(y-\eta)^2+\Delta H^2\right]^{3/2}}d\xi d\eta,(\overline{H}<H). \tag{2-40}$$

Equations (2-28), (2-29), (2-39) and (2-40) imply that: (1) Small errors in the assigned average depth of a layer create only slight changes in the variable density dependent of the error in the height ΔH ; (2) In the case of the two-dimensional distribution, a relationship exists between the true and the incorrect (distorted) density values in the form of an integral with a Poisson kernel and (3) When the error in the assigned average depth of a layer is established, the exact densities can be obtained from the distorted density values. It suffices to continue $\sigma(x)$ or $\overline{\sigma}(x,y)$ in the upward direction as harmonic functions for $\overline{H}>H$ and for $\overline{H}<H$, the continuation must proceed into the lower half-space.

These operations have a definite physical meaning such that an increase of the *bedding depth* of the layer with an unchanged gravitational anomaly implies a certain density (in particular, in the epicenter of the field of the anomaly); on the other hand, a decrease of H leads to a smoothing of the functions $\sigma(x)$. This means, when the functions $\sigma(x)$ and $\overline{\sigma}(x,y)$ can be transformed by continuation (which is possible in most cases), that their upward or downward continuation leads to a change near the epicenter. The behaviour of the density function of the periphery of the field of the anomaly is given by the change over which the depths H vary.

2.4.2 Distortions due to an assigned layer thickness or assumed density

The determination of the differential density contrasts in a horizontal layer as outlined in Section 2.3 implies the values have only a physical meaning in the horizontal layer range $H_0<h<H_0+\Delta H$. Therefore, any distortions in the assigned layer thickness alter the resulting density contrasts. To investigate these effects, let us introduce the following initial conditions with α as a constant factor based on the height of intermediate layer:

$$\begin{aligned}&\frac{H_2+H_1}{2}=\frac{\overline{H}_2+\overline{H}_1}{2}=H,\\&h=H_2-H_1,\overline{h}=\overline{H}_2-\overline{H}_1,\\&\overline{h}=\alpha h,\\&i.e.,(\overline{H}_2-\overline{H}_1)=\alpha(H_2-H_1).\end{aligned} \tag{2-41}$$

Taking into account equation (2-41), we can rewrite equation (2-20):

$$\frac{U(x)}{\alpha} = \frac{1}{2\pi\alpha h}\int_{-\infty}^{+\infty}\sigma(\xi)\ln\frac{(x-\xi)^2 + H_2^2}{(x-\xi)^2 + \overline{H}_1^2}d\xi \tag{2-42}$$

or in the Fourier-representation space:

$$U(\omega) = \overline{\sigma}(\omega)e^{-H|\omega|}\frac{e^{\frac{\alpha h}{2}|\omega|} - e^{-\frac{\alpha h}{2}|\omega|}}{\alpha h \mid \omega \mid}. \tag{2-43}$$

A similar expression results for the equation (2-19):

$$U(\omega) = \sigma(\omega)e^{-H|\omega|}\frac{e^{\frac{h}{2}|\omega|} - e^{-\frac{h}{2}|\omega|}}{h \mid \omega \mid}. \tag{2-44}$$

The fact that the left-hand sides of equation (2-43) and (2-44) are identical makes it possible to obtain, after simple calculations, relations between the Fourier transforms of the exact and the distorted density functions (2-45) and (2-46):

$$\sigma(\omega) = \overline{\sigma}(\omega)e^{\frac{h|\omega|}{2}(1-\alpha)}\frac{e^{\alpha h|\omega|} - 1}{e^{h|\omega|} - 1}, \tag{2-45}$$

$$\overline{\sigma}(\omega) = \sigma(\omega)e^{\frac{h|\omega|}{2}(\alpha-1)}\frac{e^{h|\omega|} - 1}{e^{\alpha h|\omega|} - 1}. \tag{2-46}$$

If $\alpha<1$, then equation (2-45) can be represented in the following form:

$$\sigma(\omega) = \overline{\sigma}(\omega)\sum_{i=1}^{\infty}\exp\left\{-h \mid \omega \mid \left(i - \frac{\alpha+1}{2}\right)\right\}. \tag{2-47}$$

$$\overline{\sigma}(\omega) = \sigma(\omega)\sum_{i=1}^{\infty}\exp\left\{-h \mid \omega \mid \left[\left(i - \frac{1}{2}\right)\alpha - \frac{1}{2}\right]\right\}. \tag{2-48}$$

Returning from the Fourier transform to the original functions, we obtain equations (2-49) and (2-50) as follows:

$$\sigma(x) = \sum_{i=1}^{\infty}\frac{1}{\pi}\int_{-\infty}^{+\infty}\overline{\sigma}(\xi)\frac{h\left(i - \frac{\alpha+1}{2}\right)}{(x-\xi)^2 + \left[h\left(i - \frac{\alpha+1}{2}\right)\right]^2}d\xi, (\alpha < 1), \tag{2-49}$$

$$\overline{\sigma}(x)=\sum_{i=1}^{\infty}\frac{1}{\pi}\int_{-\infty}^{+\infty}\sigma(\xi)\frac{h\left[\left(i-\frac{1}{2}\right)\alpha-\frac{1}{2}\right]}{(x-\xi)^2+\left[h\left[\left(i-\frac{1}{2}\right)\alpha-\frac{1}{2}\right]\right]^2}d\xi,(\alpha>1). \tag{2-50}$$

After similar operations, we obtain for three-dimensional distributions equations (2-51) and (2-52):

$$\sigma(x,y)=\sum_{i=1}^{\infty}\frac{1}{2\pi}\int_{-\infty}^{+\infty}\int_{-\infty}^{+\infty}\overline{\sigma}(\xi,\eta)\frac{h\left(i-\frac{\alpha+1}{2}\right)d\xi d\eta}{\left\{(x-\xi)^2+(y-\eta)^2+\left[h\left(i-\frac{\alpha+1}{2}\right)\right]^2\right\}^{3/2}},(\alpha<1) \tag{2-51}$$

$$\overline{\sigma}(x,y)=\sum_{i=1}^{\infty}\frac{1}{2\pi}\int_{-\infty}^{+\infty}\int_{-\infty}^{+\infty}\sigma(\xi,\eta)\frac{h\left[\left(i-\frac{1}{2}\right)\alpha-\frac{1}{2}\right]d\xi d\eta}{\left\{(x-\xi)^2+(y-\eta)^2+\left[h\left[\left(i-\frac{1}{2}\right)\alpha-\frac{1}{2}\right]\right]^2\right\}^{3/2}},(\alpha>1). \tag{2-52}$$

It follows from equations (2-49) and (2-51) that for $\alpha<1$ the calculations of the $\sigma(x)$ by means of $\overline{\sigma}(x)$ is accomplished by means of iterative *continuation of the unknown density* function on the level $h\left[i-(\alpha-1/2)\right]$. If $\alpha>1$, the density must be determined with an exact value of the layer thickness, using the technique outlined in section (2.3.1). When they are combined, the relations developed in section (2.3.1) and section (2.3.2), between the *distorted and the exact values* of the variable thickness, include all possible cases of inaccuracies in the assigned layer thickness and layer bedding values. These relations provide *corrections* to the results by means of inversion downward continuation analysis. This is particularly valuable when the results are reviewed on the *basis of new data on the geology* of a particular region.

2.4.3 Top surface identical to observation surfaces

The importance of the determination of density changes in a horizontal layer by means of gravitational anomalies is self-evident in cases where the *top of the layer coincides with the surface* on which observations are made. As far as the mathematics is concerned, the task is to solve the integral equations resulting from equations (2-19) and (2-30), when we assume $H_1=0$.

$$V_z(x)=f\int_{-\infty}^{+\infty}\sigma(\xi)\ln\frac{(x-\xi)^2+H_2^2}{(x-\xi)^2}d\xi, \tag{2-53}$$

$$V_z(x,y) = f\int_{-\infty}^{+\infty}\int_{-\infty}^{+\infty}\sigma(\xi,\eta)\left[\frac{1}{\sqrt{(x-\xi)^2+(y-\eta)^2}} - \frac{1}{\sqrt{(x-\xi)^2+(y-\eta)^2+H_2^2}}\right]d\xi d\eta. \tag{2-54}$$

This problem is more conveniently treated through the second derivative of the attraction potential in the vertical direction. Then we obtain instead of equations (2-53) and (2-54):

$$V_{zz}(x) = 2f\int_{-\infty}^{+\infty}\sigma(\xi)\frac{H_2}{(x-\xi)^2+H_2^2}d\xi, \tag{2-55}$$

$$V_{zz}(x,y) = 2f\int_{-\infty}^{+\infty}\int_{-\infty}^{+\infty}\sigma(\xi,\eta)\frac{H_2}{\left[(x-\xi)^2+(y-\eta)^2+H_2^2\right]^{3/2}}d\xi d\eta. \tag{2-56}$$

Dividing equation (2-55) by 2πf and equation (2-56) by 4πf, and introducing the notations:

$$\begin{aligned}\frac{V_{zz}(x)}{2\pi f} &= Q(x),\\ \frac{V_{zz}(x,y)}{4\pi f} &= R(x,y).\end{aligned} \tag{2-57}$$

We obtain integral equations with Poisson kernels:

$$Q(x) = \frac{1}{\pi}\int_{-\infty}^{+\infty}\sigma(\xi)\frac{H_2}{(x-\xi)^2+H_2^2}d\xi, \tag{2-58}$$

$$R(x,y) = \frac{1}{2\pi}\int_{-\infty}^{+\infty}\int_{-\infty}^{+\infty}\sigma(\xi,\eta)\frac{H_2}{\left[(x-\xi)^2+(y-\eta)^2+H_2^2\right]^{3/2}}d\xi d\eta. \tag{2-59}$$

The integral equations (2-58) and (2-59) have been treated by Strakhov [1963]. Let us estimate the *errors in the density determination*, which result from errors in the accepted thickness value H_2 of the layer. We assume that the function $\sigma(x)$ and its Fourier transform $S(\omega)$ were determined with the exact H_2 value, whereas $\overline{\sigma}(x)$ and $\overline{S}(\omega)$ were obtained with an inaccurate $\overline{H}_2$ value, $Q(\omega)$ is the Fourier transform of $Q(x)$. Then, with convolution theorem we can rewrite equation (2-58) as:

$$Q(\omega) = S(\omega)e^{-H_2|\omega|}, Q(\omega) = \overline{S}(\omega)e^{-\overline{H}_2|\omega|}. \tag{2-60}$$

Since the right-hand sides are equal, we obtain:

$$S(\omega) = \overline{S}(\omega)e^{-|\omega|(\overline{H}_2 - H_2)}, (\overline{H_2} > H_2), \tag{2-61}$$

$$\overline{S}(\omega) = S(\omega)e^{-|\omega|(H_2 - \overline{H}_2)}, (\overline{H_2} < H_2). \tag{2-62}$$

which corresponds to the following integral equations:

$$\sigma(x) = \frac{1}{\pi}\int_{-\infty}^{+\infty} \overline{\sigma}(\xi)\frac{\Delta H}{(x-\xi)^2 + \Delta H^2}d\xi, \quad (\overline{H}_2 > H_2; \Delta H = \overline{H}_2 - H_2). \tag{2-63}$$

$$\overline{\sigma}(x) = \frac{1}{\pi}\int_{-\infty}^{+\infty} \sigma(\xi)\frac{\Delta H}{(x-\xi)^2 + \Delta H^2}d\xi, \quad (\overline{H}_2 < H_2; \Delta H = H_2 - \overline{H}_2). \tag{2-64}$$

Similar relations hold in the three-dimensional case:

$$\sigma(x,y) = \frac{1}{2\pi}\int_{-\infty}^{+\infty}\int_{-\infty}^{+\infty} \overline{\sigma}(\xi,\eta)\frac{\Delta H d\xi d\eta}{\left[(x-\xi)^2 + (y-\eta)^2 + \Delta H^2\right]^{3/2}}, \quad (\overline{H}_2 > H_2; \Delta H = \overline{H}_2 - H_2). \tag{2-65}$$

$$\overline{\sigma}(x,y) = \frac{1}{2\pi}\int_{-\infty}^{+\infty}\int_{-\infty}^{+\infty} \sigma(\xi,\eta)\frac{\Delta H d\xi d\eta}{\left[(x-\xi)^2 + (y-\eta)^2 + \Delta H^2\right]^{3/2}}, \quad (\overline{H}_2 < H_2; \Delta H = H_2 - \overline{H}_2). \tag{2-66}$$

The equations (2-65) and (2-66) describe the effect of the layer thickness errors and the respective operations to correct them.

2.4.4 Layer approximated with a surface covered with a mass

It has been mentioned in Novoselitskii [1965; 1967] that in some cases it should be convenient to replace the exact kernel of equation (2-19) by an approximation, in essence, to solve an integral equation with a Poisson kernel:

$$U(x) = \frac{1}{\pi}\int_{-\infty}^{+\infty} \overline{\sigma}(\xi)\frac{H}{(x-\xi)^2 + H^2}d\xi. \tag{2-67}$$

This is equivalent to the approximation of the attractive potential of a horizontal layer with a variable density by means of the attractive potential of mass-loaded surfaces at the

same average depth. We are interested in establishing the relationship between $\sigma(x)$ and $\overline{\sigma}(x)$.

We derive the desired relations by representing equations (2-19) and (2-67) through their Fourier transforms and through application of the convolution theorem, i.e.,

$$U(\omega) = \sigma(\omega) e^{-|\omega|H} \frac{e^{\frac{h}{2}|\omega|} - e^{-\frac{h}{2}|\omega|}}{h \mid \omega \mid}, \tag{2-68}$$

$$U(\omega) = \overline{\sigma}(\omega) e^{-|\omega|H}. \tag{2-69}$$

By equating the right-hand sides of equations (2-68) and (2-69), we obtain

$$\overline{\sigma}(\omega) = \sigma(\omega) e^{-|\omega|H} \frac{e^{\frac{h}{2}|\omega|} - e^{-\frac{h}{2}|\omega|}}{h \mid \omega \mid}, \tag{2-70}$$

$$\overline{\sigma}(\omega) e^{-\frac{h}{2}|\omega|} = \sigma(\omega) \frac{1 - e^{-h|\omega|}}{h \mid \omega \mid}. \tag{2-71}$$

From this we obtain the integral relation in which we are interested:

$$\frac{1}{\pi} \int_{-\infty}^{+\infty} \overline{\sigma}(\xi) \frac{h/2}{(x-\xi)^2 + (h/2)^2} d\xi = \frac{1}{2\pi h} \int_{-\infty}^{+\infty} \sigma(\xi) \ln \frac{(x-\xi)^2 + h^2}{(x-\xi)^2} d\xi. \tag{2-72}$$

This integral relation determines the *error due to the approximation of the attractive potential of a horizontal layer* of finite thickness by the attractive potential of a mass-loaded surface; this relation provides also a correction to the function $\overline{\sigma}(x)$ obtained from the solution of equation (2-67). If we assume that the integral transformations in the form of upward and downward continuations can be used for the $\sigma(x)$ and $\overline{\sigma}(x)$, then the left-hand side of the integral relation has the meaning of a function $\overline{\sigma}(x)$ which was continued into the upper half-plane to the height $-h/2$; then we may denote the function by $\overline{\sigma}(x, -h/2)$; thus,

$$\overline{\sigma}\left(x, -\frac{h}{2}\right) = \frac{1}{2\pi h} \int_{-\infty}^{+\infty} \sigma(\xi) \ln \frac{(x-\xi)^2 + h^2}{(x-\xi)^2} d\xi. \tag{2-73}$$

The similarity between equations (2-53) and (2-73) is obvious. Accordingly, we can write:

$$\left[h\overline{\sigma}\left(x, -\frac{h}{2}\right) \right]_z = \frac{1}{\pi} \int_{-\infty}^{+\infty} \sigma(\xi) \frac{h}{(x-\xi)^2 + h^2} d\xi. \tag{2-74}$$

$$\left[h\overline{\sigma}\left(x,y,-\frac{h}{2}\right)\right]_z = \frac{1}{2\pi}\int_{-\infty}^{+\infty}\int_{-\infty}^{+\infty}\sigma(\xi,\eta)\frac{hd\xi d\eta}{\left[(x-\xi)^2+(y-\eta)^2+h^2\right]^{3/2}} \tag{2-75}$$

In other words, when we want to determine the density in a horizontal layer without errors by approximating its attractive potential through that of a surface loaded with mass, we may use an analytic continuation iteration outlined here. Sometimes downward continuation is more difficult to apply because the *short-wavelength terms blow up below the surface of measurement*. Even where downward continuation is geologically justified, the terms retained in the Fourier analysis must be spaced widely enough so that negligible short-wavelength components at the surface do not dominate the anomaly computed at a depth.

2.5 Height error limits in Geological and/or Geophysical Interpretations

The interpretation of gravity anomalies in terms of buried mass structures of geological importance is not as straightforward as many different distributions at the depth can yield the same anomaly. This difficulty generally arises with inverse or downward continuation problems in geophysics. Thus, the skill in interpreting gravity data does not involve the ability to understand complex mathematical theory, but rather the ability to use all the available geological and geophysical data to build a coherent story. *For geophysical methods with low resolution, like gravity, automated inversion can be dangerous unless it incorporates geological constraints*. It is essential that inversion results be checked by simple and direct computations. In both *forward and inverse modeling*, it makes little sense to create or fit models to levels exceeding the accuracy of the data of to attempt to obtain detail that lies beyond the resolution of the method.

Generally, geophysics provides only *indirect clues* to the presence of economically useful deposits. For a geophysical method to be useful, therefore, the measured physical property must be able to be interpreted in terms of geology. Such interpretations is not always straight forward because different methods sample different components or rocks – that is, the physical property measured by a geophysical method may indiscriminately sample all, or only limited, constituents of a rock. Gravity is sensitive to the average density of the rocks, for example, while seismic properties are greatly influenced by the shape and abundance of the cracks and by the pore fluids, although they also depend on the major constituents of the rock.

Many geological materials are heterogeneous at all scales from sub-grain-size zoning to rock formations found in the crust of the Earth. For thin and shallow beds, the precision needed for *geophysical interpretation* can usually be obtained – that is 0.01 g/cm^3 for 10 m bed and 0.1 g/cm^3 for 1 m bed [Sleep and Fujita, 1997, p. 98]. In fact, the variation of gravity with depth obtained from bore-hole measurements sometimes must be corrected for the *gravitational attraction of surface* and *interface topographic roughness*, as well as for localized anomalous masses that lie beneath the measured

interval [Sleep and Fujita, 1997, p. 100]. The difference between the rocks at deeper depths becomes smaller which implies the accuracy at greater depth is much more than these model values.

Chapter 3

Exercise is the beste instrument in learning.
- Robert Recorde (The Whetsone of Witte (1557)).

Practice yourself, for heaven's sake in little things nd thence proceed to greater.
- Epictectus (Discourse IV.i)

The point of philosophy is to start with something so simple
As not to seem worth stating and end with something so paradoxical that no one will believe it.
-- Bertrand Russell - "The Philosophy of Logical Atomism".

3 Modeling

3.1 Philosophical Background

Scientific work is mainly concerned with the construction, refinement or redesign of models. There exist a huge variety of models, some state a mathematical relation between observables, some predict future evolutions, some are probabilistic and some deterministic while some are simple and some complex. Models can be divided into qualitative and quantitative and differ essentially in the applicability and verifiability. Models in which physical quantities play a minor role are termed qualitative models. They describe the processes of the corresponding systems with words and assign only roughly known values or intervals to the relevant physical quantities avoiding mathematical formulae [Droste, 1998]. Normally the number of these quantities is low.

Quantitative models, in contrast, specify exact mathematical relations between physical qualities. *Verification or falsification* is more objective for quantitative models than for qualitative models, since they are formalized and even large amounts of data are treatable with the help of computers. However, even for quantitative models there is no consensus about the methods for verification. It is even possible that two individuals have different opinions about the validity of a specific model. Quantitative models contain both measurable quantities as well as quantities that are inaccessible to direct measurements. The measurable quantities are usually collected as far as possible to determine the values of the *unknown quantities*. In other words, the *free parameters* of the model are estimated. Practically quantitative models are a mixture of fundamental aspects and consist of laws that describe commonly accepted principles of physics – the laws that have been tested in many variations and their wide acceptance regard them axioms in physics; prominent of which are axioms of conservation of energy, momentum and mass [Droste, 1998].

Mathematical process modeling is one of the most important tools in geophysical sciences, since it allows quantitative prediction and establishment of relations to measurements of real objects. The results of mathematical process models, however, are directly comparable to measurements, which allow rejection or acceptance of the same, depending on the comparison between *model predictions and observations*. However, these methods of comparison are far from being unified or generally accepted

themselves. Most practicing geophysicists would say that while the motivation of inversion to get quantitative estimate of the physical properties is appealing, they would prefer to use standard methods because they do not believe inversion could work well in practice. Actually the devout inverters would reply that standard methods are inversion too because they try to obtain a picture of the sub-surface [Mora, 1987]. The strength of the *inversion philosophy* is that it tries to account for the geophysical data in terms of the Earth's properties using known equations of physics. This strength, however, is also a weakness because it often leads to impractical algorithms [Mora, 1987].

In order to understand how particular data are affected by a model, we must be able to calculate theoretical data for an assumed Earth model. This constitutes the *forward problem*. It involves deriving a mathematical relationship between data and model. It is safe to say that for many geophysical problems, the forward problems are fairly well understood in that the basic constituent equations have already been recognized and most research has focused in finding the *solutions* to these basic equations [Sen and Stoffa, 1995]. Unfortunately, the real Earth is *very complex and it is the complexity or the heterogeneity* of the Earth that is of interest to geophysicists. In many cases, however, elegant analytic solutions can be obtained when some simplistic assumptions are made for the Earth model.

3.2 Model of a Dipping Dike

The *density contrasts* is the density of the model structure minus the *remaining or surrounding geological materials*, which are mostly assumed to be *homogeneous.* When one seeks to explain the gravity anomalies in terms of density variations, we speak in terms of density contrasts, which consider the gravity effects of the models. Thus, for example a sub-surface structure with density of 2.0 g/cm^3 *surrounded or enveloped* with geological materials with a density of 2.6 g/cm^3 has a *density contrasts of –0.6 g/cm^3*. Geophysicists and/or geologists prefer models consisting of a limited number of layers or local bodies, which are relatively *homogenous* and can be separated by distinct boundaries, with or without minor transition zones. In this case therefore the density or density contrasts is clearly sought for or known for the different partitions in the structure or the sub-surface.

The gravity anomaly of a complicated two-dimensional source having arbitrary surfaces and the density distribution separated by either horizontal or vertical direction can be calculated using a combination of closed form solution or numerical interpretations [Ruotoistenmaki, 1992]. Rao [1986; 1990] considered the problem of *variable density contrasts* and derived the gravity anomalies of prisms and trapezoids having second-degree polynomial density distributions in the vertical directions. Since the anomaly equations were given in closed form, it limited the source to simple geometries bounded by planar surfaces. A more general approach was undertaken in Guspi [1990] who considered gravity sources bounded by polygons and having polynomial density distributions varying with depth.

When the geological information is particularly well defined, some prisms may have their densities assigned to specific values [Braille et al., 1974]. Some authors minimize the volume of the causative body [Green, 1975; Last and Kubik, 1983] and Guillen and Menichetti [1984] invoke minimum source moment of inertia. One may expect that density to vary slowly with position or conversely vary quickly or sharply. Smoothness or roughness of density distribution, which control gradients of parameters in spatial directions, can be introduced and has been applied in magnetic inversion by Pilkington [1997].

Li and Oldenburg [1996; 1998] proposed a sub-surface model of a *dipping dike with a constant density* throughout its volume. The gravity anomaly effect was transformed to pseudo-magnetic anomaly and adopted for the location and parameter recovery of the structure in the sub-surface. Boulanger and Chouteau [2001] on the other hand adopted a similar model but introduced the rectangular parameterizations to the sub-surface structures to aid the recovery of the sub-surface structures. We adopt a *variant* of the same but introduce a *depth-dependent density contrasts factor* in the sub-surface structure. Effectively the differential density contrasts of the dipping dike-like structure with respect to height of horizontal layers are known *apriori* and test recovery of the sub-surface dipping dike utilizing constraints. This apriori information may come from different sources either experimentally from rock density measurements or result from posteriori information of a previous inverse problem fun with a different data set [Lee and Biehler, 1991].

3.2.1 Location and Parameters

Starting from gravity anomaly effects, which explain *density variations* in the sub-surface structure, our ultimate goal is to recover the structures by invoking a valid model of the sub-surface before we can proceed to a more advanced analysis. It is often convenient to fit a number of generalized geometric forms with *different dimensions* and some cases *densities* to simulate a presumed sub-surface structure. The gravity inverse problem to estimate the sub-surface of an interface separating two or more homogenous media is an ill-posed problem; sometimes-additional information, besides gravity measurements needs to be supplied by the interpreter to transform it into a well-posed problem.

The resultant gravity anomaly effect of the possible 3-D dipping dike-like structure is obtained by the computations of the independent two 2-D faces XZ and YZ. Assuming a sub-surface structure that consists of *nearly homogenous sediments* we simulate a dipping dike-like structure with its depth to top surface i.e., model Earth surface z_1 as 0.025 km, depth to the bottom z_2 is 4.050 km and regular x and y directions widths of 3.050 km. The sub-surface *causative structure* is such that XZ face has dip angle of 45°, the YZ face appears as a finite horizontal slab and the top XY face is rectangular (a regular square). Figure 3.1 shows the three faces of sub-surface dike-like structure and the parameters given above are adopted in the independent gravity anomaly effects computations.

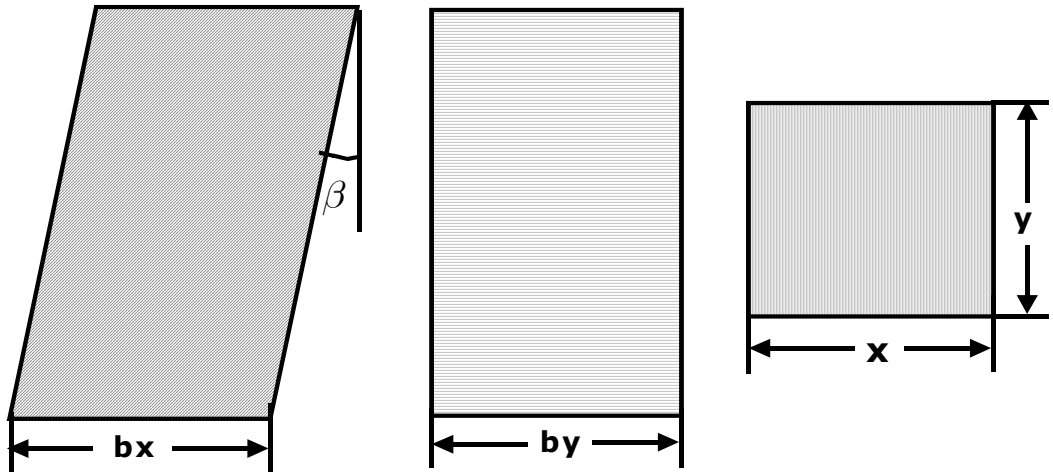

Figure 3-1: Three independent faces (XZ, YZ and XY) that constitute sub-surface dipping dike model.

3.2.2 Geological Materials

Rock densities prominently feature in the analysis of sub-surface structures and therefore before addressing the *gravity effects* it is important to consider them. The total variation in *rock densities* might be quite small relative to the other physical properties although the *density contrasts* of any sub-surface structure remarkably depend on them. The bulk density of rocks and sediments is controlled by the *densities* of the minerals present, the *amount of open space* in the rock or *sediments* and the degree to which fluids fill in these spaces.

In the interpretation of gravity anomalies, it is necessary to estimate the densities of the sub-surface rocks before one can postulate their structure. For this reason it is desirable to give some data on the densities of the *representative rocks* in regions where the gravity surveys are ordinarily made. It should be pointed out that it is not the absolute densities but the density contrasts that are significant. Table 3.1 shows the various common geologic materials that were adopted in the inversion modeling compiled from different sources. The blank spaces in Table 3.1 are due to lack of *explicit depth ranges* for the given geological materials.

Table 3-1: Densities of Common Geologic Materials

Sources: * Hirokawa [1978], + Telford et al., [1990] and ++ Burger [1992]

Geologic Materials	Density Ranges (g/cm^3)	Model Density (g/cm^3)	Depth (km)
Alluvial Deposits*	2.00 - 2.25	2.12	< 0.3
Fluvial Deposits (5Ma)*	1.95 – 2.30	2.25	< 0.4
Turbidites (Miocene)*	2.35 – 2.70	2.54	< 2.0
Sedimentary Rocks*	2.30 – 2.70	2.60	1.7 – 5.0
Igneous Rocks (Basalt)+	2.70 – 3.30	2.99	< 2.50
Metamorphic Rocks++	2.6 – 3.10	2.74	-
Igneous Rocks (Granite)+	2.50 – 2.81	2.64	-
Earth Crust*	3.27 ~	3.27	> 5.00

3.2.3 Synthetic Density Contrasts

The *variation in density contrasts with depth* can be approximated by a smooth function either quadratic or exponential by least squares fitting of the function to the observed data [Rao, 1986; Zhang et al., [2001]. Further Zhang et al. [2001] gives gravity anomalies of two-dimensional bodies with layers of variable density contrast like rectangular cylinders and inclined fault models. Following the works of Rao [1986a] and Zhang et al., [2001] we approximated the depth-dependent variable density contrasts for a sub-surface dipping dike using the common geological materials given in Table 3.1. The sub-surface depth-dependent variable density contrasts in g/cm^3 were modeled with the depth in km as:

$$\Delta\rho(z) = -0.515 + 0.109z - 0.003z^2 \qquad (3\text{-}1)$$

The *common geological materials* in Table 3.1 and the *variable density contrasts* equation (3-1) are with a few exceptions similar to those of Ateya and Takemoto [2002a; 2002b]. Table 3.2 shows the density contrasts and the differential density contrasts in the respective intermediate horizontal layers. Since equation (3-1) gives the density contrasts per a horizontal layer, the actual density of the layer is obtained additively from differential density contrasts to the *adopted or known reduction density*. The variations of the density contrasts with depth based on equation (3-1) are shown in Figure 3.2 to a sub-surface depth of 5.0 km independently while Figure 3.3 shows the combined density contrasts to depths of 5 km, 10 km and 15 km respectively.

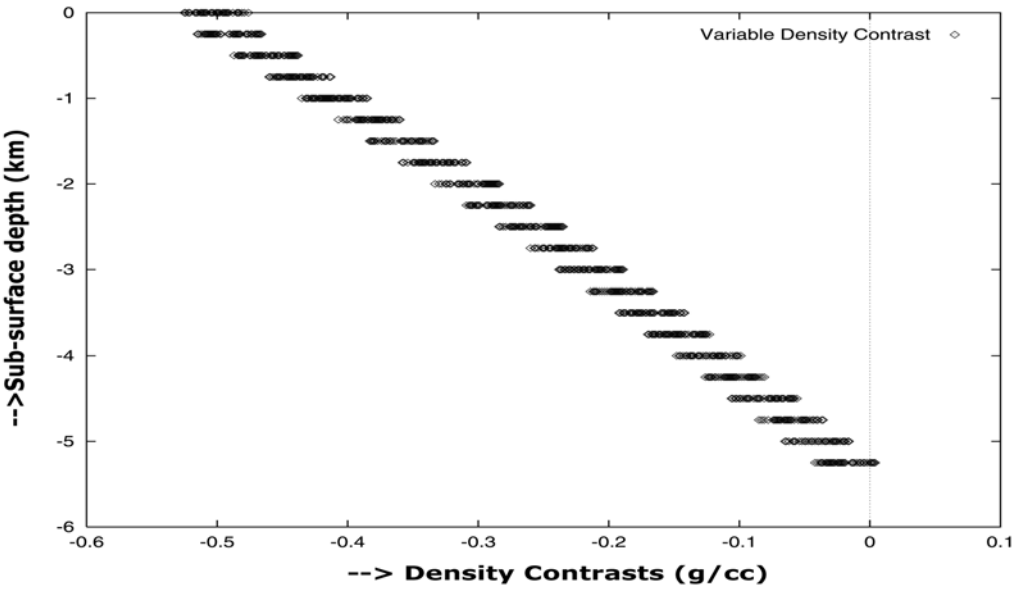

Figure 3-2: Depth-dependent variable density contrasts $\Delta\rho(z)$ to depth of 5.0 km into the sub-surface.

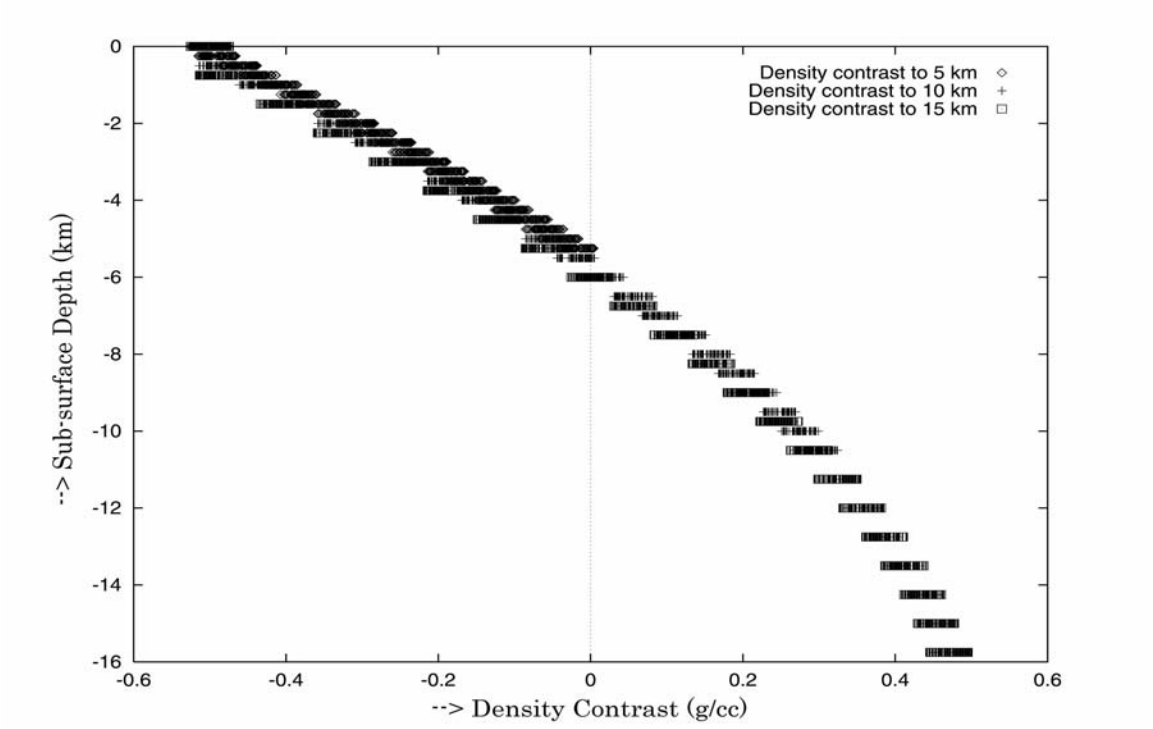

Figure 3-3: Depth-dependent variable density contrasts $\Delta\rho(z)$ for three different sub-surface depths of 5.0, 10.0 and 15.0 km respectively.

Table 3-2: Densities in a series of horizontal intermediate layers in the Dipping Dike.

Layer	Layer depth (km)	Density Contrasts (g/cm^3)	Differences in Contrasts (g/cm^3)
1	0.000	-0.525	0.000
2	0.400	-0.493	0.032
3	0.800	-0.451	0.042
4	1.200	-0.409	0.042
5	1.600	-0.368	0.041
6	2.000	-0.329	0.039
7	2.400	-0.290	0.039
8	2.800	-0.252	0.038

Most of the common geological materials used in the synthetic modeling are from Central Ranges in the Japan Alps and therefore the reduction density adopted was 2.645 g/cm^3, a value closer the average value by Yamamoto et al., [1982]. Our synthetic dike-like structure has *no outcrops* i.e., does not crop above the Earth surface and therefore the adopted surface density contrasts is $\Delta\rho(0) = -0.525$. The surface density towards Northeastern Japan is about 2.30 g/cm^3 because sedimentary and volcanic rocks and pyro-clastic flows are distributed widely over the region [Komazawa and Mishina, 2002]. The relationships between the different layers in the surface are shown by the differential density contrasts between them. Table 3.2 gives the *maximum possible values* for differential density contrasts in the horizontal layers assuming homogenous geological materials.

3.2.4 Synthetic Gravity Anomaly Effects

For simplicity we assume data interpolated onto a *regular* rectangular grid over the sub-surface dipping dike. The top surface of model is assumed to coincide with a flat Earth surface, though *dike does not outcrop*. Independently, the YZ face is modeled as sub-surface 2-D semi-finite horizontal slab with different parameters are shown in Figure 3.4 where x is the distance of an observation point P , t is the thickness of slab, β is the complement of the dip angle α while z_1 and z_2 are the depths to the top and bottom of the slab respectively. The other constants in equation (3-2) are f the gravitational constant and $\Delta\rho(z)$ the variable density contrasts. If the end of the slab is vertical

$\beta = 0$ while if the slab outcrops $z_1 = 0, z_2 = t, \theta_1 = \pi/2$ and $r_1 = x$. Thus, as the dike structure does not outcrop, the dipping dike does not have any structure's *geological materials* for z_i less z_1.

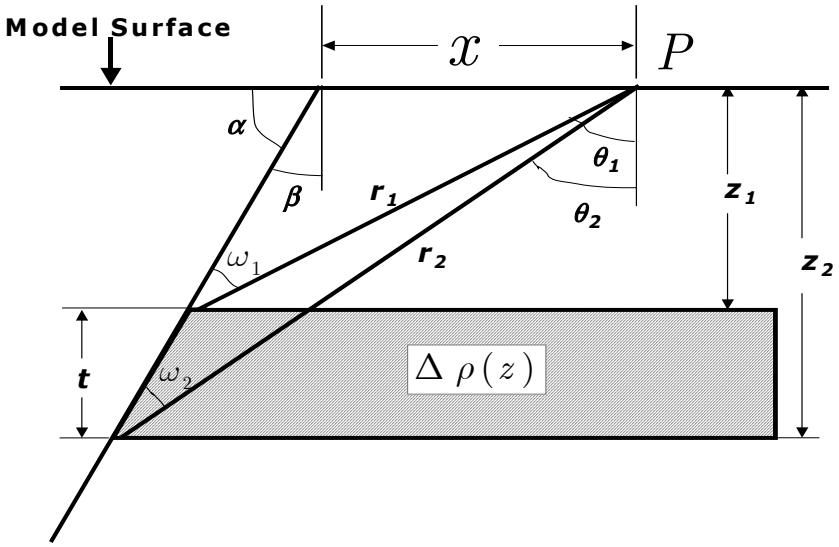

Figure 3-4: Model diagram showing the parameters and/or variables for gravity anomaly effect of a 2-D semi-infinite horizontal slab.

The gravity anomaly effect g_{obs} of a two-dimensional (2-D) semi-finite horizontal slab is given by Geldart et al., [1966] and Telford et al., [1990] (p. 43) as:

$$g_{obs} = 2f\Delta\rho(z)\begin{Bmatrix}(\pi t/2) + (z_2\theta_2 - z_1\theta_1) + x(\theta_2 - \theta_1)\sin\beta\cos\beta \\ +x\cos^2\beta\ln(r_2/r_1)\end{Bmatrix} \qquad (3\text{-}2)$$

On the other hand, the XZ face can be modeled as a sub-surface dike-like structure with its different parameters as shown in Figure 3.5. A two-dimensional dike can be obtained by the subtraction of two slabs one being displaced horizontally with respect to the other and the gravity anomaly effect g_{obs} is given by Geldart et al., [1966] and Telford et al., [1990] (p. 43) as:

$$g_{obs} = 2f\Delta\rho(z)\begin{bmatrix}z_2(\theta_2 - \theta_4) - z_1(\theta_1 - \theta_3) \\ +\sin\beta\cos\beta\left\{x(\theta_2 + \theta_3 - \theta_4 - \theta_1) + b(\theta_4 - \theta_3)\right\} \\ +\cos^2\beta\left\{x\ln(r_2r_3/r_1r_4) + b\ln(r_4/r_3)\right\}\end{bmatrix} \qquad (3\text{-}3)$$

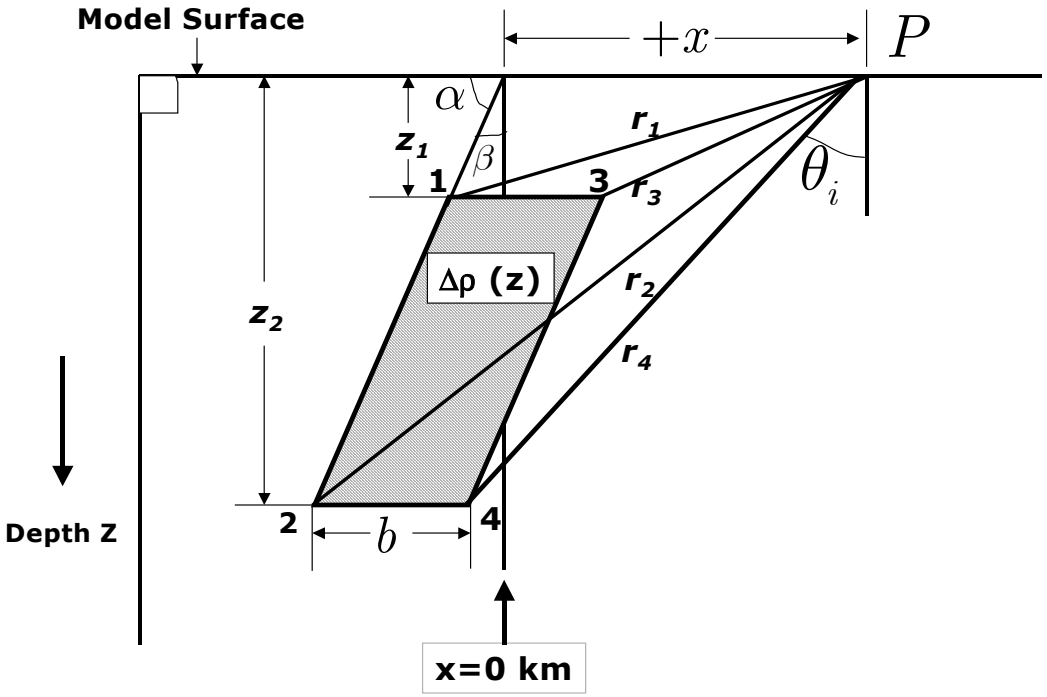

Figure 3-5: Model diagram shows the parameters and/or variables describing the gravity anomaly effect of a 2-D sub-surface dike-like structure.

The distance x is positive when the point P is to the right of central position with all angles measured in the clockwise direction β and θ_i being measured from the vertical and α from the fault plane. If the sides of the dike are vertical $\beta = 0$ while if the slab outcrops $z_1 = 0, r_1 = x, r_3 = (x - b)$ and $\theta_1 = \pi/2 = \theta_3$. In equation (3-3) f is the gravitational constant, $\Delta\rho(z)$ the density contrast and z_i is the depth in the sub-surface, x the distance to a given point on either side of the central location and inclination angle β is the complement of the dip angle α.

Ateya and Takemoto [2002a; 2002b] computed of the gravity anomaly effect for a model of sub-surface 2-D dipping dike with a *depth-dependent* variable density contrasts similar to the two-dimensional face XZ. The regular grid spacing of 0.50 km adopted in the computation of the gravity anomaly effects for both 2-D horizontal slab and 2-D dike-like structure to extend of a ± 14.00 km in x - and y -axes directions. Following the work of Ateya and Takemoto [2002a; 2002b], the independent (YZ and XZ with a dip angle $\beta = 45^\circ$) faces gravity anomaly effects were computed using equations (3-2) and (3-3). The maximum gravity anomaly effect of the two independent faces was nearly 9.50 mGals as shown in Figure 3.6.

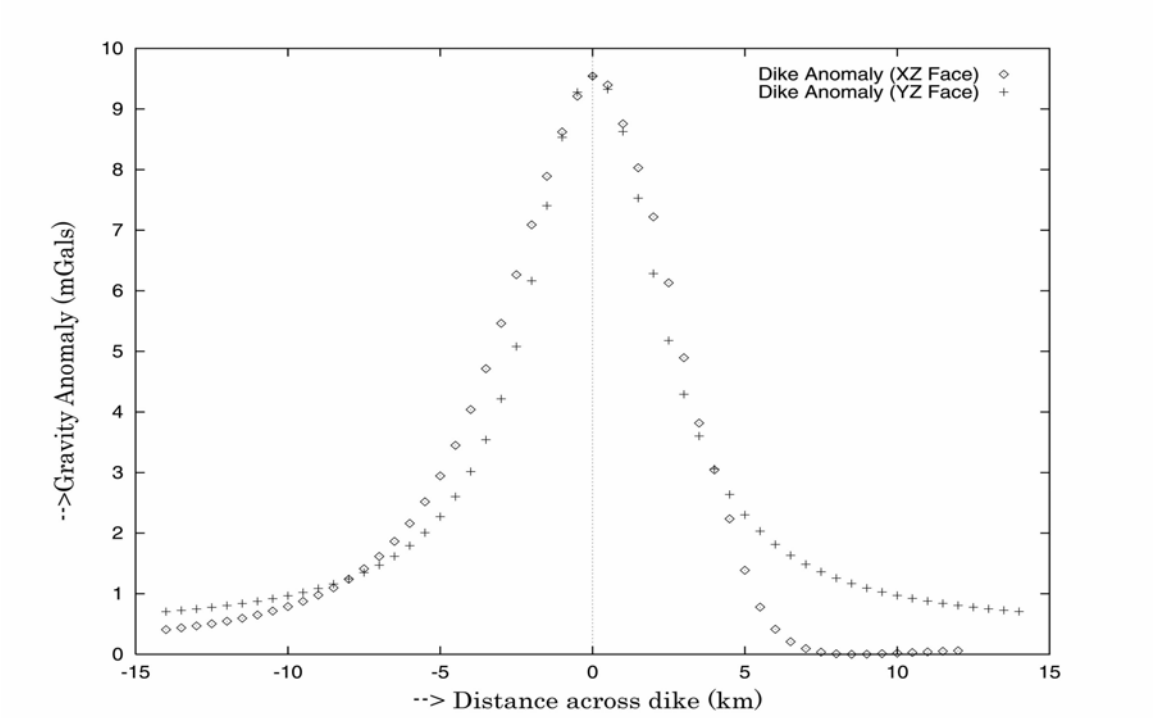

Figure 3-6: Gravity anomaly effects of the 2-D independent dike faces (XZ and YZ) with a point-to-point spacing 0.50 km.

3.2.5 Gravity Anomaly Effect for Dipping Dike

The gravity anomaly effects of the two-dimensional independent faces i.e., XZ and YZ were generated to cover the entire rectangular grid and superimposed onto each other with each co-ordinate having a gravity anomaly effect from each face interpolated directly above the grid nodes to form one system of anomaly effects. The resultant anomaly effect was then *modeled dependent* on the co-ordinate locations across the possible to have a maximum gravity anomaly effect at $(0,0)$ equal to the maximum effect of each independent face. The data was then contaminated by un-correlated Gaussian noise of maximum amplitude of 0.50 mGals. The noise vector V_n added to g_{obs} was generated as:

$$V_n = [0.5\%.\mathrm{var}(g_{obs})]^{1/2} * N(0,1) = 0.120 * N(0,1) \qquad (3\text{-}4)$$

where $N(0,1)$ denotes normally distributed random numbers with maximum amplitude of $\pm 5.\mathrm{var}(g_{obs})$ in the variance of the gravity data g_{obs}. The final gravity anomaly effect was deliberately shifted by 5.0 km eastwards and the peak anomaly maintained at 9.50 mGals to enable investigations of the *apparent shifts* in the *probable sub-surface structure*. The two-dimensional (contour interval 0.75 mGals) and three-dimensional gravity anomaly effects for the sub-surface dike are shown in Figure 3.7.

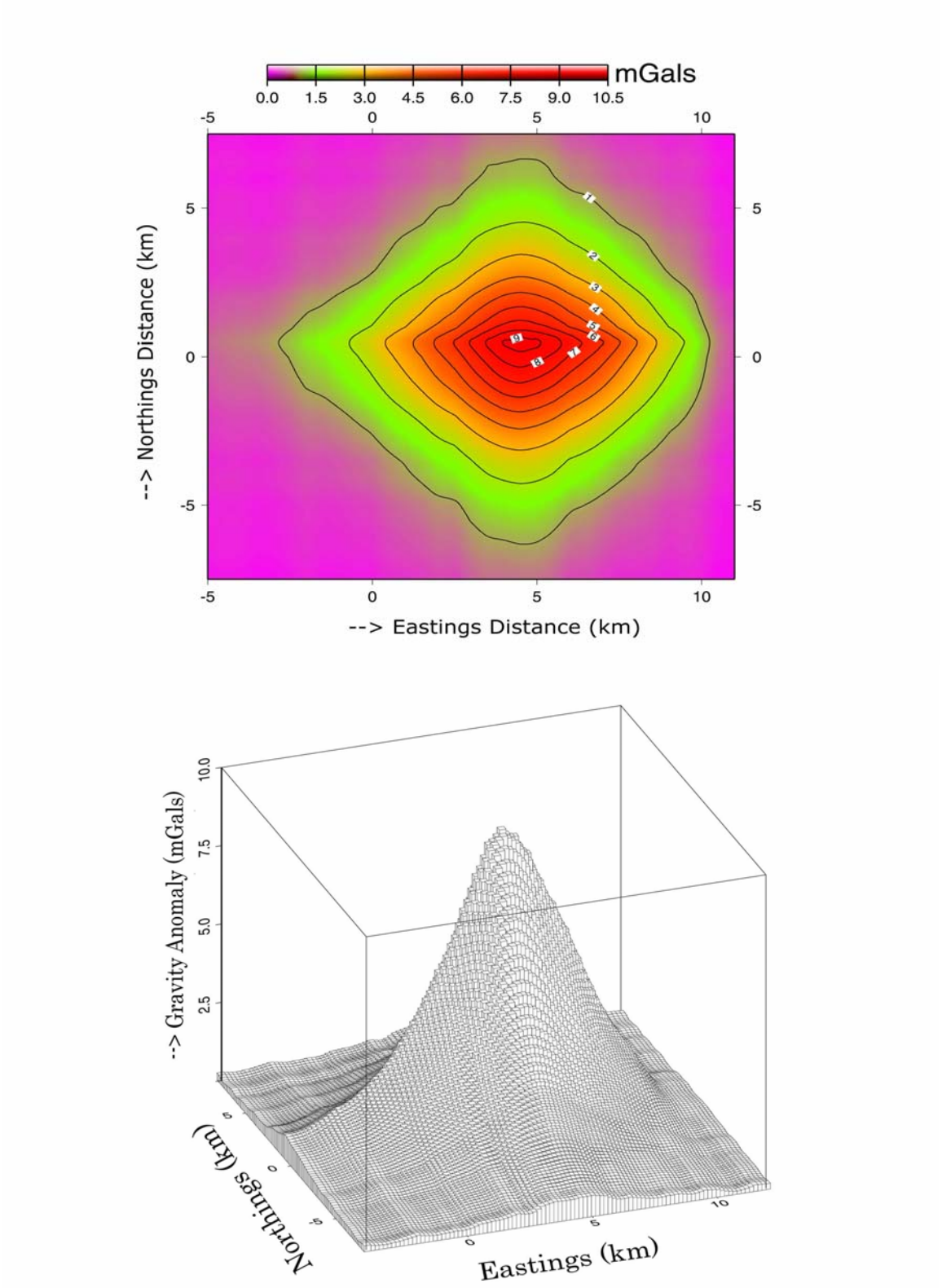

Figure 3-7: (a) Two-dimensional (contour interval of 0.75 mGals) and (b) three-dimensional resultant gravity anomaly effects of the dipping dike model displaced by 5.0 km Eastwards

3.3 Inversion Analysis

Solving an inverse problem means making inferences about physical systems from observation data. These inferences are sometimes based on the mathematical representations of the systems, which we call models. Functionals of the model represent observable properties of the system such as the *mass density* as a function of space in the Earth, the depth of continents or the radius of the core-mantle boundary [Scales and Tenorio, 2001]. Since the number of parameters can be much larger than the number of observations at the ground level, the inversion can give rise to an undetermined system of equations (*algebraic ambiguity*) [Chasseriau and Chouteau, 2003]. In addition, there are many equivalent density distributions below the surface that will reproduce the known field (*theoretical ambiguity*) because the gravity field follows the Gauss' theorem [Blakely, 1995]: the vertical component of gravity is proportional to the total mass below, so long as the mass is bounded in volume.

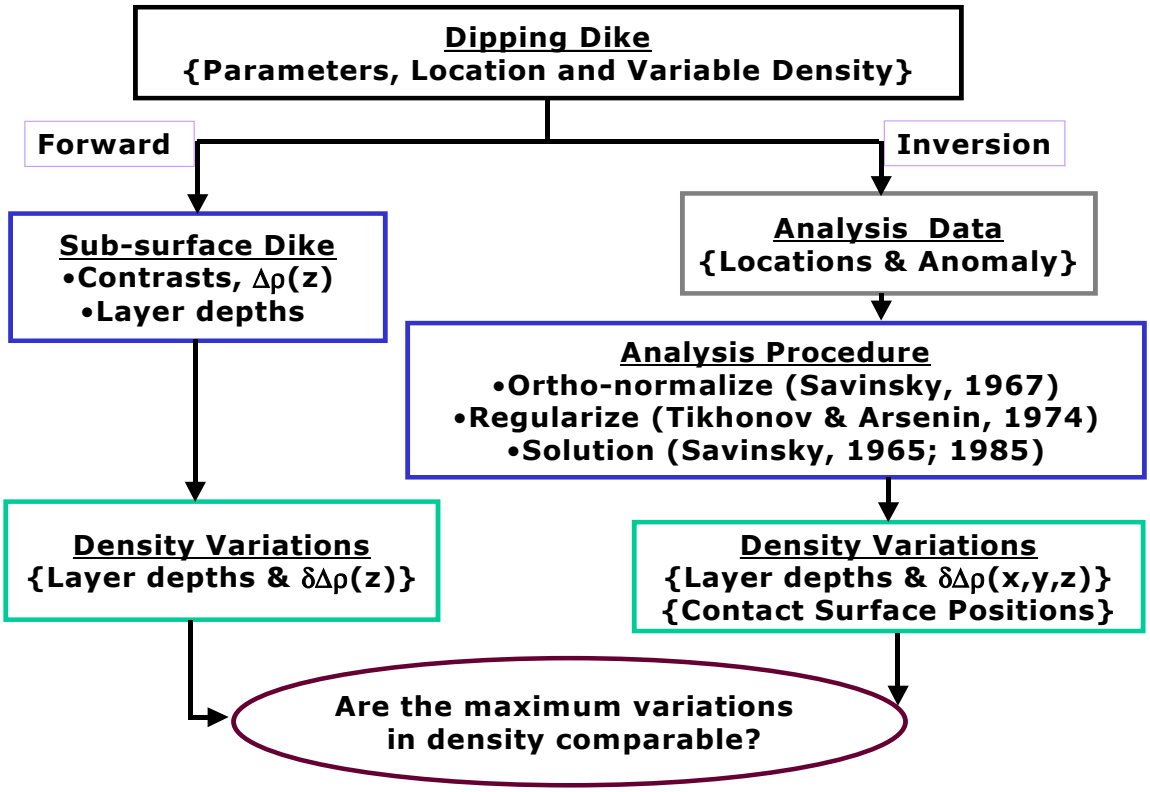

Figure 3-8: Flow diagram utilized in the quantitative determination of the horizontal layer density contrasts and position of the contact surfaces.

In our case, the goal besides the determination of the differential density contrasts in the sub-surface horizontal layers; we examine whether it is possible to determine the change in the density contrasts with respect to depth. This possible change will be determined from the apriori model, which try to recover by inversion analysis modeling.

Figure 3.8 above shows the flow diagram that adopts the sub-surface model, the procedure for determination of the disturbing masses density contrasts in a series of horizontal intermediate layers.

In formulating the inverse problems and interpreting inversion estimates, we need to address the following questions (1) how *accurately* are the data known? What does it mean to fit the data? (2) How accurately is the *physical system modeled*? Does the model include all the *physical effects* that contribute *significantly* to the data? (3) What is known about the *model* before the data are observed? What does it mean for a model to be *reasonable*? Many strategies can used to limit the number of acceptable models; they all involve some kind of *constraints* to restrict the resulting solution where *apriori* information can take several forms. It may be previously obtained from *geophysical or geological* data either on the surface or in boreholes, or it may simply be dictated by the physics of the problem [Chasseriau and Chouteau, 2003].

3.3.1 Layer density contrasts and contact surfaces positions

The *limiting (boundary) heights* of a horizontal layer with arbitrary disturbing masses $Q(x,y,h)$ has been given by equation (2-5) in Section 2.3.1 of Chapter 2 while an intermediate horizontal layer of height ΔH is diagrammatically depicted as Figure 3.9. The determined *density contrasts* for such a horizontal intermediate layer in the sub-surface have a physical meaning only at $H_0 < h < H_0 + \Delta H$ which as the *limiting heights.* The model surface has a *flat top* where all the vertical deviations from the horizontal are given as $z_j = 0.0$ depicted in Figure 3.9 and henceforth adopted in the *inversion analysis.*

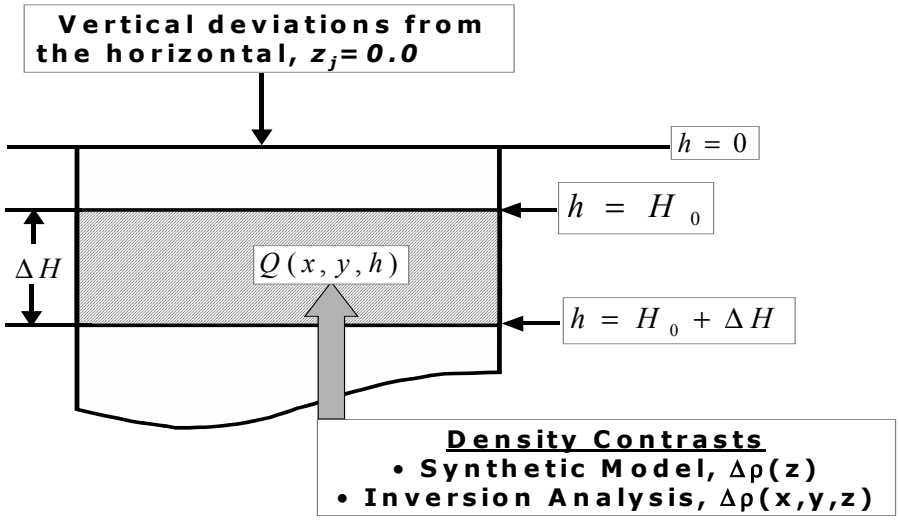

Figure 3-9: Horizontal intermediate layer for the sub-surface model with vertical deviations from the horizontal being equal to zero.

The vertical deviations in the model $z_j = 0.0$ are adopted in the inversion modeling but in actual field values they are not necessarily equal to zero. In adopting the gravity anomaly effect from Section 3.2.5, the computation of the *differential density contrasts* and *positions of the contact surfaces* in a series of horizontal layers with varying heights in the sub-surface proceeds as in the flow diagram in Figure 3.8. The forward model had *apriori* depth-dependent density contrasts as $\Delta\rho(z)$ while $\Delta\rho(x, y, z)$ are inversion analysis density contrasts. Equations (2-5) and (2-6) from Section 2.3.1 and equations (2-16) and (2-18) in Section 2.3.2 of Chapter 2 were utilized in computations of the *depth-dependent differential density contrasts* and *positions of contact surfaces* respectively. The position of contact surfaces serves two main purposes – (1) due to the direct relationship with the *maximal* differential density contrasts in the intermediate layer, checks the maximum height of contact surface which must either be *equal or less than* the height of horizontal layer height ΔH and (2) determines the actual position of the contact surfaces in the same horizontal layer.

Inversion analysis in the form of differential density contrasts and position of contact surfaces for a sub-surface horizontal layer of layer range 0.400 ~ 0.800 km is shown in Figure 3.10. The differential density contrasts for the layer range 0.400 ~ 0.800 km had a maximum value of 0.045 g/cm^3 and contact surface height of 0.400 km. *The shape and cluster of the contours gives a glimpse of the disturbing masses* in the intermediate layer. A series of horizontal layers with different heights were investigated to determine the differential density contrasts and position of contact surfaces. The summary of results for a series of horizontal layers up to a depth of 2.400 km is shown in Table 3.3. If the different horizontal layers are stack one below the other for the entire sub-surface, it *shows the shift in depth location in the sub-surface of the disturbing masses i.e., position of the dipping dike-like structure.* This effectively implies the recovery of the *actual location of the causative structure* in each horizontal intermediate layer.

The differences between the differential density contrasts from forward modeling and inversion analysis for each horizontal layer are also given in Table 3.3. It shows the extracted inversion analysis results where the heights of the *horizontal layers are kept constant at* $\Delta H = 0.400$ *km* though several different horizontal layer heights were actually investigated. The second column represents the differential density contrasts from the forward model $\Delta\rho(z)$ using a *reduction density* of 2.645 g/cm^3 given that $\Delta\rho(0) = -0.525$ while the third column represents the *maximal* differential density contrasts $\Delta\rho(x, y, z)$ in each respective horizontal layer. The differences in column 4 are a *measure of accuracy* in the recovery of the *apriori* density contrasts with the upper layers mostly able to *recover values within the limit* of a geological and/or geophysical interpretation.

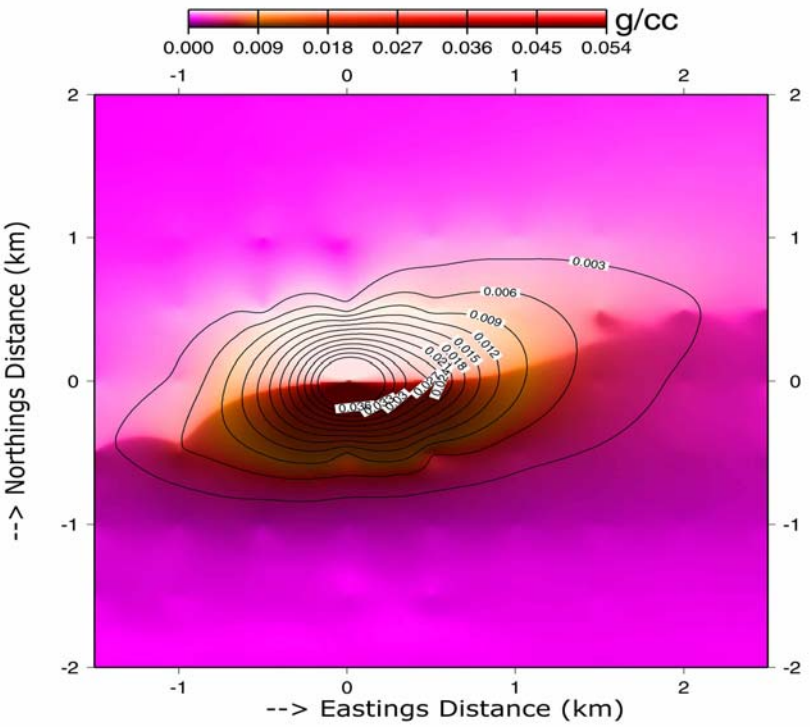
g/cc
0.000 0.009 0.018 0.027 0.036 0.045 0.054
--> Northings Distance (km)
--> Eastings Distance (km)
0.003
0.006
0.009
0.012
0.015
0.018

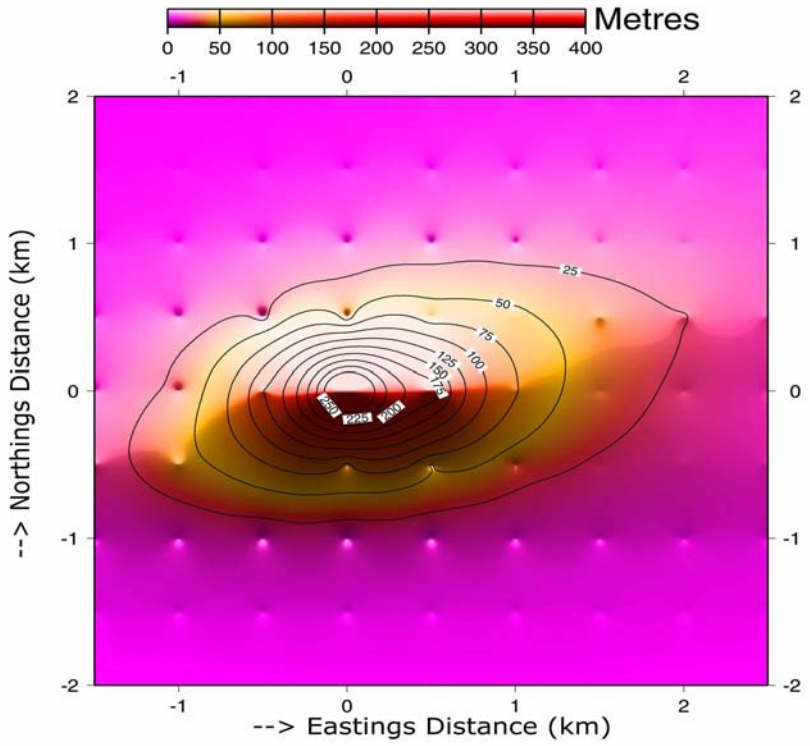
Metres
0 50 100 150 200 250 300 350 400
--> Northings Distance (km)
--> Eastings Distance (km)
25
50
75
100
125
150
175
200
225

Figure 3-10: Results for a horizontal layer of depth range 0.400 ~ 0.800 km as (a) differential density contrasts with a contour interval of 0.003 g/cm^3 and (b) position of the contact surfaces with a contour interval of 25.0 m

Table 3-3: Differences between *apriori* and inversion analysis density contrasts.

Layer Depth (km)	Forward Model Density Contrasts, $\Delta\rho(z)$ (g/cm^3)	Maximum Inversion Analysis Contrasts (g/cm^3)	Differences (g/cm^3)
0.000	0.000	0.000	0.000
0.400	0.032	0.028	0.004
0.800	0.042	0.045	-0.003
1.200	0.042	0.038	0.004
1.600	0.041	0.046	-0.005
2.000	0.039	0.054	-0.015
2.400	0.039	0.081	-0.042

3.3.2 Possible errors in determination of density contrasts and contact surfaces positions

The prevalent depth-ranges given for intermediate horizontal layers in geophysical literature for differential density contrasts or contact surface positions sometimes ignores a fundamental mathematical tenet about *rounding off*. For example Bear et al., [1995] and Nagihara and Hall [2001] determine the density contrasts of the horizontal layers, giving the depth ranges in the form 1.4 ~ 1.9 km, 2.4 ~ 2.9 km etc. The horizontal layer heights do not explicitly state to what accuracy the heights are determined and effectively blurs the idea of *errors in height measurements*. These height errors do have an effect on the *geological and/or geophysical interpretations* due to their *direct relationship with disturbing masses*. In mathematical theory, rounding off values depends on the *number decimal points* needed and therefore the values of any given layer range if not explicitly stated might imply rounding off.

In an effort to show the possible *hypothetical changes or variation ranges* in the heights of horizontal layers consider the Table 3.4 as a possible example of a horizontal intermediate layer with a height of range 1.4 ~ 1.9 km in the sub-surface or lower half-space. In Table 3.4, the *hypothetical maximum difference* in the height of the horizontal layer of depth range 1.4 ~ 1.9 km are shown as the difference between $\boldsymbol{m_2}$ for lower layer

and $\boldsymbol{m_1}$ for the upper layer i.e., 1.944 – 1.349 = 0.595 km. Similarly, the *hypothetical minimum difference* is the difference between $\boldsymbol{m_1}$ for the lower layer and $\boldsymbol{m_2}$ of the upper layer i.e., 1.849 – 1.444 = 0.405 km. In terms of differential density contrasts these *errors could significantly* affect the geological and/or geophysical interpretations since the density contrasts have a *physical meaning* only in the *explicit range* as depicted in Section 2.4 of Chapter 2. This is especially serious as density differences if the neighbouring geologic materials varies and thus difficult to *clearly delineate between them for observations obtained on the Earth surface*. Hence, it is imperative to *explicitly state the accuracy of the height measurements* for a horizontal layer

Table 3-4: Hypothetical height ranges for a sub-surface horizontal intermediate layer

	Depth (km)	**Minimum possible value, m_1 (km)**	**Maximum possible value, m_2 (km)**
H_1	1.4	1.349	1.444
H_2	1.9	1.849	1.944
$\Delta H = H_2 - H_1$	0.5	0.500	0.500

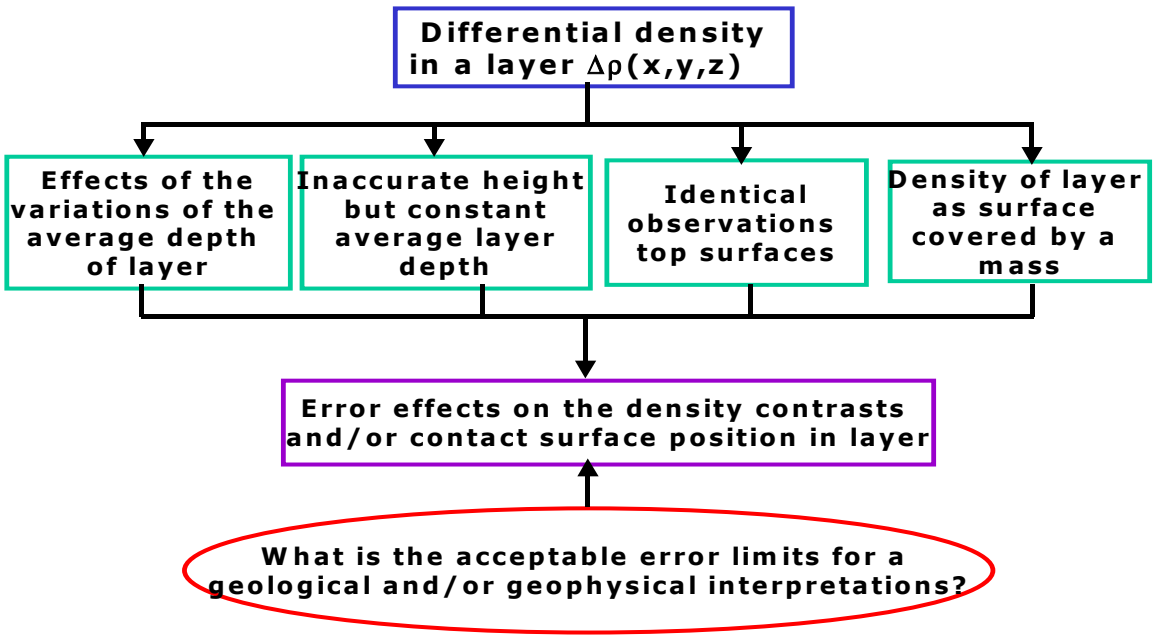

Figure 3-11: Flow diagram to show for the possible errors on heights on an intermediate horizontal layer problem.

The possible height errors effects on a sub-surface horizontal layer have been developed from a combination of *Fourier analysis techniques* and the *convolution theorem* as outlined in Section 2.4 of Chapter 2. Figure 3.11 shows the different possible kinds of errors on height or density for the disturbing masses in a horizontal layer. Each horizontal layer had a *height error* introduced and the *respective height errors effects* on the differential density contrasts and positions of contact surfaces determined. Concurrently, the *height error limits* are investigated for meaningful geological and/or geophysical interpretations in an intermediate horizontal layer. The differential density contrasts and positions of contact surfaces are computed similar to those in Section 3.3.1 using equations (2-5) and (2-6) in Section 2.3.1 and equations (2-16) and (2-18) in Section 2.3.2 of Chapter 2. In this case too the adopted gravity anomaly effect is from Section 3.2.5.

3.3.2.1 Deviations due to inaccurate average depth of horizontal layer

The position of the horizontal layer in the sub-surface could be given inaccurately without any alteration in the actual height of the horizontal layer, ΔH . The result could either be an upward or downwards shift as shown in Figure 3-12. Even though the shifts might be minimal, it is our interest to find out how *significantly they alter or affect* the determination of the disturbing masses in the horizontal layer depending on the actual thickness of layer and its location in the lower half-space. The disturbing masses are computed for a possible height error on the intermediate layer and the height error effects accordingly investigated.

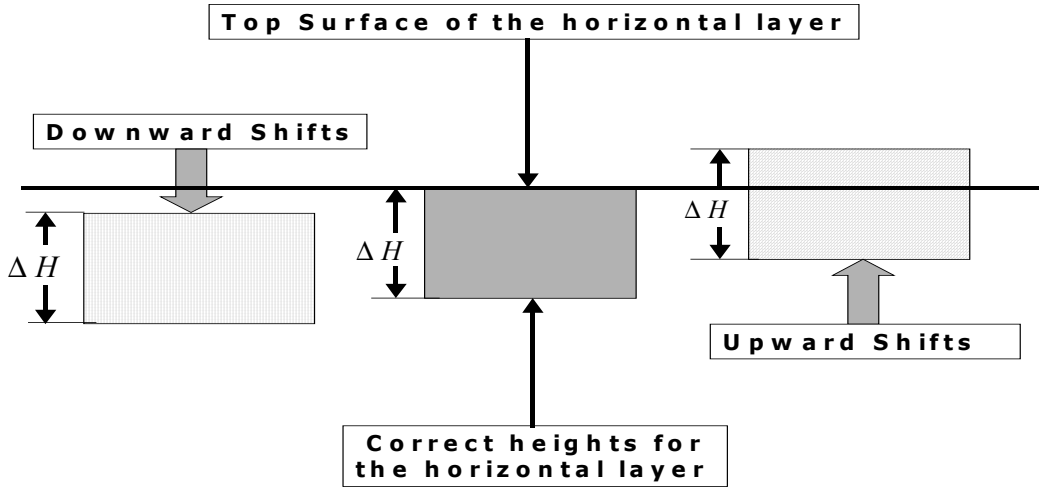

Figure 3-12: Diagram to depict the apparent shifts in a horizontal intermediate layer in a sub-surface with a height of the horizontal layer thickness, ΔH **.**

In order to investigate the error effects, a pair of specific error values was arbitrarily chosen for a known lower half-space layer given in Table 3.5. The actual shift from the correct position without the alteration of the height of horizontal layer height is shown in the central part of Figure 3-12. The table sums the actual changes in the average depth, the error in the average height of a layer and the positions of the effective layer relative to the correct layer. Two arbitrary height errors were chosen as 5.0 m and –10.0 m on a horizontal layer of height 0.750 km.

Table 3-5: Possible height errors on a horizontal layer of thickness $\Delta H = 0.750$ km.

	Correct height of horizontal layer (km)	**#1 – Inaccurate layer height (km)**	**#2 – Inaccurate layer height (km)**
H_1	0.250	0.255	0.240
H_2	1.000	1.005	0.990
$\Delta H = H_2 - H_1$	0.750	0.750	0.750
Mean H = $(H_2+H_1)/2$	0.625	0.630	0.615
Error dh in the mean H	0.000	+0.005	-0.010
Height position relationship	-	Mean H greater than correct mean value	Mean H less than correct mean value

In Section 2.4.1 of Chapter 2 the development by downward continuation of *height error effects* on the differential density contrasts and positions of the contact surfaces arising thereby have been shown wherefrom equations (2-39) and (2-40) are now utilized in the inversion analysis. The first *case* had a maximum error in differential density contrasts of 1.80 mg/cm^3 and 65.0 cm in the position of the contact surface, while the second *case* had a maximum error effects of –3.50 mg/cm^3 and -78.0 cm in the density contrasts and position of contact surface respectively. The resulting height error effects for the two possible errors on heights above are given in Figure 3.13 and Figure 3.14 respectively

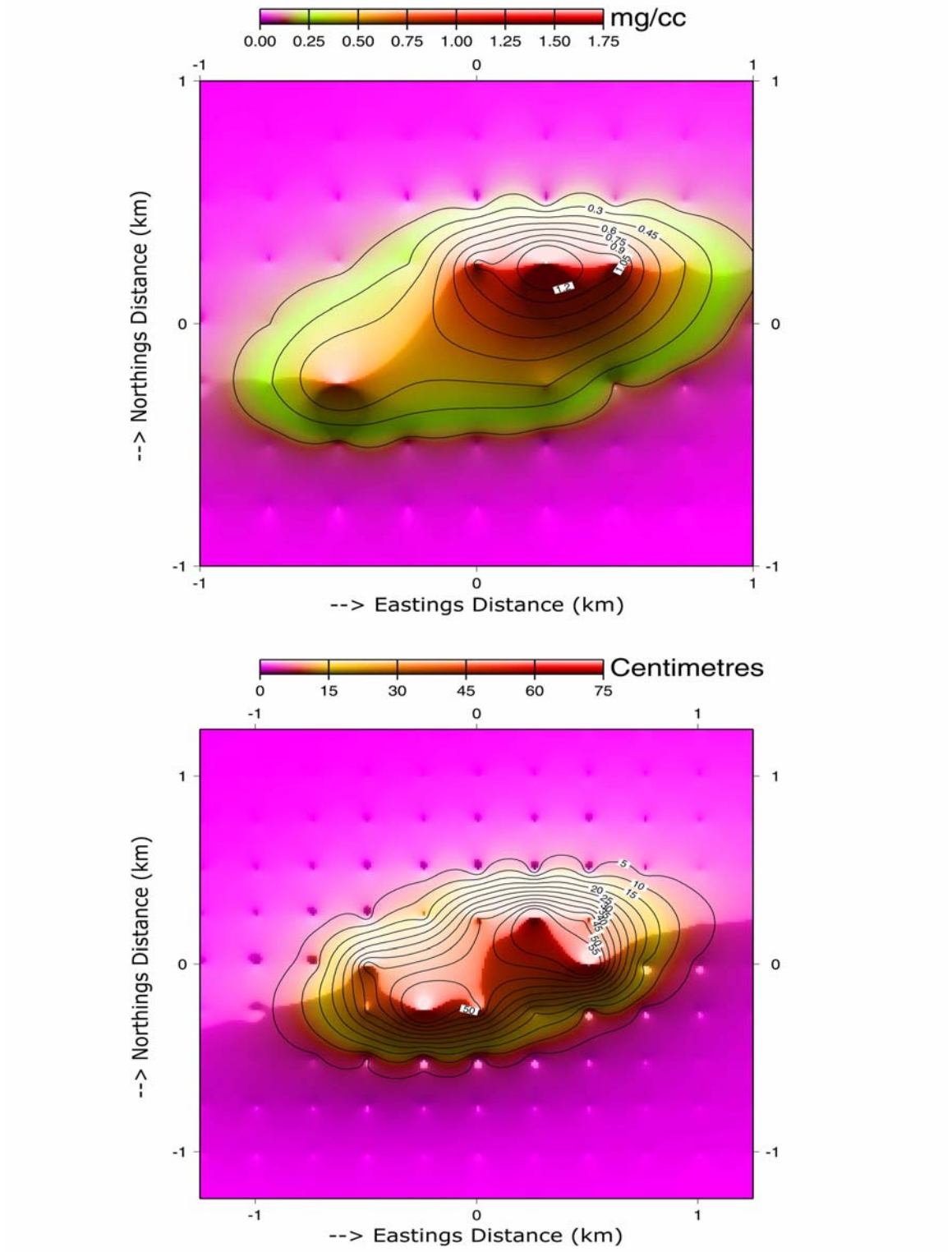

Figure 3-13: Error effects due to average height greater than correct height of layer for a range of 0.250 ~ 1.000 km as (a) differential density contrasts with a contour interval of 0.150 mg/cm^3 and (b) position of contact surfaces with a contour interval of 5.0 cm

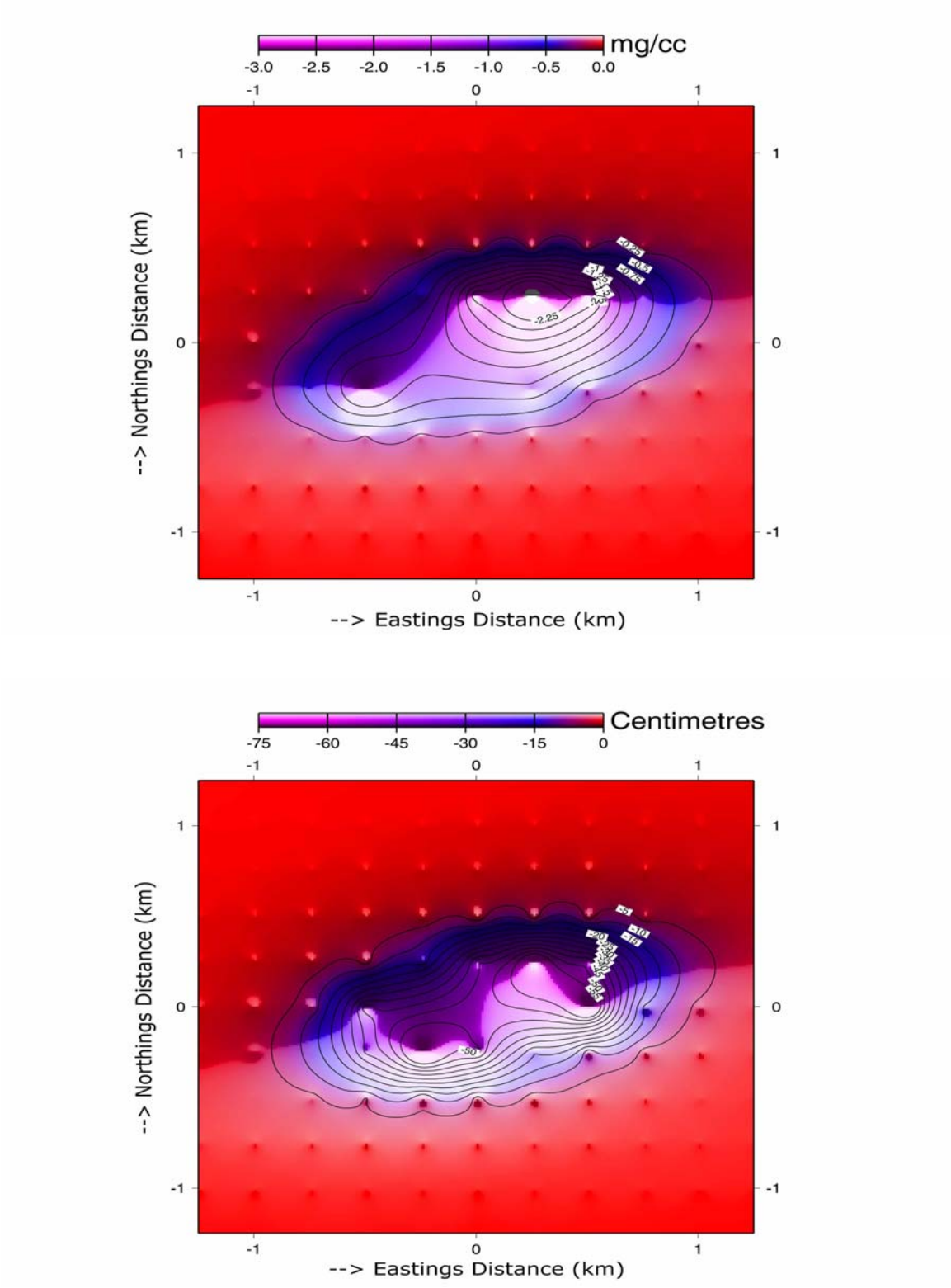

Figure 3-14: Error effects due to average height less than correct height of layer for a range of 0.250 ~ 1.000 km as (a) differential density contrasts with a contour interval of 0.250 mg/cm^3 and (b) position of contact surfaces with a contour interval of 5.0 cm

3.3.2.2 Distortions on the density contrasts due to an assigned layer thickness

The *distortion* in the assigned layer thickness is also a source of error in the resulting disturbing masses for an intermediate horizontal layer of thickness ΔH. Two possible scenarios arise where the average height of the horizontal layer though constant has either (1) the height of layer ΔH_1 being less than ΔH i.e., a compressed thickness effect of intermediate layer or (2) height of layer ΔH_2 being greater than ΔH i.e., a stretched thickness effect of intermediate layer. Both cases are diagrammatically depicted in Figure 3.15 and a possible numerical rendering on heights in Table 3.6.

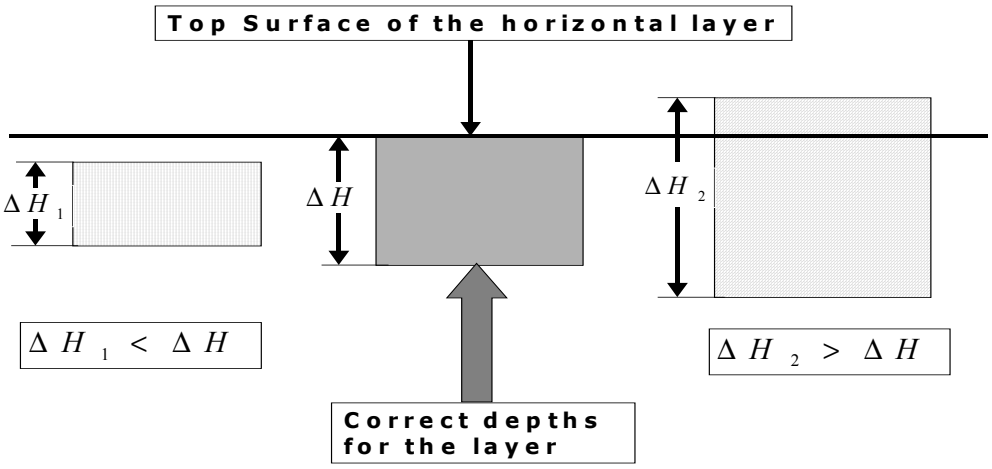

Figure 3-15: Diagram for the apparent sub-surface layer location due to errors on for an intermediate horizontal layer.

Table 3-6: Distortions due to assigned layer thickness and/or assumed density.

	Correct height of horizontal layer (km)	**#1 – Compressed layer height (km)**	**#2 – Stretched layer height km)**
H_1	0.250	0.255	0.240
H_2	1.000	0.995	1.010
$\Delta H = H_2 - H_1$	0.750	0.740	0.770
Mean H = $(H_2+H_1)/2$	0.625	0.625	0.625
Factor α = ΔH/Actual height	1.000000	0.986667	1.026667

The same possible errors on height as in Section 3.3.2.1 are applied whereby equations (2-51) and (2-52) in Section 2.4.2 show the development by downward continuation of the height errors and their effects on the disturbing masses. When the equations are adopted in the inversion analysis, the first *case* had a maximum error effect in differential density contrasts of 8.560 mg/cm^3 and 78.0 cm in the position of the contact surface, while the second *case* has a maximum error effect of 8.847 mg/cm^3 and 75.0 cm on density contrasts and the position of the contact surfaces respectively. The error effects for the two above cases are shown in Figures 3.16 and Figure 3.17 respectively.

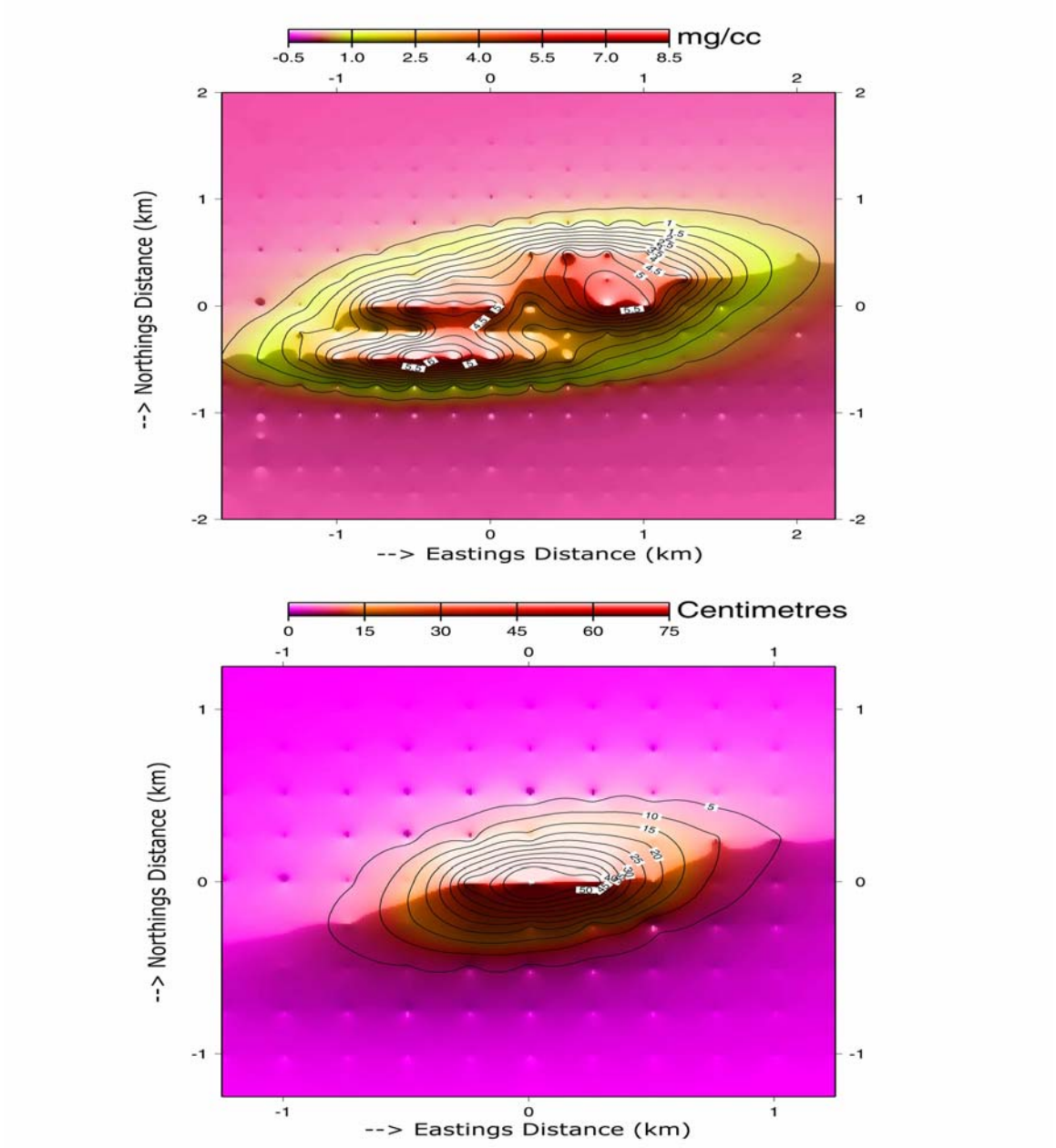

Figure 3-16: Error effects for thickness of the layer less than correct thickness for a range of 0.250 ~ 1.000 km as (a) differential density contrasts with a contour interval of 0.500 mg/cm^3 and (b) position of contact surfaces with a contour interval of 5.0 cm

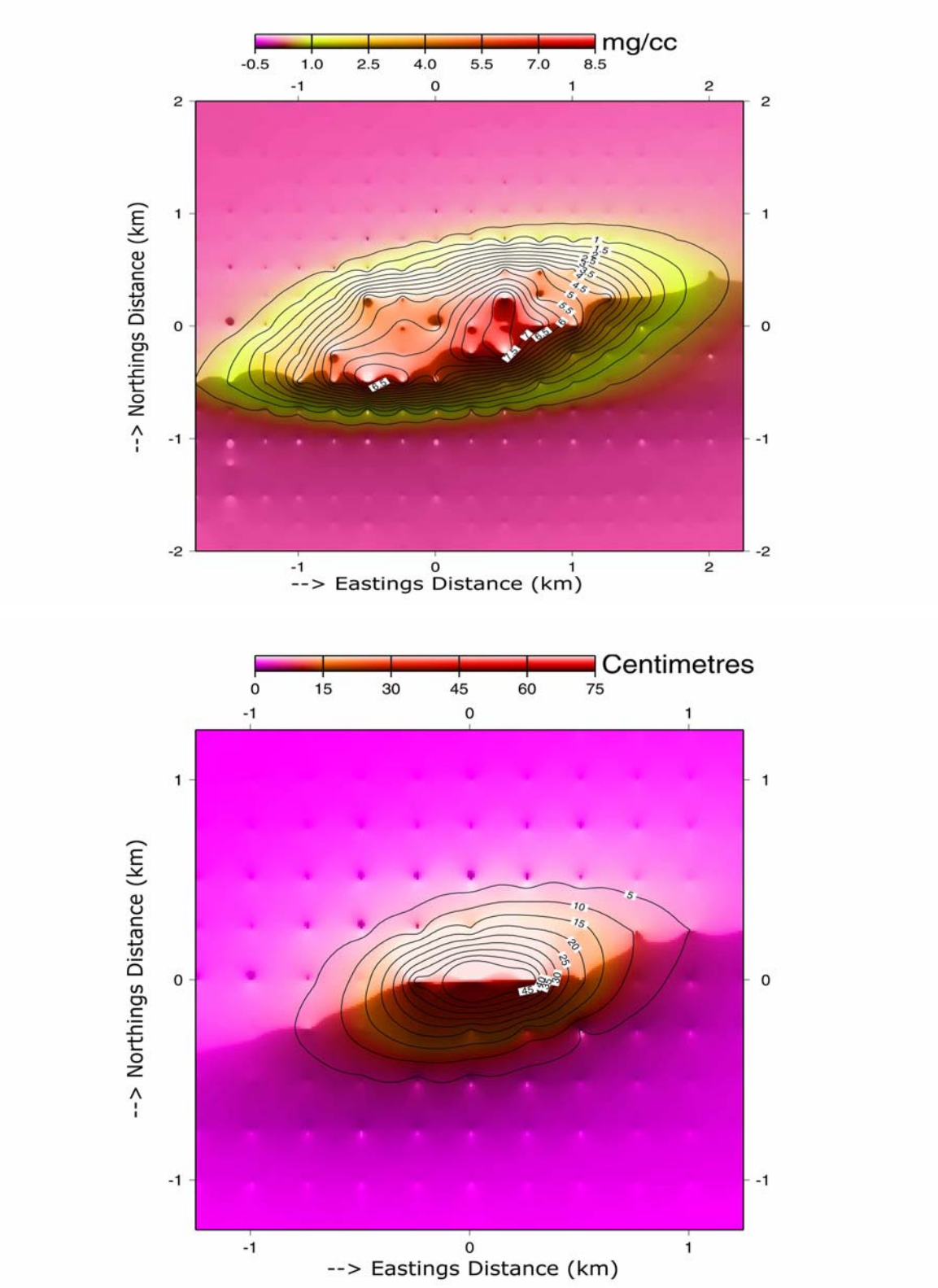

Figure 3-17: Error effects for the thickness of the layer greater than correct thickness for a range of 0.250 ~ 1.000 km as (a) differential density contrasts with a contour interval of 0.500 mg/cm^3 and (b) position of contact surfaces with a contour interval of 5.0 cm

3.3.2.3 Density changes due to top surface being identical to the observation surfaces

The assigned layer thickness can be altered with the top surface being correctly given while the bottom surface is erroneous. In this case, the bottom surface has a height error and thus an error effect on the computed density contrasts in layer. This has two possible cases too such that (1) height of the layer ΔH_2 is greater than ΔH i.e., a stretched intermediate layer effect or (2) the height of the layer ΔH_1 is less than ΔH i.e., a compressed intermediate layer effect. The height errors for two cases have the top surfaces being identical but the bottom surfaces are erroneous as shown in Figure 3.18 and the possible case values given in Table 3.7.

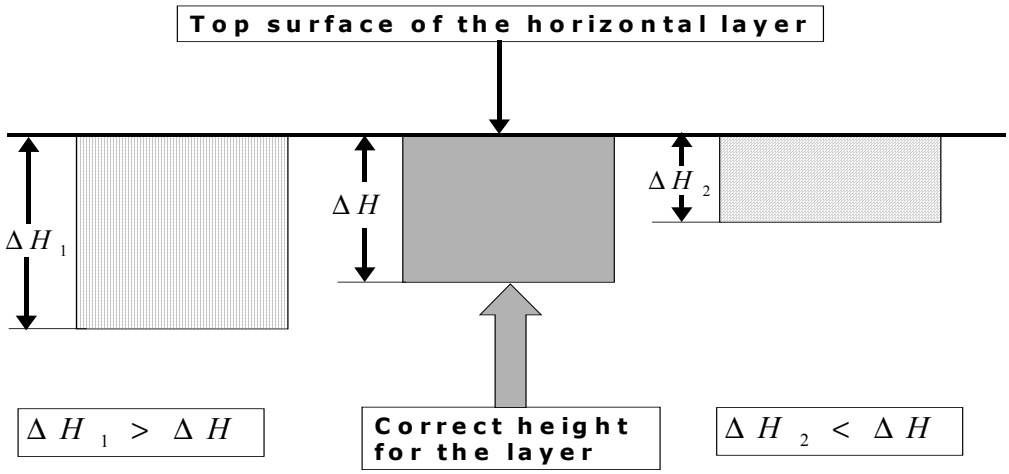

Figure 3-18: Diagram showing the thickness variations in the sub-surface due on the horizontal layer.

Table 3-7: Density changes for top surface identical to the observation surfaces.

	Correct height of horizontal layer (km)	**#1 – Stretched layer height (km)**	**#2 – Compressed layer height (km)**
H_1	0.250	0.250	0.250
H_2	1.000	1.010	0.995
$\Delta H = H_2 - H_1$	0.750	0.760	0.745
Mean H = $(H_2+H_1)/2$	0.625	0.630	0.6225
Relative Height position	-	Mean H greater than correct mean value	Mean H less than correct mean value

Two possible errors on heights cases are chosen as +10.0 m and -5.0 m on the horizontal layer height of thickness 0.750 km. Equations (2-65) and (2-66) in Section 2.4.3 shows the development by downward continuation of the *height errors* and *their effects* on the disturbing masses on an intermediate layer. When these equations are adopted in the inversion analysis, the first case has a maximum error in differential density contrasts of –7.374 mg/cm^3 and –43.0 cm in the position of the contact surface, while the second case has a maximum error of 5.530 mg/cm^3 and 75.0 cm on the density contrasts and the position of the contact surface respectively. The error effects resulting from the errors on thickness are shown in Figure 3.19 and Figure 3.20 respectively.

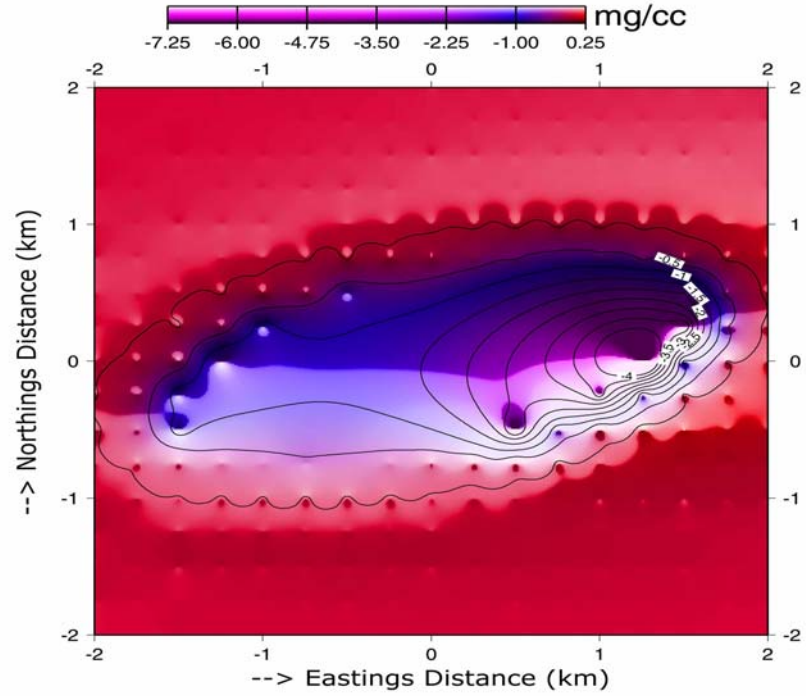

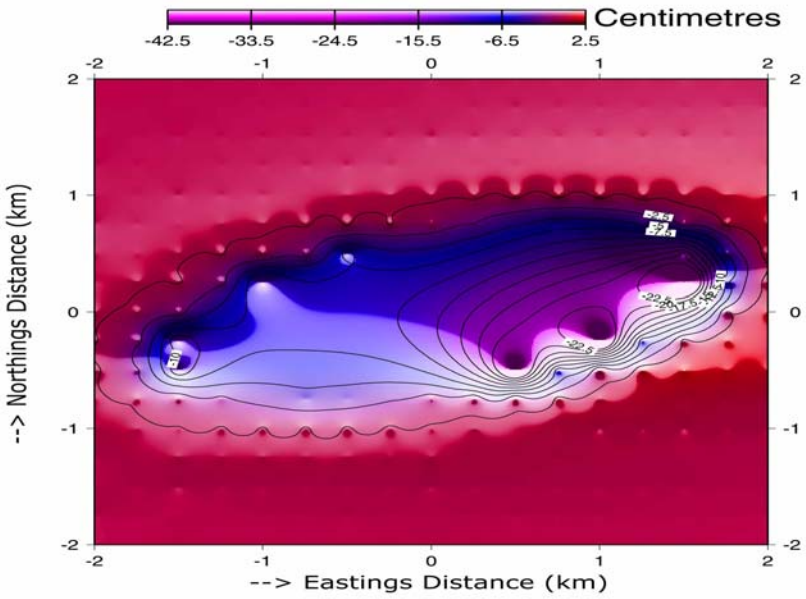

Figure 3-19: Error effects due to identical surfaces but thickness of layer greater than actual thickness for a range of 0.250 ~ 1.000 km as (a) differential density contrasts with a contour interval of 0.500 mg/cm^3 and (b) position of contact surfaces with a contour interval of 5.0 cm.

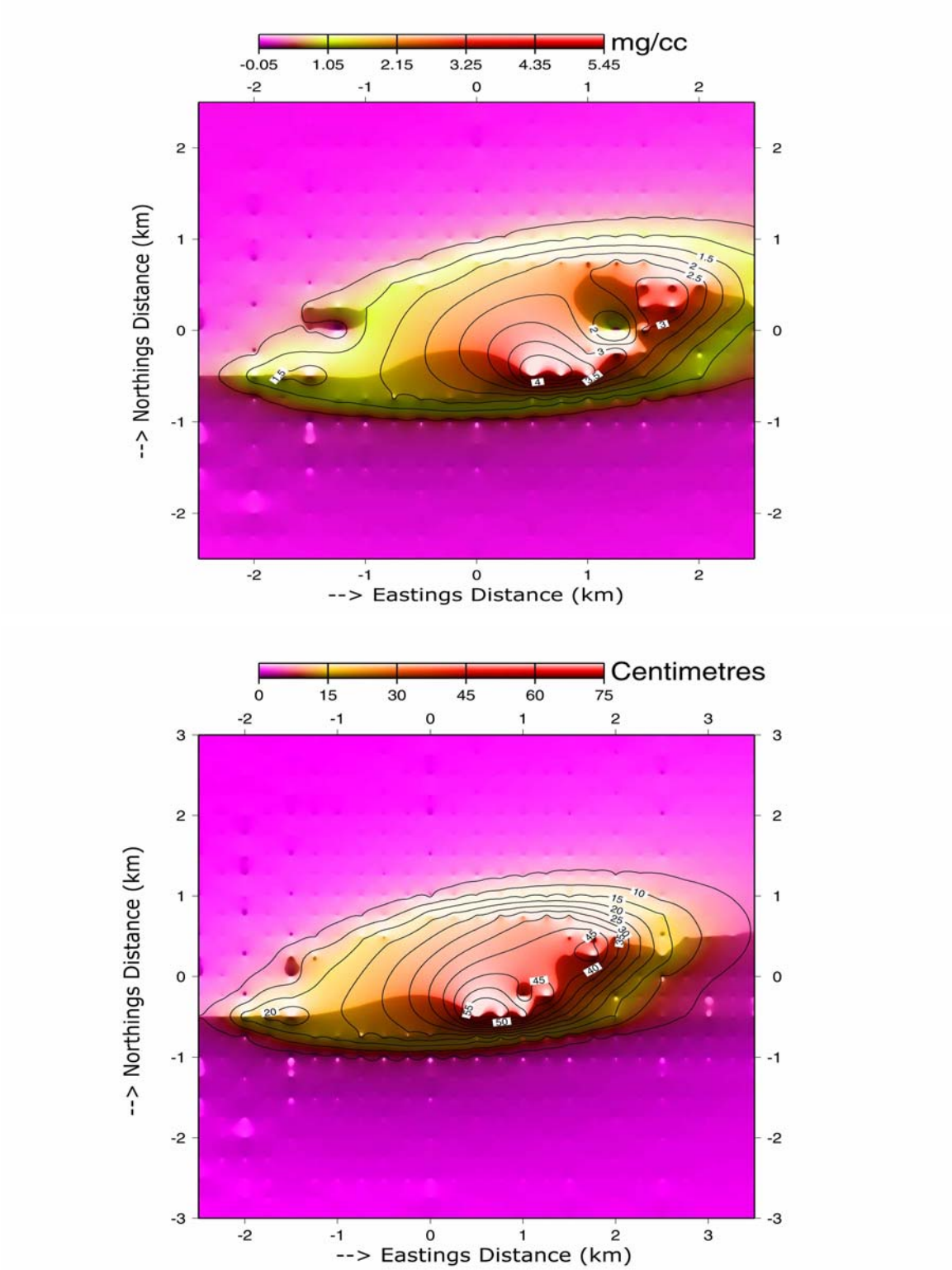

Figure 3-20: Error effects due to identical surfaces but thickness of layer less than actual thickness for a range of 0.250 ~ 1.000 km as (a) differential density contrasts with a contour interval of 0.500 mg/cm^3 and (b) position of contact surfaces with a contour interval of 2.5 cm

3.3.2.4 Deviations in density due to a surface loaded with a mass

Sometimes the density contrasts can be approximated as a surface loaded with a mass and the actual density contrasts can then be computed. It can provide for the *corrections* or *computations* of the correct values for an intermediate horizontal layer especially with new geophysical data e.g. gravity or geology data.

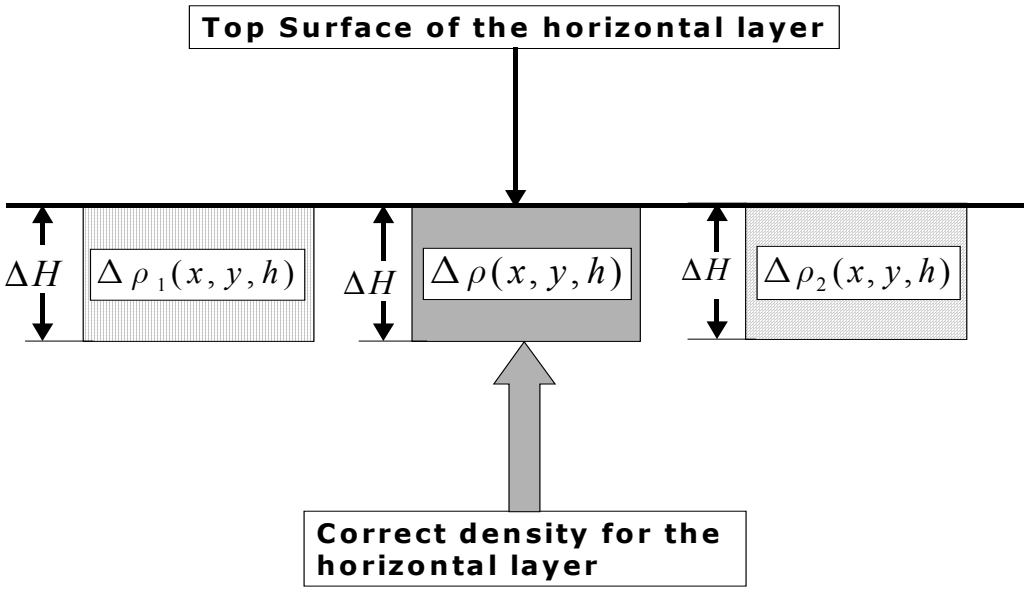

Figure 3-21: Diagram depicting the approximate density contrasts in the sub-surface besides the actual density or density contrasts in the sub-surface layer

This could is achieved by approximation of the *attractive potential of a horizontal layer* with a variable density by means of the attractive potential of a mass-loaded surface at the same average depth. The development by downward continuation of height error effects is given in Section 2.4.4 in Chapter 2 while the possible parameter changes are shown in Figure 3.21. A possible error on height of 10.0 m on the intermediate horizontal layer of thickness 0.750 km is adopted for the investigation.

From Section 2.4.4 of Chapter 2, equation (2-75) is adopted in the inversion analysis. A maximum error effect on differential density contrasts of 8.833 mg/cm^3 and 75.0 cm in the position of the contact surface were realized. The resulting error effects on

differential density contrasts and the position of the contact surfaces are shown in Figure 3.22.

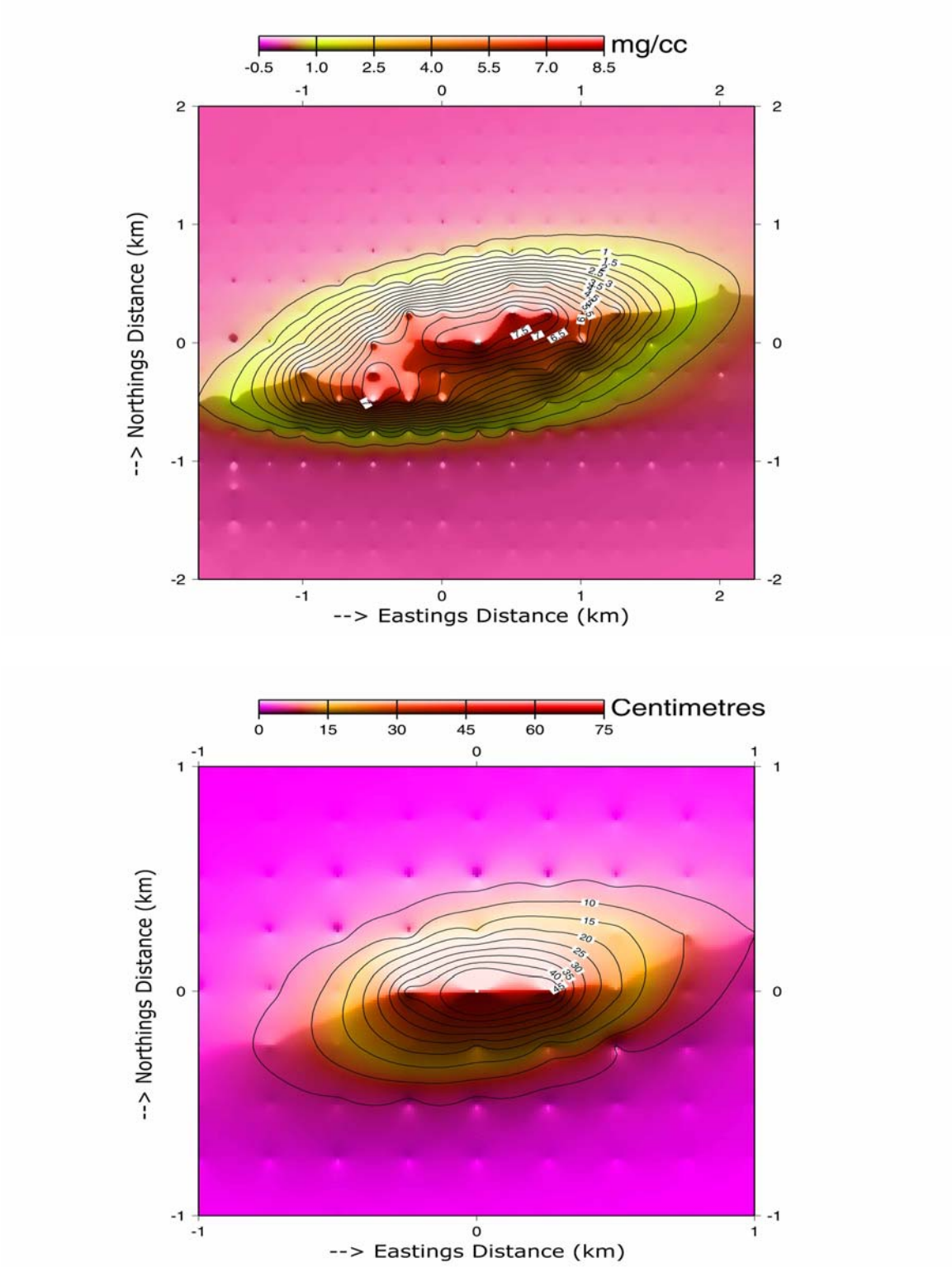

Figure 3-22: Error effects due to a surface covered with a mass for a range of 0.250 ~ 1.000 km as (a) differential density contrasts with a contour interval of 0.500 mg/cm^3 and (b) position of contact surfaces with a contour interval of 5.0 cm

3.4 Error limits for a geological and/or geophysical interpretation

In the geological and/or geophysical interpretations the height error limits for height measurements for a horizontal layer are vital. As long as the stated height limits do not exceed the accuracy of the geophysical data *measuring instruments*, it is very important to ensure the use of as accurate height measurements as possible. The height error limits are dependent on the accuracy of the differential density contrasts in the intermediate horizontal layer, which in turn depends of the rocks density at a particular depth. In the computation of the height error effects in Section 3.3 above, we similarly tested for the *height error limits*. Table 3.8 shows the height limits in errors on heights for our case synthetic dipping dike to a depth of about 1.000 km in the sub-surface.

Table 3-8: Error limits for the geological and/or geophysical interpretations.

	Effects of variations in average depth	**Inaccurate height but constant average depth**	**Identical top layer surfaces**	**Approximate density for a layer with mass**
Density contrasts (mg/cm^3)	0.50	0.50	0.50	0.50
Height error limits (cm)	5.0	2.0	2.0	2.0

The height error limits given in Table 3.8 are allowable on the height measurements for intermediate layer in the given range possible without *effective alteration* of the density contrasts and/or position of the contact surfaces. The meaningful interpretation depends on the ability to *differentiate or delineate* the densities of different rocks, which might become less distinct with increases in the depth. It is seldom, however, that the geophysicist must base his interpretation on *gravity data* alone. Using other data such as drilling logs, seismic data to reduce the ambiguity in the interpretation, narrows the range of *uncertainty*. The more the available data from other sources, the more restricted will the questions that the gravity information is called upon to answer and the more definite the answers that can be expected.

Chapter 4

The essential quality of a proof is to compel belief.
- Pierre de Fermat

-

"That which is well conceived can be expressed clearly
And the words for saying it will come easily"
- Nicolas Boileau, 1636 – 1711.

And now I see with eye severe, the very pulse of the machine.
- William Wordswork (She was a Phantom of Delight (1804)).

4 A Case Study - Chubu District, Japan

4.1 Physiography and Geology

4.1.1 Physiography

In the case study, an investigation site located in the Central Ranges of Chubu District, Japan was chosen. The Central Ranges consist of the *Hida*, *Akaishi* and *Kiso* mountain ranges and are bounded by the Itoigawa-Shizuoka Tectonic Line (ISTL) to the east and the Atera fault to the southwest across which the *regional Bouguer anomaly pattern changes sharply*. The Hida, Akaishi and Kiso mountain ranges accompany the Matsumoto basin - the northern Fossa Magna and the Kofu basin - the southern Fossa Magna) and the Ina basin on their eastern part. The Fossa Magna has a complex geologic history but it is presently a strongly folded zone forming the Matsumoto sedimentary basin northward and southward, the Fuji River Valley as a thick sedimentary trough [Huzita, 1980]. The effect of the *lateral variation of density* is difficult to evaluate. If for example, the Matsumoto sedimentary basin at relatively high altitudes of about 600 meters had a density 10% smaller than the average, the use of the value 2.64 g/cm^3 would have led to an *overestimation* of negative anomalies of this basin by an amount of 7.00 mGals [Yamamoto et al., 1982].

The Atera fault is a first-class active fault along which a narrow but very clear *Bouguer low* is observed that may be attributed to fault gouge material [Yamamoto et al., 1982]. It marks the western margin of the Fossa Magna, which is known as the greatest depression in Central Honshu. The *correlation of Bouguer anomaly* with topography is strongly negative in the Hida Mountains, marginally in the Akaishi Mountains and significantly positive in the Kiso range, suggesting that the correlations becomes progressively negative with increasing massiveness of the mountain structure. The strongly negative Bouguer anomaly can be attributed to thick late Tertiary to Quaternary sediments.

The Itoigawa-Shizuoka Tectonic Line (ISTL) - a major fault in Honshu extends from Itoigawa on the coast of Sea of Japan to Shizuoka on the Pacific Coast. In the northern ranges along ISTL, it is recognized that several faults trend from north to south. For the inversion analysis a wider encompassing region was chosen as given in Table 4.1.

The larger area provides for redundancy and enables for the regional *computation for topographic loading and terrain corrections*. The region in a regular grid given in Table 4.1 covers an area of approximately of 15.0 km by 15.0 km on the Earth's surface and it is generally flat rising at the edges to about 800 meters above Sea Level. On the other hand, the actual investigation site covers an area of 9.0 km by 9.0 km as shown in Table 4.2 wholly encompassed in the wider region in Table 4.1. The investigation site is generally flat with an incline of about 1 in 500 especially towards the edges. The elevation heights as given in Table 4.1 and Table 4.2 show the relative topography prevalent in the regions.

Table 4-1: Regional Location in the Chubu District - Japan.

	Longitude (Deg.)	**Latitude (Deg.)**	**Height above Sea Level (m)**	**Bouguer Anomaly (mGals)**
Minimum	137.830	36.265	500.378	-32.576
Maximum	138.000	36.432	704.545	-18.475
Difference	0.170	0.167	204.167	14.101
Contour Intervals	-	-	10.0	1.0

Table 4-2: Location of the Investigation Site in Chubu District – Japan.

	Longitude (Deg.)	**Latitude (Deg.)**	**Height above Sea Level (m)**	**Residual Anomaly (mGals)**
Minimum	137.875	36.320	500.342	-5.425
Maximum	137.975	36.420	702.808	8.175
Difference	0.100	0.100	202.466	13.600
Contour Intervals	-	-	10.0	0.5

4.1.2 Geological and Tectonic Setting

Modern inversion techniques presume that geophysical data are *inaccurate* i.e., they have both measurement errors and noise; *incomplete* i.e., the relevant physical properties cannot be completely determined and yet *redundant* (and thus probably

inconsistent). Without redundancy, error estimates cannot be quantified and the separations of the signal become more difficult, if not impossible. In its broadest sense, noise is any information that obscures the *signal* i.e., the information that is useful for interpretation. Isolation of the signal is easiest when the data are redundant and experiments have been designed with this goal in mind. Geological application of geophysical results requires consideration of the target, that the technique is actually measuring and which results are conclusive and which strongly depends on interpretation, that is, the *limitations*.

Gravity is sensitive to the *average density* of the rocks while seismic properties are greatly influenced by the shape and abundance of the cracks and by pore fluids, although they also depend on the major constituents of the rock. In Nagano and the Matsumoto basins, *alluvial* and *diluvial* deposits are spread widely with the *Tertiary sedimentary rocks* are partly exposed in certain locations. The geological features naturally give rise to a *fairly large contrasts* or *rock density* between formations of the pre-Neogene and those of the Neogene and the Quaternary. Itoigawa-Shizuoka Tectonic Line (ISTL) is a geological boundary between the Pre-Tertiary unit to the west and the Neogene units to the East. The Pre-Tertiary basement deepens to the East. The northern segment of ISTL is an active thrust. The recurrence time of the Earthquake faulting is estimated as less than 1000 years from the trenching of the active segment in Matsumoto [Okumura et al., 1994].

Table 4-3: Densities of Rock Types in the Chubu District, Japan.

Sources: ***** Hirokawa [1978], $^{+}$ Telford, et al. [1990] and $^{++}$ Burger [1992]

Geological Materials	Density Ranges (g/cm^3)	Average Density (g/cm^3)	Rock Depths (km)
Alluvial Deposits*	2.00 - 2.25	2.12	< 0.30
Fluvial Deposits (5Ma)*	1.95 – 2.30	2.25	< 0.40
Turbidites (Miocene)*	2.35 – 2.70	2.54	< 2.00
Sedimentary Rocks* (Paleo-Mesozoic)	2.30 – 2.70	2.60	1.70 - 5.00
Igneous Rocks (Basalt)$^{+}$	2.70 – 3.30	2.99	< 2.50
Metamorphic Rocks^{++}	2.60 – 3.10	2.74	-
Igneous Rocks (Granite)$^{+}$	2.50 – 2.81	2.64	-
Earth Crust*	3.27 ~	3.27	> 5.00

Rock densities of the pre-Neogene are generally larger than those of the Neogene and the Quaternary formations and so high gravity anomalies of short wavelengths are coincident to pre-Neogene formations whereas low gravity anomalies to that of the Neogene and the Quaternary formations [Hagiwara, 1967]. The basins have combination of a wide variety of geological materials namely: - (1) quaternary sediments (2) tertiary sediments, (3) basal sediments (4) igneous rocks and/or metamorphic rocks, and (4) metamorphic rocks with ultra-basic rocks besides shallowly lying fluvial and alluvial deposits. Paleozoic and Mesozoic rocks are mainly distributed west of Itoigawa-Shizuoka Tectonic Line (ISTL). They are characterized by a strongly *negative Bouguer anomaly* that can be *attributed to the thick Tertiary to Quaternary sediments*. The anomaly reaches the maximum in the western periphery of each basin using an average Bouguer reduction density of 2.64 g/cm^3 [Yamamoto et al., 1982]. Table 4.3 shows the common *geological materials* prevalent in the Central Ranges of Japan with the blank spaces are being to lack of the *explicit depth ranges* for the respective geological materials.

4.2 Data types adopted in the Modeling

4.2.1 Regional Topography

Geographical Survey Institute (GSI) situated in Tsukuba City, Ibaraki Prefecture – Japan prepared the Digital Terrain Elevation Data (DTED) for entire Japanese Islands. It is a raster source topographic database with a grid spacing of 1.5 by 2.5-arc seconds and translates to approximately 50 m by 50 m between the abutting points. The Geodetic Reference System used with an the Tokyo datum based on Bessel (1841) ellipsoid and origin at latitude 36° North and longitude 136° East on a polyconic projection. For any Digital Elevation Model (DEM) e.g., DTED, the differences in topographic detail depend on the size and positions of the details. Small artificial mounds and depressions may be present in localized areas, particularly where steep topography is adjacent to relatively low areas and hypsography was sparse. The locations of points in region are such that a larger area is possible as the topographic heights are for the centre of the grid and not the nodal locations.

Regular grid topographical data are well known to offer advantageous characteristics especially for the *distant* and *intermediate zones surrounding* the gravity stations. The situation is clearly dependent on the ruggedness of the topography and the accuracy specifications for the terrain effects [Blais and Ferland, 1984]. Terrain corrections for gravimetric measurements require topographical data of appropriate *accuracy and density*. The results rely strongly on the DEM's and their accuracy depends most strongly on how well the DEM represents the *terrain in the vicinity of the gravity station* as well as how accurately the location of the gravity station is known. However when relief is great, corrections calculated for the innermost terrain can still be inaccurate even though the interpolated and actual station elevations are often due to errors in the gravity station location rather than to inaccuracies in the DEM.

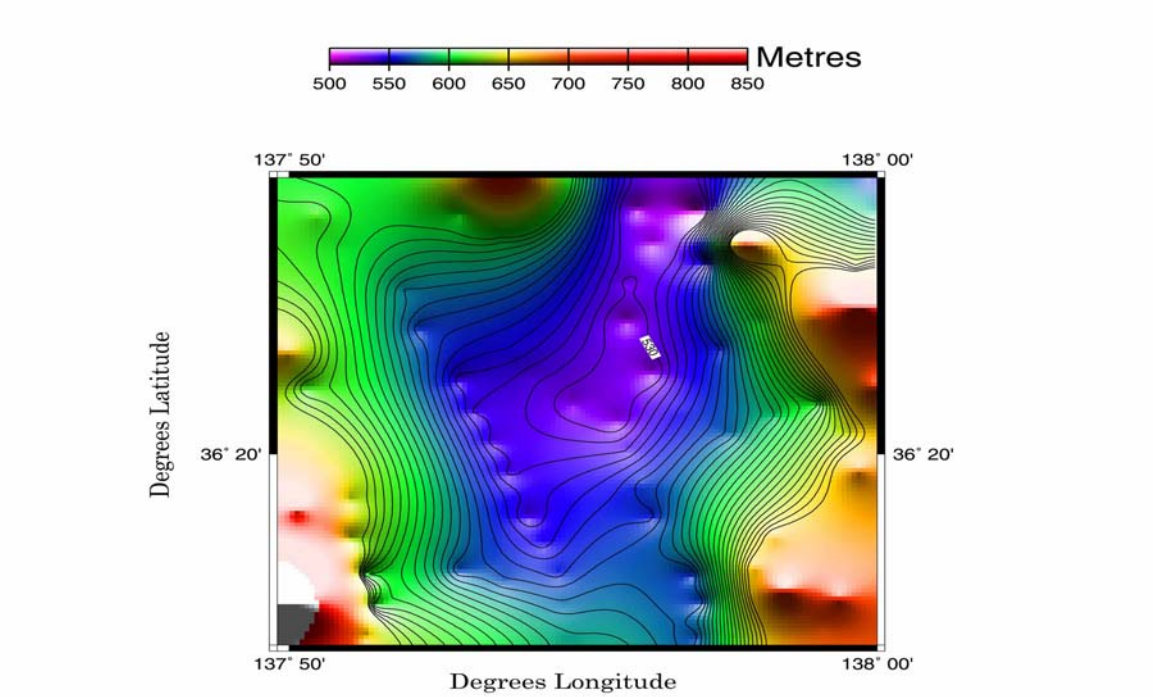

Figure 4-1: Regional topography of Case Study Region in Chubu District with contour interval of 10.0 m.

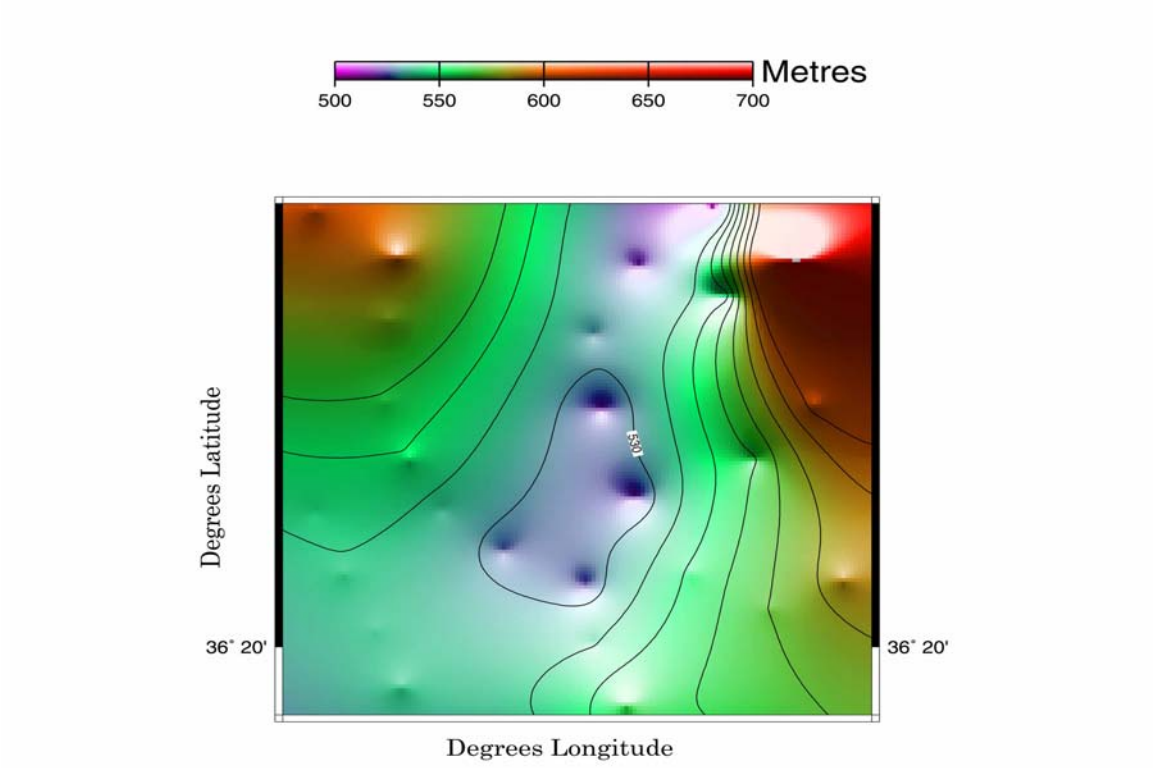

Figure 4-2: Topography of structural investigation site in Chubu District with a contour interval of 10.0 m.

4.2.2 Gravity Data

The gravity method being a part of applied geophysics has shown numerous advances in the data acquisition, processing and interpretation techniques to meet certain often-changing demands. In particular, improvements in gravity acquisition systems, aided by rapid computer technology, leads to the detection of *weak signal gravity anomalies* that are in the *range of few micro-gals*. This highly precise gravity data enables the detection of the sub-surface mass distributions, whose existence was not observable in the past. But, on the other hand, does demand high precision data processing and interpretation techniques. In practical work, it is not only the *perturbation forces* that make the measurement(s) and analysis of geophysical data complicated but also the precision of the *data acquisition*, *processing and interpretation*.

The gravity data used was mainly from a Geological Survey of Japan (GSJ) CD ROM released on 24th March 2000 and compiled from gravity data measurements of 347,979 points on land and 691,766 points in the Ocean. Many institutions in Japan – both academic and private involved in the gravity, mining and geological explorations contributed the data. The absolute gravity data is based on the Japan Gravity Standardization Net 1975 (JGSN1975) which is referred to as the International Gravity Standardization Net 1971 (IGSN1971), while the normal gravity has been calculated according to the Geodetic Reference System 1980 (GRS1980).

Corrections for *terrain effects* are required for virtually all gravity measurements acquired in *mountainous areas*, as well for high-precision surveys, even in *areas of low relief*. An indicator of the reliability of the corrections is the difference between the *actual* and *interpolated* elevations of the gravity station where such differences are large the calculated correction is suspect. However, when relief is great, corrections calculated for the innermost terrain can still be inaccurate even though the interpolated and actual station elevations are often due to errors in the gravity station location rather than to inaccuracies in the DEM.

4.2.2.1 Bouguer Anomaly

Gravity anomaly can be generally divided into two parts; one is characterized by the *broad spatial variations* reflecting the deep geological structure, which is supposed to reach the upper mantle of the Earth, and the other is due to the *crustal geological features* [Hagiwara, 1967]. A good analysis should be able to distinguish these two types of anomaly so that they can be examined one by one in relation to the topographical undulations and geological features [Hagiwara, 1967]. The *complete Bouguer anomaly reflects* the *lateral variation of density* at depth and therefore the density chosen for the final Bouguer reduction is the one that probably produces the gravity profiles that illustrates the least correlations with topography [Burger, 1992]. The Bouguer reduction density is an *important factor* in the *determination of the sub-surface structures* and the size of the area affects which reduction density value is adopted.

The choice of final reduction density is to minimize the correlation of the gravity with topography because the search for gravity anomalies arises from these sub-surface density variations. Of course, sampling rocks and sediments and determining densities in the laboratory determine the best reduction values. In most cases however surveys cover so large an area that such sampling is not practical or exposures are not sufficiently numerous to permit reliable and representative samples to be gathered.

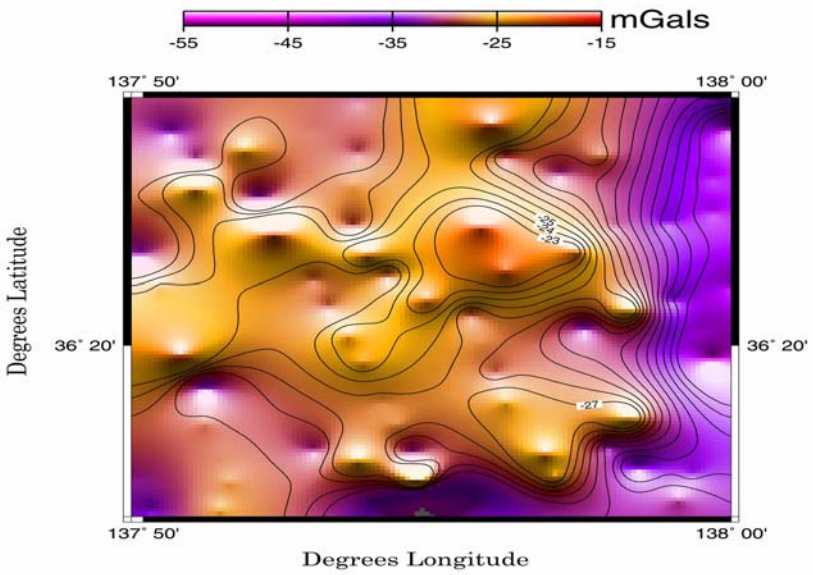

Figure 4-3: Complete Bouguer anomaly for the Case Study area with a contour interval of 1.0 mGals.

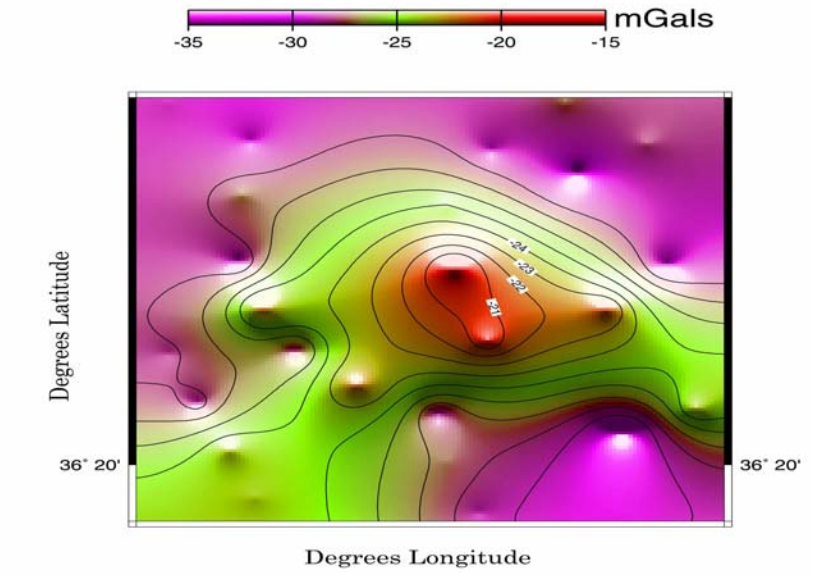

Figure 4-4: Complete Bouguer anomaly of the structural investigation site with a contour interval of 1.0 mGals.

Many gravity surveys select a density of 2.67 g/cm^3 for the Bouguer reduction, an important factor in the determination of the sub-surface structures and the size of the area affects which reduction density value is adopted. This enables the values to be combined with other surveys for production of regional maps but may not be suitable for some purposes. A technique after works by Nozaki [1981] that utilizes the DTED provided by GSI was used in the computations of the terrain corrections.

In the computations, the *complete Bouguer anomaly* was calculated using a topographic or reduction density of 2.64 g/cm^3 and the *terrain corrections* were applied to a distance of about 25 km around the gravity station. The adopted average topographic density was 2.64 g/cm^3 after works by Yamamoto et al., [1982]. The value was obtained using a newly proposed least squares method that incorporates the topography that covers an extensive area of 40,000 km^2 with elevation heights ranging from 0 to 3000 m for which the Earth's sphericity may not be ignored [Hagiwara, 1975].

4.2.2.2 Residual Anomaly

It has long been recognized that the largest regional gravity response comes from the gravity effects of both topography and the crustal structures [Chapin, 1996]. In most areas where gravity surveys are carried out there are deep-seated structural features causing variations in gravity at the surface, which are much larger in areal extent than the structures ordinarily of interest. A major step in the analysis of the gravity data is the process of isolating observed anomaly patterns into regional and residual components. The gravity anomaly is often the sum of the overlapping gravitational effects of two or more separate geologic structures of varying dimensions and depths and thus an objective separation criterion in not possible.

These effects can be hundreds of milligals. Since the Bouguer anomaly contains all the density deviations from an ideal Earth, residualizing gravity data to take out the deeper anomalous effects has been a major problem for a long time. In Hagiwara [1967] it is suggested that frequency analysis technique would be one of the best ways of separating the broad variations from local anomalies. In recent years, the application of digital filters to achieve this *regional-residual separation* has become increasingly popular among geophysicists. A high-pass filter is useful for emphasizing anomalies of short wavelength while the upper mantle structure could be effective by making use of a low pass-filter [Hagiwara, 1967].

However, the effectiveness of these mathematically derived maps from the viewpoint of quantitative gravity modeling is still debatable [Gupta and Ramani, 1980]. All residual maps generally follow the outlines of the geologic units and are probably equally useful for studying anomaly shapes and trends sometimes with slight discrepancies [Gupta and Ramani, 1980]. It is important that the residual anomaly contains the effects of the *local* and *near-surface masses* and be possible to explain the *most highs and lows* by the observed geology besides the effects of deep crustal features.

The separation of the Bouguer gravity field into its regional and residual components is always *ambiguous* and rather troublesome. There have been many approaches to solve this problem (e.g. Nettleton [1954]; Skeels [1967]; Fuller, [1967]) and they all have relied on the method of subtracting a *long-wavelength mathematical surface* from the data. In general Bouguer anomalies are smooth, but they contain a trend depending on the horizontal position of the measuring point. A linear trend must be removed from the data because its presence distorts the power estimate at all frequencies particularly near the zero frequency [Kanasewich, 1990; Meyer, 1974]. Assuming that the anomaly is given as Δg can be split into two jointly un-correlated parts, a horizontal trend AX and the residual Δg^r (cf. Sunkel and Kraiger, 1993):

$$\Delta g = AX + \Delta g^r \tag{4-1}$$

Now the horizontal trend must be expressed by a suitable function. In this case a *multivariate polynomial* of degree k has to be chosen as trend function that, in the plane, has the following form:

$$AX = a_0 + a_1 x + a_2 y + a_3 x^2 + a_4 xy + ... + a_n y^k \tag{4-2}$$

The coefficients a_i are determined by least squares regression k denotes the degree of the polynomial and (x, y) are the coordinates of the data points. The reduction due to a horizontal trend is necessary because least-squares prediction works best with quantities that contain no symmetrical part [Moritz, 1980, p. 76]. The residuals Δg^r satisfy this assumption much better than the gravity anomalies, Δg . In general, polynomials equations higher than fourth degree are incapable of algebraic solution in terms of a finite number of additions, subtractions, multiplications, divisions and root extractions as demonstrated by Abel (i.e., Abel's impossibility theorem) and also shown by Ruffini in 1813 [Wells, 1986, p. 59].

For the case study, the complete Bouguer anomaly was de-trended i.e. removal of the trend by utilizing polynomial functions to the fourth degree *for any degree greater than four becomes unsolvable.* Optimum filters are designed to separate the components or to *enhance or suppress specific wavelengths*, which correspond to certain geologic features. The filters are designed from power spectrum particularly unique to the set of data after the separation of the components has been determined. Therefore, the resultant values were filtered to obtain the *residual anomaly* for both the regional location and the investigation site and are shown in Figure 4.5 and Figure 4.6 respectively. In both de-trending and filtering we utilized GMT software prepared by Wessel and Smith [1995].

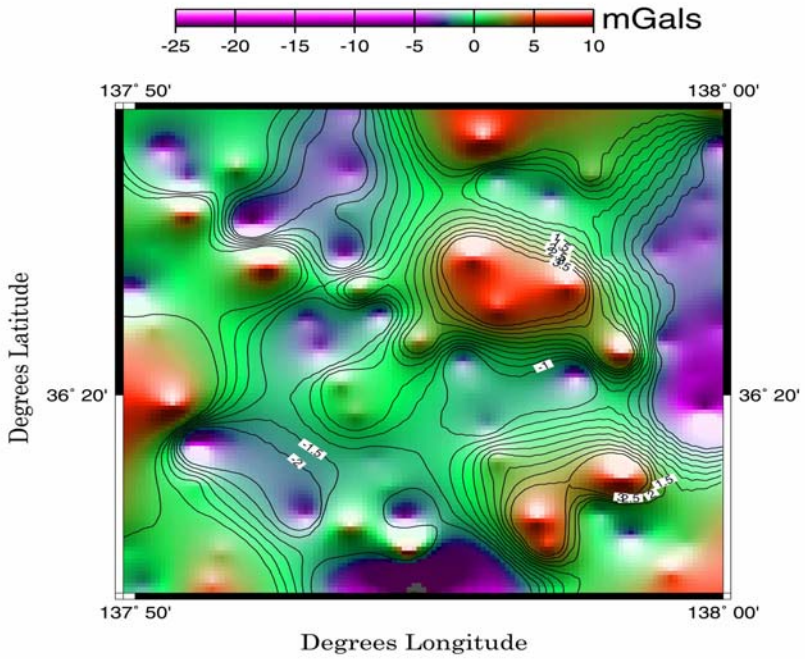

Figure 4-5: Residual anomaly of Case Study area with a contour interval of 0.50 mGals.

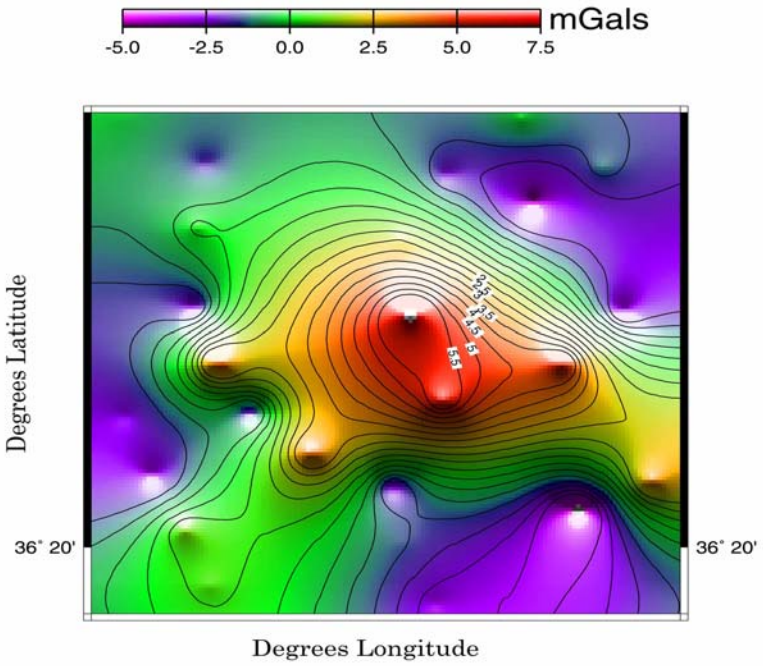

Figure 4-6: Residual anomaly of structural investigation site of area approximately 9.0 km by 9.0 km with a contour interval of 0.50 mGals.

4.3 Inversion Analysis

The gravity inverse problem is an ill-posed problem in the sense of Hadamard [1902] because its solution is neither unique nor stable. The non-uniqueness of the inverse problem increases rapidly for bodies with *in-homogenous* density and rapidly becomes *unmanageable.* Generally, geophysics provides only *indirect clues* to the presence of *economically useful deposits*. For a geophysical method to be useful, therefore, the measured physical property must be able to be interpreted in terms of geology. Such interpretation is not always straightforward because different methods sample different components of rocks, that is, the physical property measured by a geophysical method may indiscriminately sample all or only limited, constituents of a rock.

In geophysics this is primarily because one cannot afford to model the complexity of the Earth. Even if this were possible, it might not be worth the effort given the instrument's resolution and the noise level in the data. Even in the *absence of measurement and modeling errors*, the forward operator might not be invertible and the set of models that predict the data equally well may be quite large [Scales and Tenorio, 2001]. This in itself is not a problem; the problem is when these equally predicting models yield wildly different values for the model functional one wants to estimate. Many geophysical formulas are however *homologous* – that is, the structure of the formulae are identical and one equation can be obtained from the other by renaming the variables.

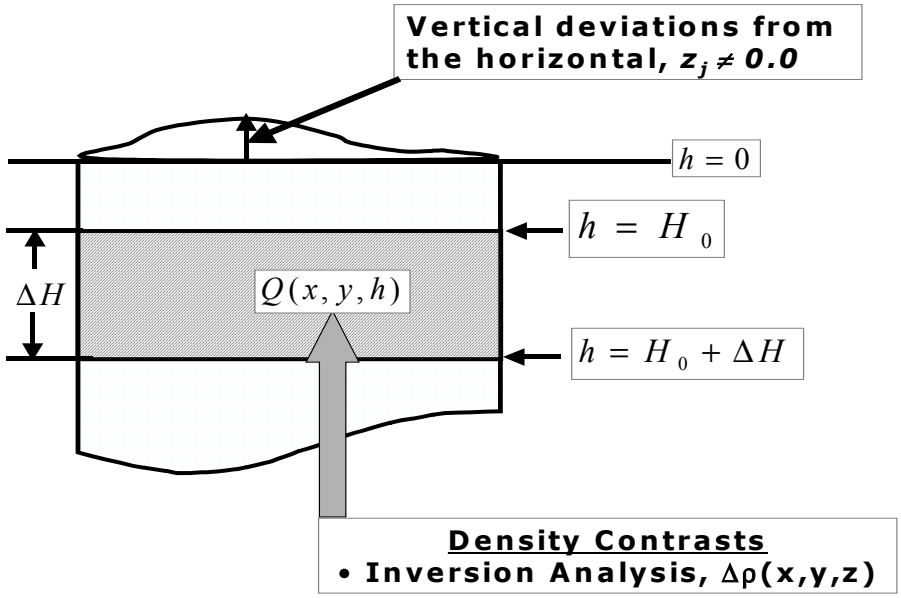

Figure 4-7: Model of the disturbing masses for a case where the deviations from the horizontal level are not equal to zero

4.3.1 Density contrasts and contact surfaces positions in an intermediate layer

The differential density contrast obtained in the sub-surface for a horizontal layer in the sub-surface has a *physical meaning* only at $H_0 < h < H_0 + \Delta H$. In the actual field, observations of rugged terrain (topography), the deviations from the vertical are not zero i.e. $z_j \neq 0.0$. Figure 4.7 shows the diagrammatic relationship of the vertical deviations from the horizontal level position and the horizontal layer. The *vertical deviations* have to be incorporated in the inversion analysis unlike the inversion analysis for the synthetic model. The vertical deviations are only values above horizontal level taken as $h = 0$. In the test site the maximum vertical deviation was 0.200 km.

Adopting the residual anomaly in Section 4.2.2.2, the computation of the *differential density contrasts* and *positions of the contact surfaces* in a series of horizontal layers with different thickness in the sub-surface proceeds as in Figure 4.8. It helps determine the depth-dependent density contrasts $\Delta\rho(x, y, z)$ from the *residual anomaly by inversion analysis*. Equations (2-5) and (2-6) in Sections 2.3.1 and equation (2-16) and (2-18) in Section 2.3.2 of Chapter 2 do contain the relevant equations. The computation proceeds similar to the modeling in Section 3.3.1 of Chapter 3 for the layer *disturbing masses*. The computation of differential density contrasts and the position of the contact surfaces is due to their *direct relationship* with disturbing masses in each of the series of intermediate horizontal layers.

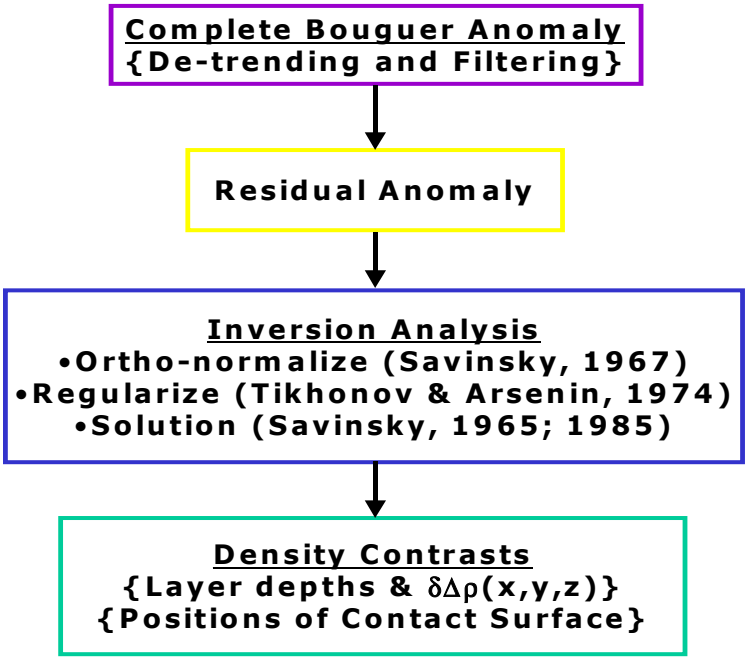

Figure 4-8: Flow diagram to determine of the differential density contrasts and position of the contact surface in a horizontal layer.

The inversion analysis for the *differential density contrasts* and *position of contact surfaces* for a sub-surface horizontal layer of range 0.350 ~ 0.650 km are shown in Figure 4.9 and Figure 4.10 respectively. Similar inversion analysis results for a *series of horizontal layers of similar heights i.e., each with a layer height of thickness 0.300 km* was performed and the summary is given in Table 4.4.

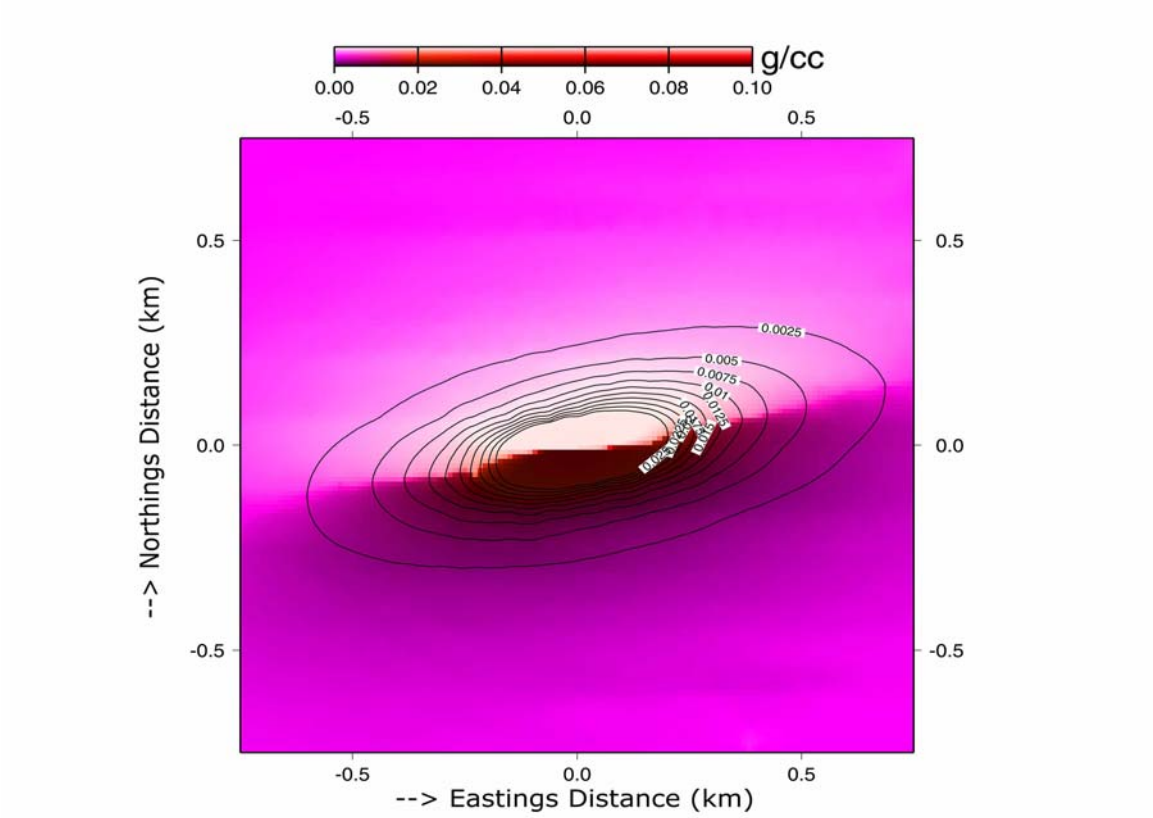

Figure 4-9: Results for a horizontal layer of range 0.350 ~ 0.650 km for differential density contrasts with a contour interval of 0.0025 g/cm^3.

The position of contact surfaces serve two purposes (1) due to the direct relationship with the maximal differential density contrasts in the layer, it checks the *maximum height of contact surface* which must either be equal or less the height of horizontal layer ΔH and (2) determines the *actual position of the contact surfaces* in the same horizontal layer. Table 4.4 gives the differential density contrasts for possible sub-surface structure in the investigation site. The inversion analysis was performed to a depth of 1.60 km.

Table 4.4 shows the *maximum density contrasts* for a possible structure in our investigation site. The density or density contrasts of the sub-surface could then be obtained *adding to the density or density contrast on the Earth surface* to the differences between the subsequent intermediate horizontal layers. The actual location of the disturbing masses could be obtained by stacking together the different layers for the entire lower half-space.

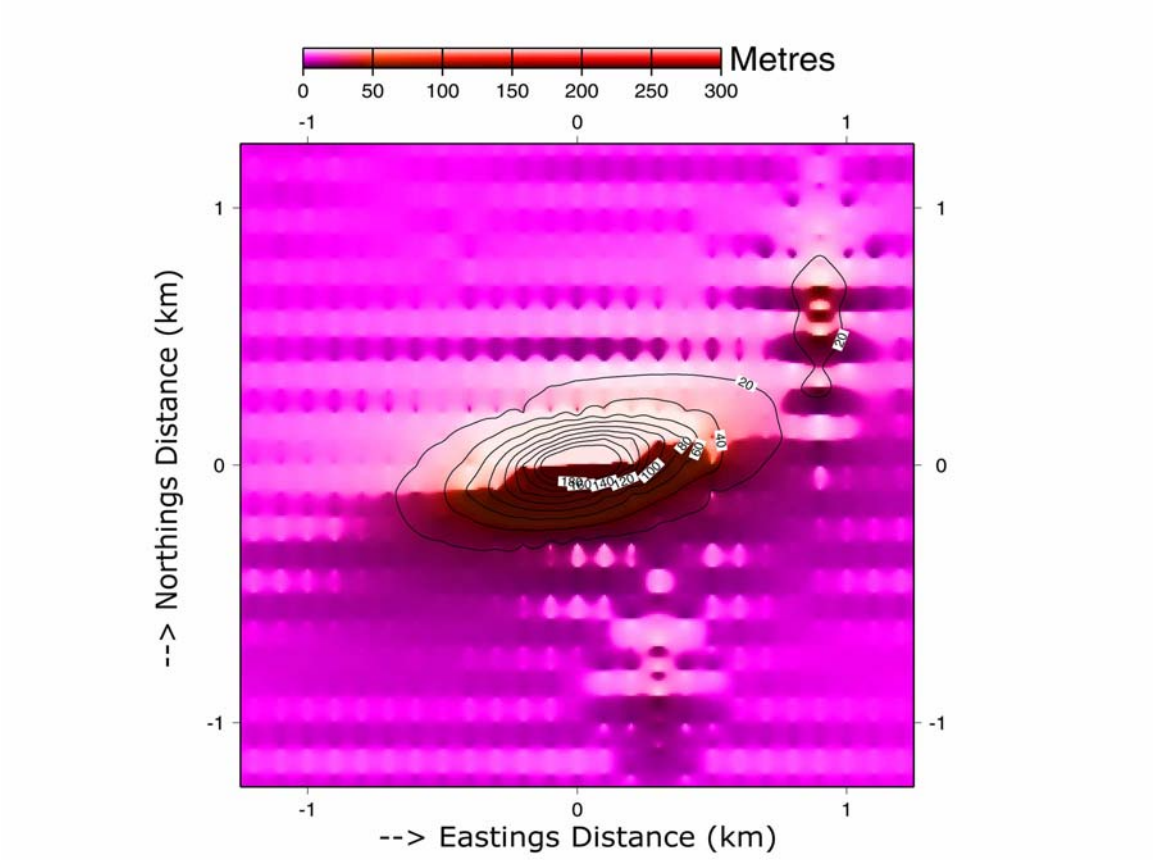

Figure 4-10: Results for a horizontal layer range 0.350 ~ 0.650 km for position of the contact surfaces with a contour interval of 10.0 m.

Table 4-4: Differential Density Contrasts for Layers in Investigation Site**.**

Layer	Horizontal Layer Range (km)	Maximum Layer height (km)	Maximum Density Contrasts (g/cm^3)
1	0.050 ~ 0.350	0.300	0.0800
2	0.350 ~ 0.650	0.300	0.0910
3	0.650 ~ 0.950	0.300	0.2012
4	0.950 ~ 1.250	0.300	0.3585
5	1.250 ~ 1.550	0.300	0.4253

4.3.2 Errors on differential density contrasts and contact surfaces positions

In Section 3.2.2 of Chapter 3 we showed the *hypothetical changes or variation ranges* in the heights of horizontal intermediate layers as depicted in Table 3.4. We proceeded there to investigate the *height error effects* on synthetic gravity anomaly effect of dipping dike in Sections 3.3.2.1, 3.3.2.2, 3.3.2.3 and 3.3.2.4. Here for the *actual gravity anomaly,* investigations on three different kinds of *height errors* on the differential density contrasts and position of the contact surfaces are as shown Figure 4.11.

We proceed as in Section 3.2.2 of Chapter 3 except for a *surface loaded with a mass case* which needs actual layer density contrast that is not *available presently*. In all the three cases, each intermediate horizontal layer had a *height error* introduced and the respective *height error effects* on the differential density contrasts and positions of contact surfaces determined for the actual geophysical data. Concurrently, the *height error limits* were investigated for meaningful geological and/or geophysical interpretations in an intermediate horizontal layer based on the geophysical data of the Chubu District – Japan.

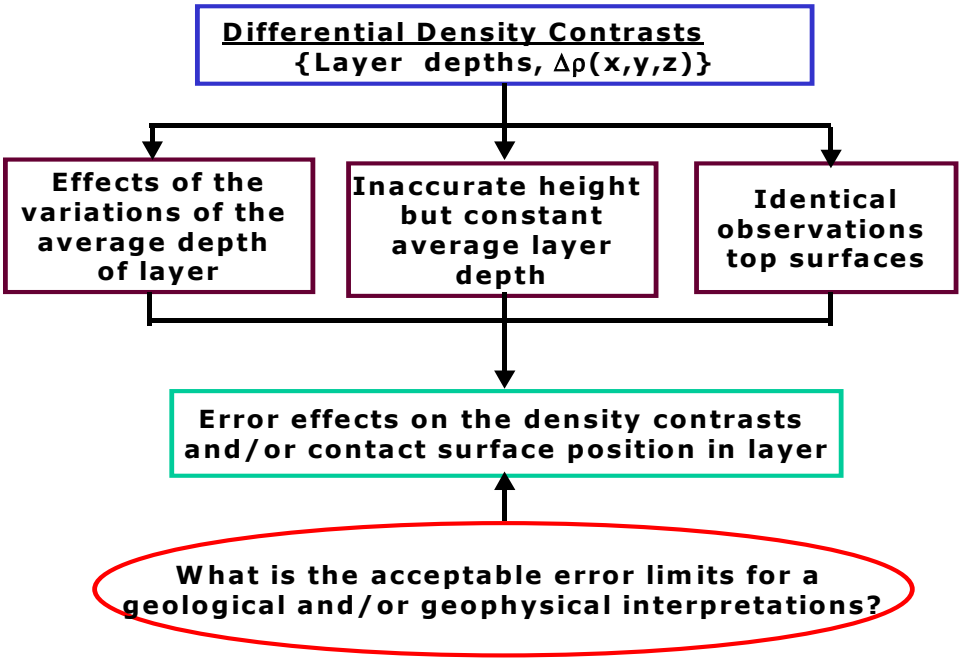

Figure 4-11: Flow diagram for the determination of height error effects at the Investigation Site in Chubu District – Japan.

4.3.2.1 Deviations due to inaccurate average depth of horizontal layer

The position of the horizontal layer in the sub-surface could be given inaccurately without any change in average height of the intermediate horizontal layer, ΔH. This could either be a *shift either upwards* or *downwards* as depicted by Figure 3.11 in Section 3.3.2.1. Even though the shifts might be minimal but their effects might significantly alter the resultant differential density contrasts and the position of the contact surfaces in an intermediate horizontal layer as was shown in Section 3.2.2 of Chapter 3. In the present case as shown in Table 4.5, we vary the horizontal layer heights i.e., a *case one* with an error of +5.00 m and *case two* as –10.0 m respectively on an intermediate horizontal layer of height $\Delta H = 0.300\,\text{km}$.

Table 4-5: Error on heights on horizontal layer of $\Delta H = 0.300\,\text{km}$.

	Correct height of horizontal layer (km)	**#1 – Inaccurate layer height (km)**	**#2 – Inaccurate layer height (km)**
H_1	0.250	0.255	0.240
H_2	0.550	0.555	0.540
$\Delta H = H_2 - H_1$	0.300	0.300	0.300
Mean H = $(H_2+H_1)/2$	0.400	0.405	0.390
Error dh in the mean H	0.000	0.005	-0.010
Height position relationship	-	Mean H greater than correct mean value	Mean H less than correct mean value

Equations (2-39) and (2-40) in Section 2.4.1 in Chapter 2 give the *height error effects* in the differential density contrasts and positions of the contact surfaces arising thereby are utilized in a pattern similar to synthetic modeling in Section 3.3.2.1 of Chapter 3. From the inversion analysis, the *first case* has a maximum error effects in differential density contrasts of 9.604 mg/cm^3 and 14.5 cm in the position of the contact surface, while the *second case* has a maximum error in differential density contrasts of –8.92 mg/cm^3 and -13.6 cm in the position of the contact surface. The *height error effects* for the two cases are shown in Figure 4.12 and Figure 4.13 respectively.

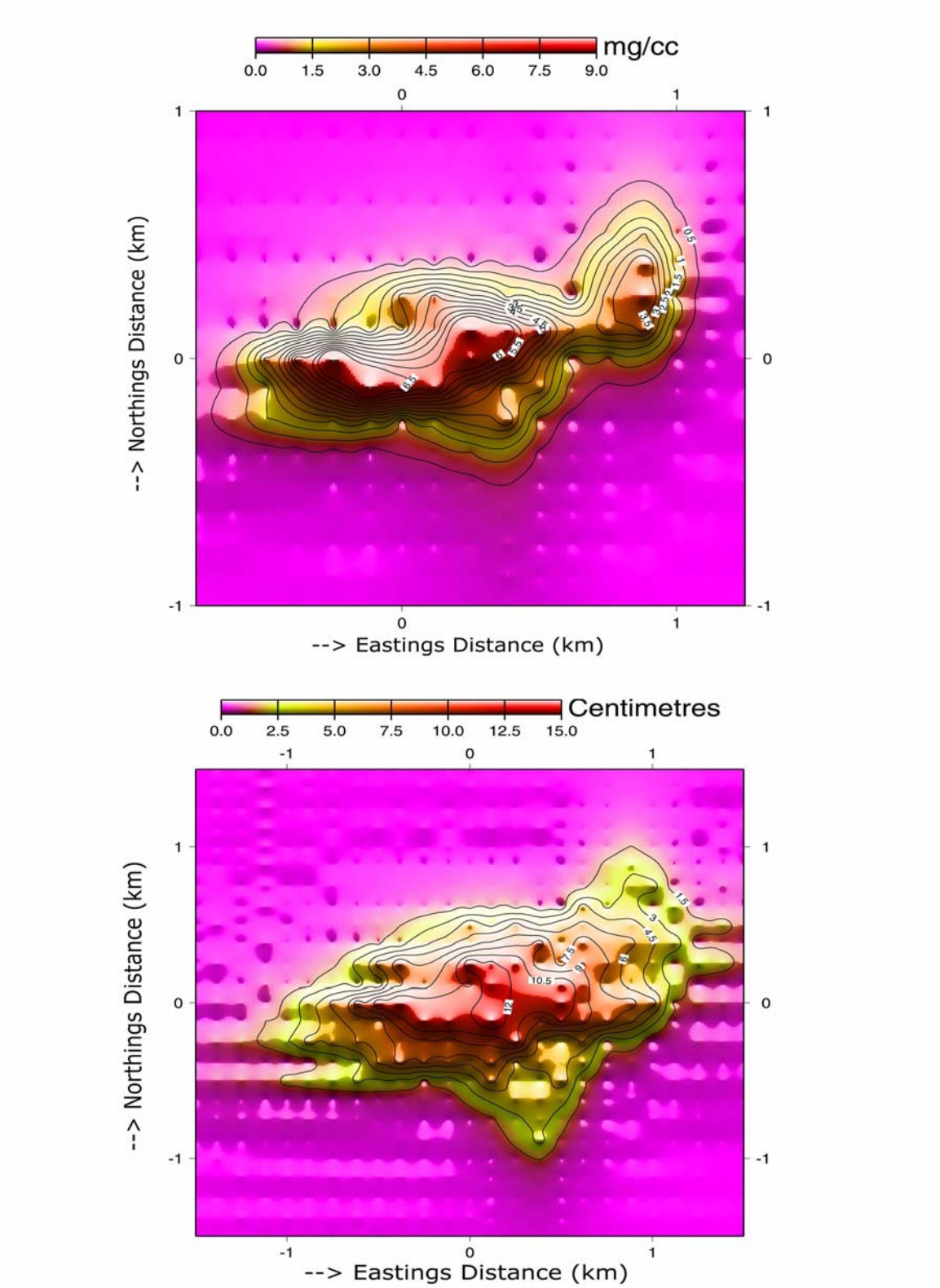

Figure 4-12: Error effects due to average height greater than correct height of layer for a range of 0.350 ~ 0.650 km as (a) differential density contrasts with a contour interval of 0.50 mg/cm^3 and (b) position of contact surfaces with a contour interval of 1.50 cm.

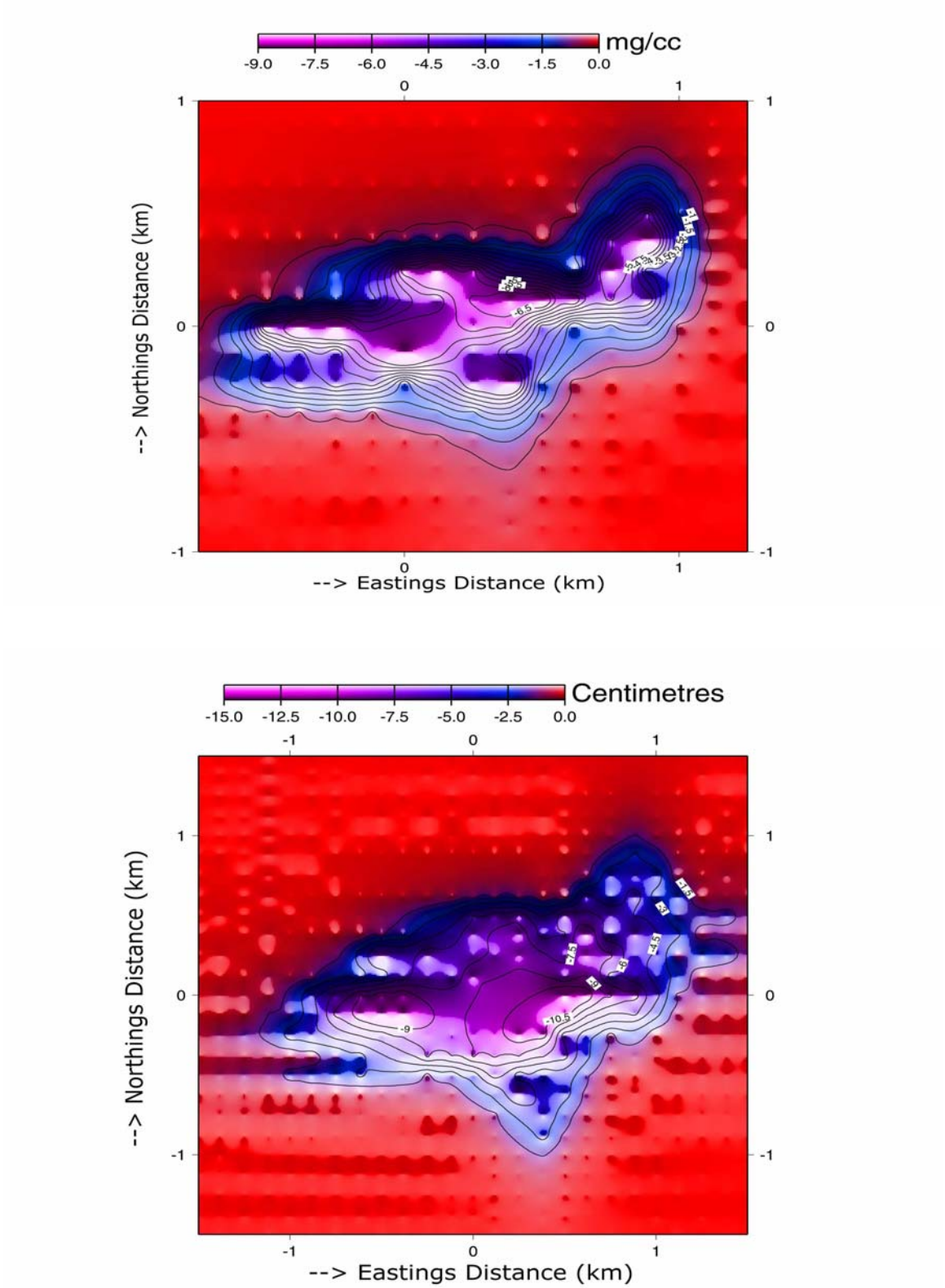

Figure 4-13: Error effects due to average height less than correct height of layer for a range of 0.350 ~ 0.650 km as (a) differential density contrasts with a contour interval of 0.50 mg/cm^3 and (b) position of contact surfaces with a contour interval of 1.50 cm.

4.3.2.2 Distortions due to an assigned layer thickness and/or assumed layer density

The *distortion* in the assigned layer thickness is also a source of error in the computed differential density contrasts in the horizontal layer as was shown in Section 3.2.2.2 of Chapter 3 using *synthetic gravity anomaly*. Two specific *height error* cases where the average height of the horizontal layer though remaining constant has either (1) the height of the layer ΔH_1 being less than ΔH i.e., a compressed intermediate layer effect or (2) height of the layer ΔH_2 being greater than ΔH i.e., a stretched intermediate layer effect are considered. Figure 3.14 in Section 3.3.2.2 in Chapter 3 diagrammatically depicts the two cases and *possible height errors* for the case study are given in Table 4.6. In this case, we vary the average height of intermediate horizontal layer i.e., a *case 1* with an error of -5.0 m and *case 2* as +10.0 m on the lower and upper parts of the layer of height $\Delta H = 0.300$ km as shown in Table 4.6.

Equations (2-51) and (2-52 in Section 2.4.2 on the height error effects for the differential density contrasts and positions of the contact surfaces arising thereby are utilized in a pattern similar to *synthetic data modeling* in Section 3.3.2.2 of Chapter 3. The determination of the disturbing masses, the *case 1* has a maximum error effect in differential density contrasts of 11.53 mg/cm^3 and 15.5 cm in the position of the contact surface, while the *case 2* has a maximum error of 11.34 mg/cm^3 and 13.3 cm in the position of the contact surface. The *height error effects* arising from the two cases for an intermediate horizontal layer of height $\Delta H = 0.300$ km are shown in Figure 4.14 and Figure 4.15 respectively

Table 4-6: Distortions due to assigned layer thickness and/or assumed density

	Correct height of horizontal layer (km)	**#1 – Compressed layer height (km)**	**#2 – Stretched layer height (km)**
H_1	0.250	0.255	0.240
H_2	0.550	0.545	0.560
$\Delta H = H_2 - H_1$	0.300	0.290	0.320
Mean H = $(H_2+H_1)/2$	0.400	0.400	0.400
Value of factor α = ΔH/Actual height	1.000000	0.966667	1.066667

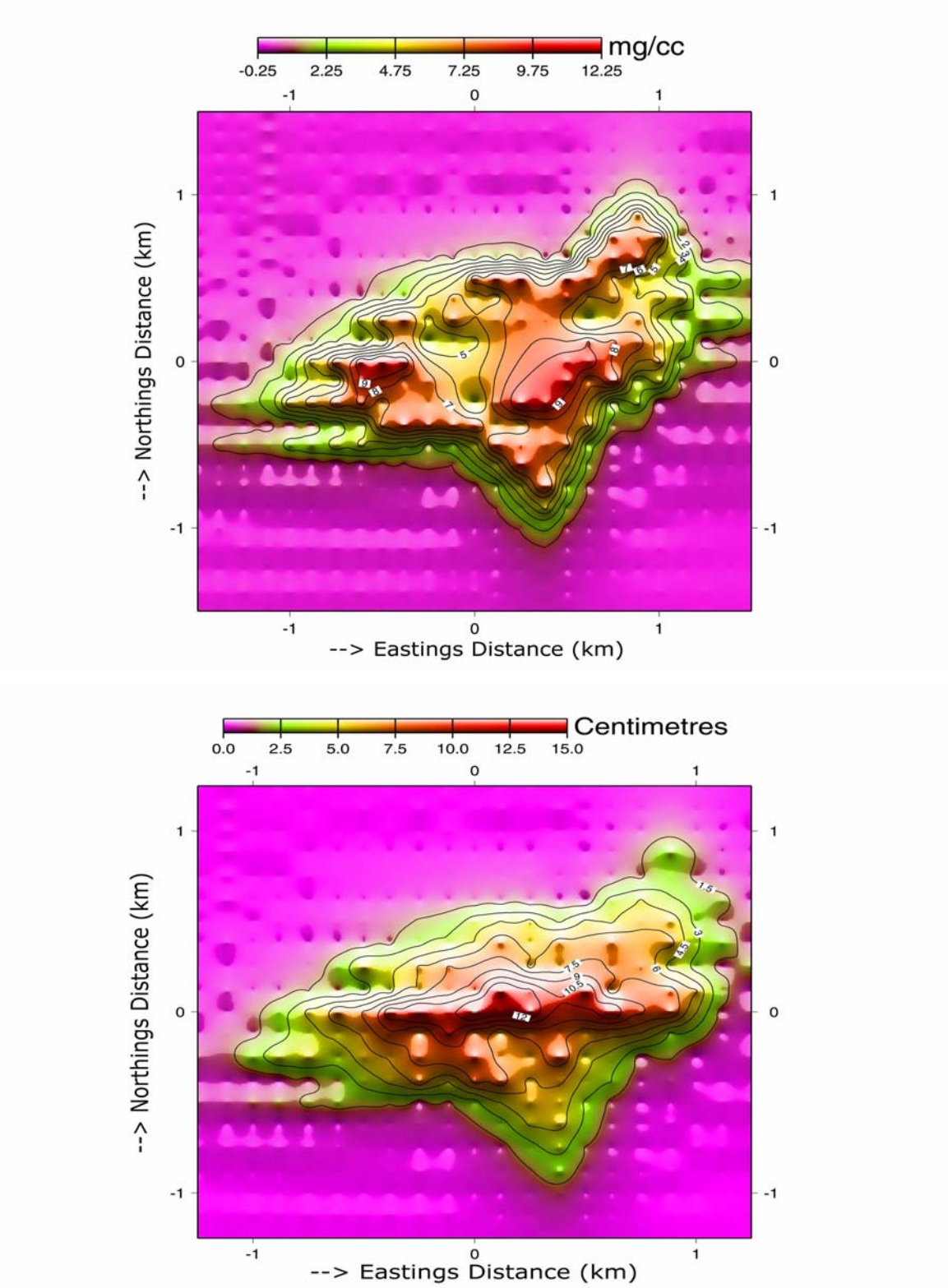

Figure 4-14: Error effects for the thickness of the layer less than correct thickness for a range of 0.350 ~ 0.650 km as (a) differential density contrasts with a contour interval of 1.00 mg/cm^3 and (b) position of contact surfaces with a contour interval of 1.50 cm.

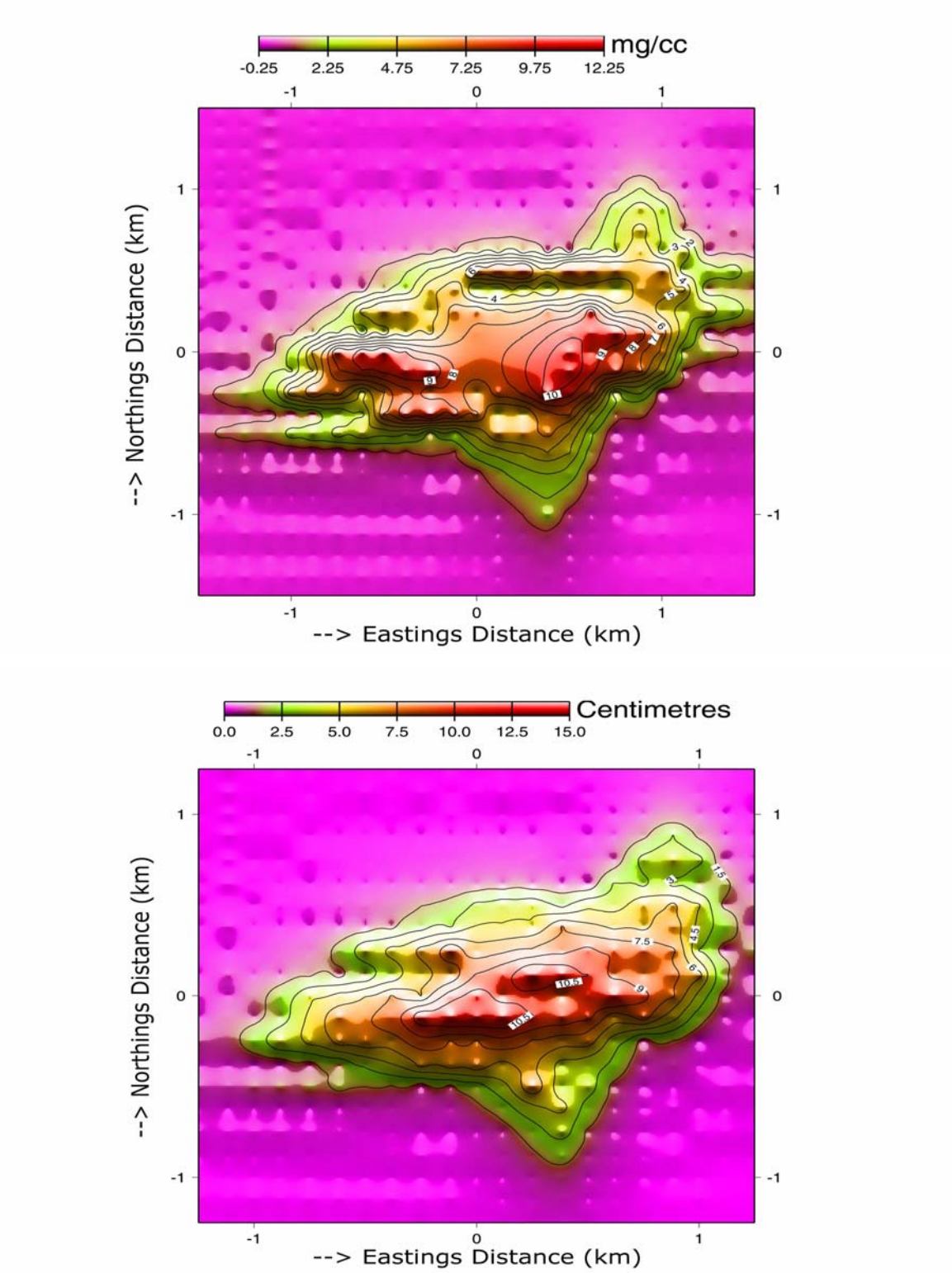

Figure 4-15: Error effects for the thickness of the layer greater than correct thickness for a range of 0.350 ~ 0.650 km as (a) differential density contrasts with a contour interval of 1.00 mg/cm^3 and (b) position of contact surfaces with a contour interval of 1.50 cm.

4.3.2.3 Density changes due to the top surface identical to observation surfaces

The assigned layer thickness can be *altered* such that the top surfaces though being identical, the bottom surfaces have a *height error*. As has been established in Chapter 3, two possible error cases where the top surface though identical i.e., top surface of layer not erroneous but the bottom surfaces are in error are depicted in Figure 3.17 of Section 3.3.2.3 and the test values as shown in Table 4.7. The two cases are such that (1) height of intermediate layer ΔH_2 is greater than ΔH i.e., a stretched intermediate layer effect and (2) the height of layer ΔH_1 is less than ΔH i.e., a compressed intermediate layer effect. We have demonstrated by inversion analysis the *height error effects* of such an alteration of intermediate horizontal layer in Chapter 3, Section 3.3.2.3 using synthetic gravity anomaly and follow the same pattern to investigate height error effects on this actual field geophysical data.

Table 4-7: Density changes due to top surface being identical to observation surfaces

	Correct height of horizontal layer (km)	**#1 – Stretched layer height (km)**	**#2 – Compressed layer height (km)**
H_1	0.250	0.250	0.250
H_2	0.550	0.560	0.540
$\Delta H = H_2 - H_1$	0.300	0.310	0.290
Mean H = $(H_2+H_1)/2$	0.400	0.405	0.395
Height position relationship	-	Mean H greater than correct mean value	Mean H less than correct mean value

Two possible cases are (1) height error of +10.0 m and (2) height error of -10.0 m on the horizontal intermediate layer of thickness $\Delta H = 0.300$ km. Equations (2-65) and (2-66) in Section 2.4.3 of Chapter 2 are adopted for the computations. The *first case* had a maximum error effect on differential density contrasts of –13.05 mg/cm^3 and 9.6 cm in the position of the contact surface, while the *second case* had a maximum error effect of 13.25 mg/cm^3 on the differential density contrasts and 16.8 cm in the position of the contact surface. The height error effects for the two cases are shown in Figure 4.16 and Figure 4.17 corresponding to *case 1* and *case 2* respectively.

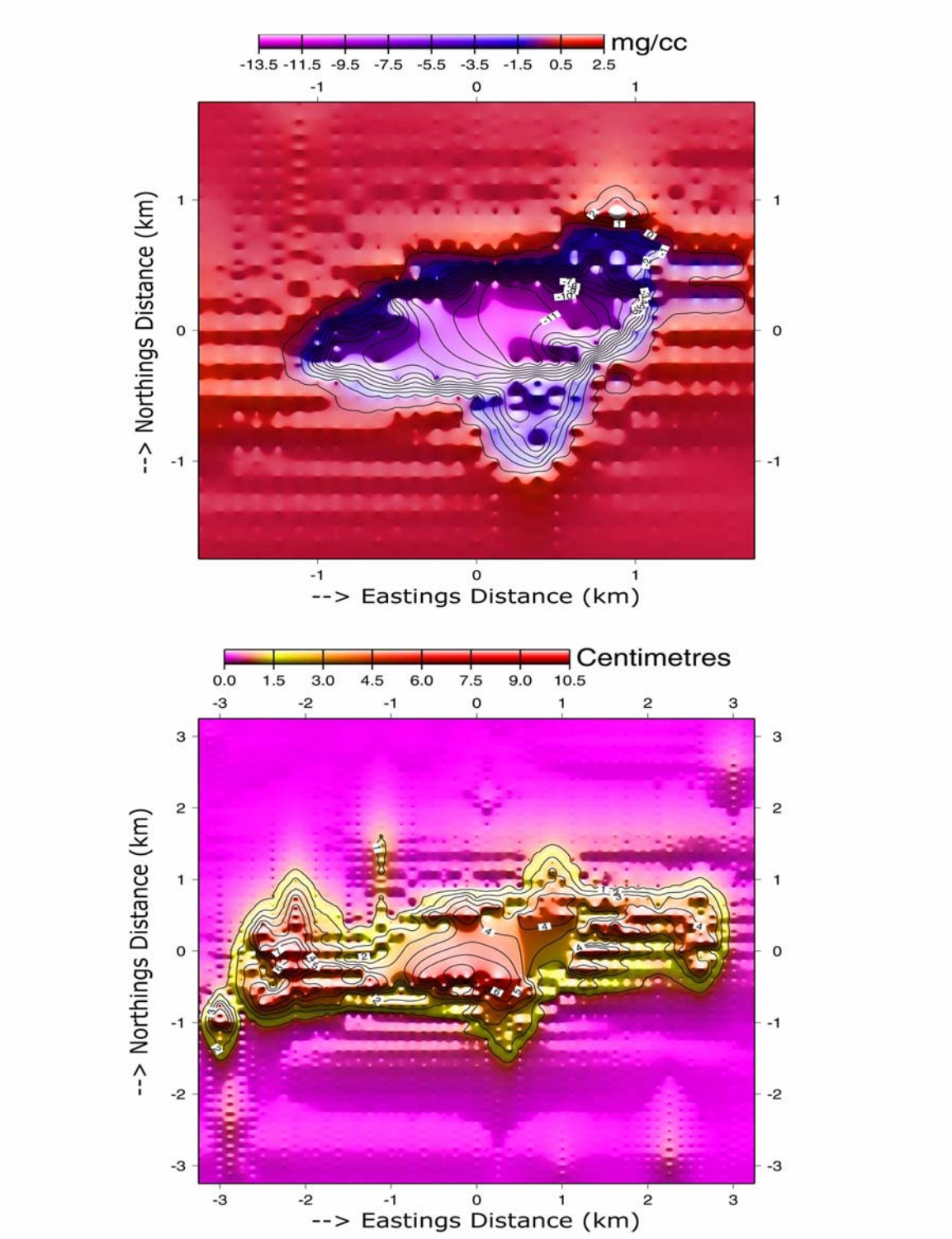

Figure 4-16: Error effects due to identical surfaces but thickness of layer greater than actual thickness for range of 0.350 ~ 0.650 km as (a) differential density contrasts with a contour interval of 1.00 mg/cm^3 and (b) position of contact surfaces with a contour interval of 1.00 cm.

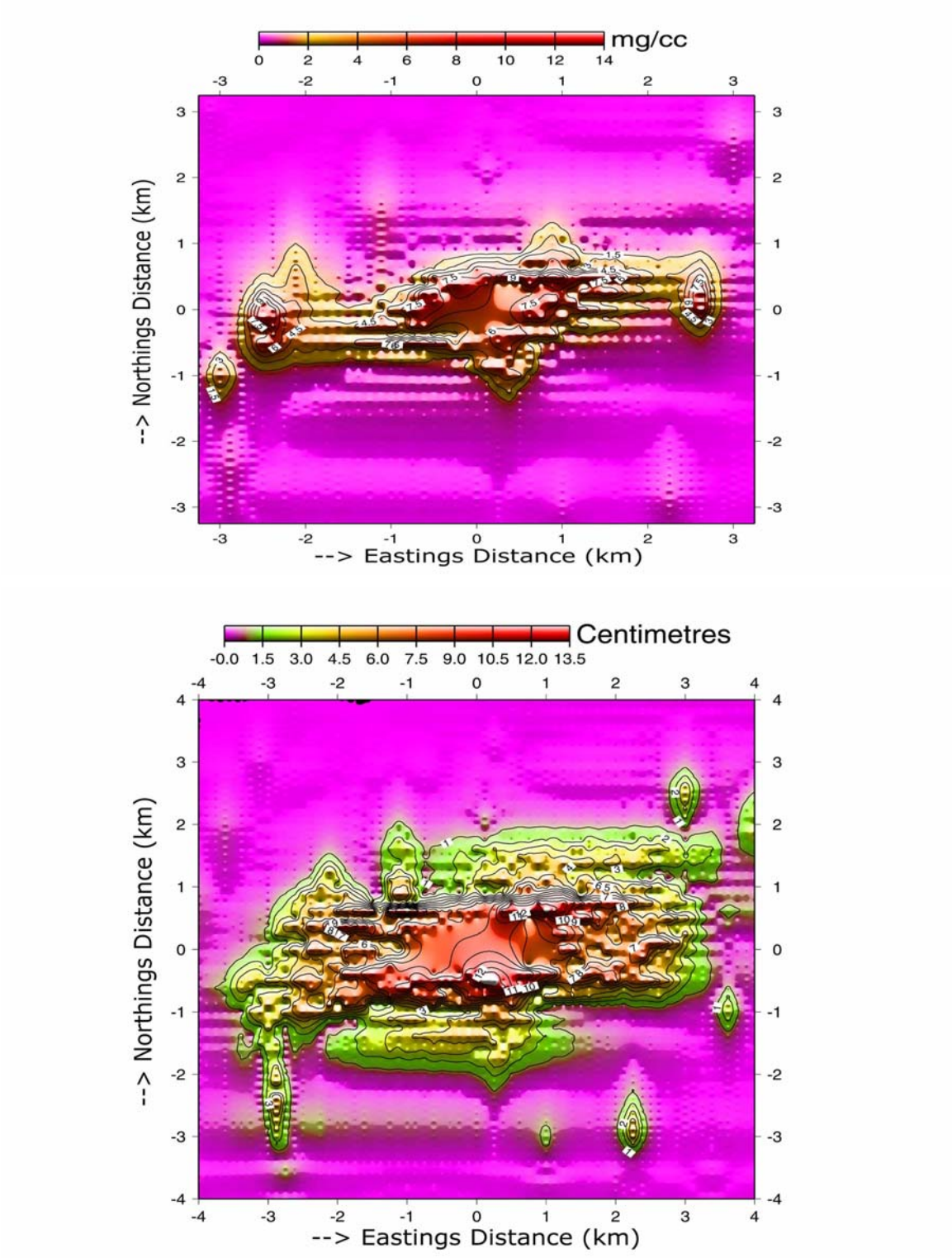

Figure 4-17: Error effect due to identical surfaces but thickness of layer less than actual thickness for range of 0.350 ~ 0.650 km as (a) differential density contrasts with a contour interval of 1.00 mg/cm^3 and (b) position of contact surfaces with a contour interval of 1.00 cm.

4.4 Height error limits for geological and/or geophysical interpretations

In the computation of the *height error effects* in Section 4.2 above, we similarly as in Chapter 3 for the *synthetic gravity anomaly* computed the *height error limits* for each type of alteration of the horizontal intermediate layer. Table 4.8 shows the error limits for the height errors on the *three error types investigated* i.e., (1) effects of the variations in average depth of horizontal intermediate layer, (2) inaccurate layer heights but constant average depth and (3) use of identical top layer though the bottom surface is erroneous. These *error limits* for a horizontal intermediate layer of height $\Delta H = 0.300\,\text{km}$ i.e., Table 4.8 are due to a depth of about 0.600 km from the Earth surface location. These values are solely dependent on the *depth* in sub-surface and the density contrasts or disturbing masses and might *var*y from one location to another.

Table 4-8: Error limits for a geological and/or geophysical interpretations.

	Effects of variations in average depth	**Inaccurate height but constant average depth**	**Identical top layer surfaces**
Density contrasts (mg/cm^3)	1.0	1.0	1.0
Maximum height error (cm)	3.0	1.0	1.0

For the inversion analysis in an area with no *independent information on sub-surface geology*, it is seldom possible to translate gravity data into reliable indications of structure. The more the available data from other sources, the *more restricted* will be the questions that gravity information is called upon to answer and the more the definite answers that can be expected. It is important for all who use gravity data like geologists and geophysicists to realize that interpretation in not a clear-cut process, which can be relied on for unique solution but instead subject to *numerous limitations*, which decrease as the *independent control increases*. Sometimes substantial overlap between densities of different rocks types would complicate the interpretations.

Chapter 5

What one might see as a job well done; is just the start for a true professional.
- Scientific Lore.

Originally humans were ignorant and yet they had an internal model of the world.
In the course of time, this model has been updated many times, following the development
Of new experimental possibilities or the development of their intellect.
– Albert Tarantola, Paris 1986.

5 Summary and Conclusions

In summary, Chapter 3 has demonstrated the *quantitative determination* of the *depth-dependent (variable) density contrasts* in the lower half-space from *inversion analysis modeling*. The *depth-dependent density contrasts* forward model $\Delta\rho(z)$ was computed apriori for a series of intermediate horizontal layers with *varying heights and at different depths* though results adopt a single layer thickness for all of them. It has been shown that from a sub-surface *forward model* with *apriori* depth-dependent density contrasts, it is possible to *determine or recover the differential density contrasts* $\Delta\rho(x,y,h)$ *changes with respect to depth*. The same heights were utilized in the inversion analysis to determine if it is possible to recover the *maximum values i.e., quantities* from the forward model. The maximum values or quantities were chosen per each intermediate layer since the *maximum gravity anomaly effect* was maintained at either central or shifted locations. Each maximum value gives the highest possible value of density contrasts for each intermediate layer as per the gravity anomaly effect of the dipping dike. Similar inversion analysis was later applied to an investigation site in Chubu District, Japan as a real case study in Chapter 4.

Table 3.3 shows the maximum inversion *differential density contrasts*, where column 3 can be compared to the *apriori* density contrasts in column 2. The differences between the forward model density contrasts $\delta\Delta\rho(z)$ and inversion analysis *density contrasts* $\delta\Delta\rho(x,y,h)$ are in column 4. Thus, for a series of horizontal intermediate layers, it highlights the *accuracy of determination* of disturbing masses. The differences are less than 5.0 mg/cm^3 up to a depth of 2.00 km for the horizontal layers of 0.400 km thickness. The differences increase gradually after a depth of 2.00 km in the sub-surface. One possibility for the increase is due to use of greater *point-to-point* separation distance with increasing depth. It effectively smoothens the *effective gravity anomaly effect* as pointed out in Savinsky [1967], i.e., set of inversion results become poorly defined at increasing depths H_0 due the influence of the accumulated errors or smoothing of the gravity anomaly effect with increase in the point-to-point separations. These accumulated errors are causes for the need for the regularization techniques applied in the inversion analysis [Tikhonov and Arsenin, 1974; Koch, 1990]. Results of the investigation site for a possible sub-surface structure in Chubu District are depicted in column 4 of Table 4.4 with *maximum density contrasts* for a series of intermediate horizontal layers.

In Chapter 3 we further demonstrate the *height error effects* on the density contrasts for an intermediate horizontal layer due to the height errors or alteration of the thickness. In this regard we considered four cases namely (1) deviations due to an *inaccurate average depth* of horizontal layer, (2) *distortions due to assigned layer thickness* or assumed density, (3) top surface being *identical to the observations surfaces* and (4) layer approximated with a *surface covered with a mass*. In *case 1*, a height error of +5 m or –10 m had error effects in *density contrasts of 1.80* and *-3.50 mg/cm*^{3} for a layer height of 0.750 km while *case 2* had *8.56* and *8.85*, *case 3* had *-7.37* and *5.53* respectively. The height error effect in *density contrasts* due to height error of +5 m in *case 4* as *8.83 mg/cm*^{3}. From the results, it implies in *case 1* that *minimal errors in the assigned average depth of a layer create only slight changes in the variable density* compared to cases 2, 3 and 4 respectively. Thus, any shift of the horizontal intermediate layer *without alteration of the layer height*, ΔH as in *case 1*, has only slight changes on the resulting density contrasts compared to cases 2, 3 and 4. Therefore as long as the layer thickness is maintained the error effects due to small height changes are *minimal.*

Similar results are reflected in the *height error effects* on the contact surfaces positions too. In *case 1*, a height error of +5 m or –10 m had height error effects in *position of contact surfaces as 65.0* and *–78.0 cm* for a layer height of 0.750 km while *case 2* had *78.0* and *75.0 cm*, *case 3* had *–43.0* and *75.0 cm* respectively. The error in *density contrasts* due to height error of +5 m in *case 4* as *75.0 cm.* The results imply that the effect of variation of the height of horizontal layer considerably affects the position of the contact surface and depends the position of horizontal layer and quantity of the disturbing masses. The height error effects on both *differential density contrasts* and positions of contact surfaces implies *that a relationship exists between the true and the incorrect (distorted) density values such as when the error in the assigned depth of a layer is established, the exact densities and/or density contrasts can be obtained from the distorted density values.*

In Table 3.8 in Chapter 3 the *height error limits* and their effects for an intermediate layer of height 0.750 km are given. These are the values beyond which any accuracy in height measurements does not have an effect in the *geological and/or geophysical interpretation of the sub-surface density or localized structures*. Chapter 4 has results for a investigation site in Chubu District - Japan, for cases 1, 2 and 3 in an intermediate horizontal layer of height $\Delta H = 0.300\,\text{km}$ that corroborate quite well with those from in Chapter 3 on synthetic gravity anomaly effects. In *case 1*, a height error of +5 m and –10 m had height error effects in *density contrasts of 9.60* and *–8.92 mg/cm*^{3} for a layer height of 0.300 km while *case 2* had *11.53* and *11.34*, *case 3* had *–13.05* and *13.25* respectively. On the hand, in *case 1*, a height error of +5 m or –10 m had height error effects in *position of contact surfaces of 14.5* and *–13.60 cm* for a layer height of 0.300 km while *case 2* had *15.50* and *13.30 cm*, *case 3* had *9.6.0* and *-16.80 cm* respectively

When combined the four cases developed in Sections 2.3.1, 2.3.3, 2.3.3 and 2.3.4 of Chapter 2 for the relations between the *distorted and the exact values of the variable thickness (height of intermediate layer)* about the inaccuracies in the assigned

intermediate layer thickness and bedding values demonstrate the corrections of the possible *error effects*. In terms of differential density contrasts these *height errors significantly* affect the geological and/or geophysical interpretations since the density contrasts have a *physical meaning* only in the *explicit range* as depicted in Section 2.4 of Chapter 2. This is especially serious as *density differences* in the neighbouring geologic materials vary and it becomes difficult to clearly *delineate* between them. It has also been shown in Section 3.3.3 of Chapter 3 for synthetic modeling and Section 4.3 in Chapter 4 in the real case study the maximum *height error limits* needed in the geophysical and/or geological interpretation for a horizontal intermediate layer..

The determination of the disturbing masses in a horizontal layer as depicted in the above computations is also an indication of the *recovery of the causative structure*. This was shown by the shift in the sub-surface of the location of the disturbing masses as had been proposed in the *deliberate shift by 5.00 km Eastwards* of the gravity anomaly effect of the synthetic dipping dike. The actual location of the disturbing masses is made possible by stacking together horizontal layers in the lower half-space. The operations as demonstrated in both *synthetic modeling* and *actual case* studies have a *definite physical meaning* such that for *unchanged gravitational anomaly* these *effective distortions* in intermediate layer implies *certain density variations*. These relations provide for corrections to the height error effects by means of *inversion downward continuation analysis* and are particularly valuable when the results are reviewed on the basis of *new data on the geology* of a particular region. The revised density variations are thus useful in the improving for a given gravity anomaly the *geological and/or geological interpretations* of the sub-surface.

In conclusion in the present study, the *determination* of *apriori* depth-dependent density contrasts and position of the contact surfaces within an intermediate horizontal layer has been quantitatively demonstrated. Closely related to the disturbing masses in an intermediate horizontal layer, the recovery of the *actual location* of the *causative structure* in the sub-surface has been demonstrated too. Further, the possible *height errors* and the *height error effects* arising there from have been investigated and conclude that it is *vital* to *explicitly state* the height of the intermediate horizontal layer since the *physical meaning* of the determined disturbing masses holds *only within* the layer. The explicit *height error limits* are useful for a meaningful geological and/or geophysical interpretation the geological materials (i.e., densities) at a particular sub-surface depth. Therefore, it is imperative, if possible to state and adopt in the computations layer heights to the either *centimeters level accuracy or accuracy of height measuring instrument(s)*. Finally, the determination of disturbing masses is more effective in *microgravimetry studies* and/or *localized structures* without the effects long-wavelength anomalies and a more *accurate interpretation* is dependent on abundance of the geological information. In order to obtain a better understanding of the subsurface structure, it is necessary to incorporate other geophysical and geological constraints such as seismic survey data and information from drill holes.

References

Abd-Elmotaal, H. (1992): Statistical behaviour of the free-air, Bouguer and isostatic anomalies in Austria. Bulletin Geodesique, **66**, pp. 325-335.

Ateya, I. L. (2000): Influence of Actual Gravity Variation on Height Determination. MSc. Thesis (Unpublished). Department of Geophysics, Kyoto University, Japan.

Ateya, I. L. and S. Takemoto (2002a): Inversion of gravity across a sub-surface dike-like structure in two dimensions. Western Pacific Geophysics Meeting 2002 (WPGM), Wellington, New Zealand, EOS, Transactions, American Geophysical Union, **83**, No. 22, pp. 112.

Ateya, I. L. and S. Takemoto (2002b): Gravity inversion modeling across a 2-D dike-like structure – A Case Study. Earth Planets Space (EPS), **54**, pp. 791 – 796.

Ateya, I. L., S. Okuyama and S. Takemoto (2003): Gravity inversion modeling across Fault/Tectonic Lines in the Central Ranges in Honshu, Japan, Journal of the Geodetic Society of Japan, **49**, No. 1, pp. 101 – 111.

Ando, M. (1975): Possibility of a major earthquake in the Tokai District, Japan and its pre-estimated seismo-tectonic effects. Tectonophysics, **25**, pp. 69 – 85.

Barbosa, V. C. F., Silva, J. B. C., and Medeiros, W. E. (1999): Stable inversion of gravity anomalies of sedimentary basins with non-smooth basement relief's and arbitrary density contrast variations. Geophysics, **63**, pp. 754 – 764.

Bear, G. W., Al-Shukri, H. J. and Rudman, A. J. (1995): Linear inversion of gravity data for 3-D density distributions, Geophysics, **60**, No. 5, pp. 1354 – 1364.

Bell, R. (1998): Gravity gradiometry, Scientific American, **278**, pp. 74 – 79.

Bell, R, Anderson, R. and Pratson, L. (1997): Gravity gradiometry resurfaces. The Leading Edge, **16**, pp. 55 – 60.

Blais, J. A. R. and Ferland, R. (1984): Optimization in gravimetric terrain corrections. Canadian Journal of Earth Sciences, **21**, pp. 505 – 515.

Blakely, R. J. and Simpson, R. W. (1986): Locating edges of source bodies from magnetic or gravity anomalies. Geophysics, **51**, pp. 1494 – 1498.

Blakely, R. J. (1995): Potential Theory in Gravity and Magnetic Applications, Cambridge University Press.

Boulanger, O. and Chouteau, M. (2001): Constraints in 3D gravity inversion. Geophysical Prospecting, **49**, pp. 265 – 280.

Braille, L. W., Keller, G. R. and Peeples, W. J. (1974): Inversion of gravity data for two-dimensional density distribution. Journal of Geophysical Research, **79**, pp. 2017 – 2021.

Burger, H. R. (1992): *Exploration Geophysics of the Shallow Subsurface,* Prentice Hall, Englewood Cliffs, New Jersey 07632.

Butler, D. K. (1979): Assessment of micro gravimetric techniques for site investigations. Presented at the 49th Annual International SEG Meeting (Abstracts), New Orleans. Geophysics, **45**, pp. 549.

Butler, D. K., Gangi, A. F., Wahl, R. E., Yule, D. E. and Barnes, D. E. (1982): Analytical and data processing techniques for interpretation of geophysical survey data with special application to cavity detection, Miscellaneous paper GL-82-16, US Army Engineer Waterways Experiment Station, Vicksburg, MS.

Butler, D. K. (1983): Micro-gravimetry and the theory, measurements and application of gravity gradients, PhD, Thesis, Texas, A & M University, College Station, USA.

Butler, D. K. (1984): Micro gravimetric and gravity gradient techniques for detection of subsurface cavities. Geophysics, **49**, No. 7, pp. 1084 – 1096.

Butler, D. K. (1995): Generalized gravity gradient inversion for 2-D inversion. Geophysics, **64**, No. 4, pp. 1018 – 1028.

Chai, Y. and Hinze, W. J. (1998): Gravity inversion of an interface above, which the density contrast varies exponentially with depth. Geophysics, **53**, pp. 837 – 845.

Chasseriau, P. and Chouteau, M. (2003): 3D gravity inversion using a model of parameter covariance. Journal of Applied Geophysics, **52**, pp. 59 – 74.

Chapin, D. A. (1996): A deterministic approach toward isostatic gravity residuals – A case study from South America. Geophysics, **61**, No. 4, pp. 1022 – 1033.

Cordell, L. and Henderson, R. G. (1968): Iterative three-dimensional solution of gravity anomaly data using a digital computer. Geophysics, **33**, No. 4, pp. 596-601.

Cordell, L. (1973): Gravity analysis using an exponential density-depth function - San Jacinto Graben, California. Geophysics, **38,** pp. 684 - 690.

Cordell, L. and Grauch, V. J. S. (1982): Reconciliation of the discrete and integral Fourier transforms. Geophysics, **47,** pp. 237 – 243.

Damiata, B. N. and Lee, T. (2002): Gravitational attraction of solids of revolution – Part I: Vertical circular cylinder with radial variation of density. Journal of Applied Geophysics, **50**, pp. 333 – 349.

Damiata, B. N. and Lee, T. (2002): Gravitational attraction of solids of revolution – Part II: General expressions, Journal of Applied Geophysics, **50**, pp. 351 – 373.

Ditmar, P. (2002): Finding the shape of a local heterogeneity by means of a structural inversion with constraints. Geophysical Prospecting, **30**, pp. 209 – 223.

Droste, C. (1998): *Uncertainty in Parameter Estimation for Nonlinear Dynamical Models,* Ph.D. Dissertation at University of Bonn, Munchen.

Evjen, H. M. (1936): The place of the vertical gradient in gravitational interpretations, Geophysics, **1**, pp. 127 – 136.

Fuller, B. D. (1967): Two-dimensional frequency analysis. Mining Geophysics, Volume II, Theory: Society of Exploration Geophysics, pp. 658 – 708.

Geldart, L. P., Gill, E. D. and Sharma, B. (1966): Gravity anomalies of two-dimensional faults. Geophysics, **31**, No. 2, pp. 372 – 397.

Geological Survey of Japan (2000): Gravity CD-ROM of Japan published on 24th March 2000, URL http://www.gsj.go.jp

Goad, C. C., Tscherning, C. C. and Chin, M. M. (1984): Gravity Empirical Covariance Values for the Continental United States. Journal of Geophysical Research, **89**, No B9, pp. 7962 – 7968.

Glasko, V. B., Ostromogilskiy, A. H. and Filatov, V. G. (1970): On the reconstruction of depth and form of contact surface on the basis of the regularization method. J. Comp. Math. Math. Phys., **10** (5), pp. 1292 – 1297.

Glasko, V.B., Volodin, B. A., Mudretsova, Y. A., and Nefedova, N. Yu (1973): Solution of the inverse problem of the gravimetry for a contact surface with the aid of the Regularization Method. Izv., Earth Physics, No. 2, pp. 30 – 41.

Glasko, V.B., Mudretsova, E. A., and Strakhov, V. N. (1987): Inverse problems in gravimetry and magnetometry, *in* A. N. Tikhonov and A. V. Goncharsky, Eds. Ill-posed problems in natural sciences: MIR, pp. 115 – 129.

Grant, F. S. and West, G. F. (1965): *Interpretation Theory in Applied Geophysics.* McGraw-Hill Book Company. New York.

Grauch, V. J. S. and Cordell, L. (1987): Limitations of determining density or magnetic boundaries from gravity data, Geophysics, **52**, pp. 118 – 121.

Green, W. R. (1975): Inversion of gravity profiles by use of Backus-Gilbert approach. Geophysics, **40**, pp. 763 – 772.

Guillen, A. and Menichetti, V. (1984): Gravity and magnetic inversion with minimization of a specific functional. Geophysics, **49**, pp. 1354 – 1360.

Gupta, V. K. and Ramani, N. (1980): Some aspects of regional-regional separation of gravity anomalies in a Precambrian Terrain. Geophysics, **45**, No. 9, pp. 1412 - 1426.

Guspi, F. (1990): General 2-D gravity inversion with density contrast varying with depth. Geo-exploration, **26**, pp. 253 – 265.

Hadamard, J. (1902): *Sur les problemes aux derive espartielles et leur signification physique*. Bulletin of Princeton University, **13**, pp. 1-20.

Hagiwara, Y. (1967): Analyses of Gravity Values in Japan, Bulletin of the Earthquake Research Institute, University of Tokyo, **45**, pp. 1091 – 1228.

Hagiwara, Y. (1975): Conventional and spherical Bouguer correction. Journal of the Geodetic Society of Japan, **21**, pp. 16 – 18.

Hammer, S. and Anzoleaga, R. (1975): Exploring for stratigraphic traps with gravity gradients, Geophysics, **40**, pp. 300 – 312.

Hinze, W. J. (1990): The role of gravity and magnetic methods in engineering and environmental studies, *in* Ward, S. H., Ed., Geotechnical and environmental geophysics, **1**, Soc. Exploration Geophysics, pp. 75 – 126.

Hirokawa, O. (1978): Geological Map of Japan, 1:1,000,000 (2nd Edition), Geological Survey of Japan.

Hubbert, M. K. (1948): Gravitational terrain effects of two-dimensional topographic features. Geophysics, **13**, pp. 226 – 254.

Huzita, K. (1980): Role of the Median Tectonic Line in the Quaternary tectonics of the Japanese Islands, Memoirs of Geological Society of Japan, **18**, pp. 129 – 153.

Ikami, A., Yoshii, T., Kubota, S., Sasaki, Y., Hasemi, A., Moriya, T., Miyamachi, H., Matsu'ura, R. S. and Wada, K. (1986): A Seismic-refraction Profile in and around Nagano Prefecture, Central Japan. Journal of Physics of Earth, **34**, pp. 457 – 474.

Jackson, M. P. A. and Talbot, C. J. (1989): Salt Canopies: 10th Ann. Res. Conf., Gulf Coast Soc. Econ. Paleontology. And Mineral. Found. Proceedings, pp. 72 – 78.

Jekely, C. (1988): The gravity gradiometer survey system (GGSS). EOS Transactions of the American Geophysical Union, **69**, pp. 116 – 117.

Kanasewich, E. R. (1990): *Time sequence analysis in geophysics*: Edmonton, The University of Alberta Press, 352 pages.

Kobrunov, A. I. (1988): Theory of Interpretation of Gravimetric Data for Stratified Media (Uniform Optimization), Izv., Earth Physics, **24**, No. 8, pp. 618 – 626.

Koch, M. (1990): Optimal regularization of the linear seismic inverse problem, Technical Report No., FSU-SCRI-90C-32, Florida State University, Tallahassee, Florida.

Komazawa, M. and Mishina, M. (2002): Caldera structure inferred from gravity anomalies west of Nagamachi-Rifu Fault, Northeast Japan. Earth, Planets and Space, **54**, pp. 1049 – 1053.

Kraiger, G. (1987): Influence of the curvature parameter on least-squares prediction. Manuscripta Geodetica, **13**, pp. 164-171.

Last, B. J. and Kubik, K. (1983): Compact gravity inversion. Geophysics, **48**, pp. 713 – 721.

Lee, T.-C. and Biehler, S. (1991): Inversion modeling of gravity with prismatic mass bodies, Geophysics, biased linear estimation, and nonlinear estimation, Technometrics, **12** (3).

Lewi, E. (1997): *Modeling and Inversion of High Precision Gravity Data*, Ph.D. Dissertation at the Institute of Physical Geodesy, Technical University of Darmstadt, Germany.

Li, Y. and Oldenburg, D. W. (1996): 3-D inversion of magnetic data. Geophysics, **61**, pp. 394 – 408.

Li, Y. and Oldenburg, D. W. (1998): 3-D inversion of gravity data. Geophysics, **63**, No. 1, pp. 109 – 119.

Li, X. and Gotze, H. (2001): Tutorial – Ellipsoid, geoid, geodesy and geophysics. Geophysics, **66,** No. 6, pp. 1660 – 1668.

Marson, I. and Klingele, E. E. (1993): Advantages of using the vertical gradient of gravity for 3-D interpretation. Geophysics, **58**, No. 11, pp. 1588 – 1595.

Martin-Atienza, B. and Garcia-Abdeslem, J. (1988): 2-D gravity modeling with analytically defined geometry and quadratic polynomial density functions. Geophysics, **64,** pp. 1730 - 1734.

Meyer, F. D. (1974): Filter techniques in gravity interpretation. Geophysical Prospecting, **36**, pp. 475 – 488.

Mickus, K. L. and Hinojosa, J. H. (2001): The complete gravity gradient tensor derived from the vertical component of gravity: a Fourier transform technique. Journal of Applied Geophysics, **46**, pp. 159 – 174.

Mironov, V. S. (1980): Course in Gravitation Prospecting, 543 pp., Nedra, Leningrad, 1980.

Moon, W. (1981): A new method of computing geopotential fields, Geophysical Journal of Royal Astronomical Society, **67**, pp. 735 – 746.

Mora, P. (1987): Nonlinear two-dimensional elastic inversion of the multi-offset seismic data. Geophysics, **52**, No. 9, pp. 1211 – 1228.

Moritz, H. (1970): Least squares estimation in physical geodesy. (OSU Rep. No. 130) DGK, Reihe A, Nr. 69, Munchen, Germany.

Moritz, H. (1980): *Advanced Physical Geodesy*. H. Wichmann Verlag, Karlsruhe, Germany.

Murthy, I. V. R. and Rao, D. B. (1979): Gravity anomalies of two-dimensional bodies of irregular cross-section with density contrast varying with depth. Geophysics, **44,** pp. 1525 – 1530.

Nagihara, S. and Hall, S. A. (2001): Three-dimensional gravity inversion using simulated annealing: Constraints on the diapiric roots of alloch-thonous salt structures. Geophysics, **66**, No. 5, pp. 1438 – 1449.

Nettleton, L. L. (1954): Regional, residuals and structures. Geophysics, **19**, pp. 1 – 22.

Nettleton, L. L. (1976): Gravity and Magnetics in Oil Prospecting, McGraw Hill.

Novoselitskii, V. M. (1965): On the theory of determining the Density Variations in a Horizontal Layer through Gravitational Anomalies, Bull. Izv., Academy of Sciences USSR, Earth Physics, No. 5.

Novoselitskii, V. M. (1967): Possible errors in the determination of the variable density of a horizontal layer by means of gravitational anomalies. Izvestiya Earth Physics, No. 5, 1967, pp. 54 – 61.

Nozaki, K. (1981): A Computer Program for Spherical Terrain Correction. Journal of the Geodetic Society of Japan, **27**, No. 1, pp. 23-32 (*Japanese with English Abstract*).

Okumura, K., Shimokawa, K., Yamazaki, H. and Tsukuda, E. (1994): Recent surface faulting along the middle section of Itoigawa-Shizuoka tectonic line – trenching survey of the Gofukuji fault near Matsumoto, central Japan. Zishin, **46**, pp. 425 – 438, (In *Japanese*).

Okubo, S., Ikeda, Y., Kumamoto, T., Seta, G., Matsuta, N., Chiba, H., and Arai, Y. (2000): 2-D and 3-D Subsurface Density Structure in the Northern Part of the Itoigawa-Shizuoka Tectonic Line Derived by Gravity Surveying. Journal of Geodetic Society of Japan, **46**, No. 3, pp. 177 – 186, (*Japanese with English Abstract*).

Oldenburg, D. W. (1974): The inversion and interpretation of gravity anomalies, Geophysics, **31**, pp. 363 – 368.

Parasnis, D. S. (1961): Exact expressions for the gravitational attraction of a circular lamina at all points of space and of a right circular vertical cylinder at points external to it, Geophysical Prospecting, **9**, pp. 382 – 398.

Parasnis, D. S. (1997): *Principles of Applied Geophysics,* Chapman & Hall.

Paterson, N. R. and Reeves, C. V. (1985): Applications of gravity and magnetic surveys: The state-of-art in 1985: Geophysics, **50**, pp. 2558 – 2594.

Peters, L. J. (1949): The direct approach to Magnetic Interpretation and its practical application, Geophysics, **14**, pp. 290 – 319.

Prieto, C. (1998): *Gravity/Magnetic Signatures of Various Geologic Models – An Exercise in Pattern Recognition* in Eds. Gibson, R. I. and Millegan, P. S – Geologic Applications of Gravity and Magnetics: Case Histories. AAPG Studies in Geology, No. 43, pp. 20 – 27.

Rao, D. B. (1986a): Analysis of gravity anomalies over an inclined fault with quadratic density function. Pageoph, **123**, pp. 250 – 260.

Rao, D. B. (1986b): Modeling of sedimentary basins from gravity anomalies with variable density contrast. Geophysics Journal of the Royal Australian Society, **84**, pp. 207 – 212.

Rao, D. B. (1990): Analysis of gravity anomalies of sedimentary basins by asymmetrical trapezoidal model with quadratic function. Geophysics, **55**, pp. 226 – 231.

Ruotoistenmaki, T. (1992): The gravity anomaly of two-dimensional sources with continuous density distribution and bounded by continuous surfaces. Geophysics, **57**, No. 4, pp. 623-628.

Savinsky, I. D. (1963): On solving inverse geophysical problems represented by the Fredholm integral equations of the first order, Izv, Academy USSR Ser. Geofiz. No. 5, pp. 712 – 721.

Savinsky, I. D. (1967a): Solution of an Incorrectly Posed Problem in the Conversion of Potential Field into the Underlying Level, Izv. Akad. Nauk SSSR, Fizika Zemli, No. 6, 1967.

Savinsky, I. D. (1967b): On solving incorrect problems of recalculation of the potential field to underlying levels. Izv, Academy of Sciences, USSR Physics of Solid Earth, No. 6, pp. 72 – 92.

Savinsky, I. D., Briskin, V. L and Petrova, A. A. (1981): Reduction of the Gravitational and Magnetic inclined and Vertical Planes in the Lower Half-Space. Izv. Earth Physics, **17**, No. 12, pp. 934 – 943.

Savinsky, I. D. (1984): Solving inverse problems on gravity data with help of kern functions of integral equations, *in* Applied Geophysics, **109**, pp. 86 – 95, Nedra, Moscow.

Savinsky, I. D. (1995): On determination of the contact interface from gravitational and magnetic fields. Physics of the Solid Earth, English Translation, **30**, No. 10, pp. 903 – 907.

Scales, J. A. and Tenorio, L. (2001): Tutorial – Prior information and uncertainty in inverse problems. Geophysics, **66**, No. 2, pp. 389 – 397.

Schwarz, K. P. and Lachapelle, G. (1980): Local characteristics of the gravity anomaly covariance function. Bulletin Geodesique, **54**, pp. 21-36.

Sen, M. and Stoffa, P. L. (1995): *Global optimization methods in geophysical inversion.* Elsevier Science, 1995.

Skeels, D. C. (1976): Short Note – What is residual gravity? Geophysics, **32**, pp. 872 - 876.

Sleep, N. H. and Fujita, K. (1997): *Principles of Geophysics*, Blackwell Science, Massachusetts and Toronto, 1997.

Starostenko, V.I. and Zavorot'ko, A. N. (1982): Solution of inverse gravimetric problems for several contact surfaces, Izvestiya Earth Physics, **18**, No. 3, pp. 196 – 206.

Starostenko, V.I., Chernaya, N. N., and Chernyi, A. V. (1992): Gravity data inversion for a contact surface, Part I. Izvestiya Earth Physics, **28**, No. 6, pp. 494 – 501.

Starostenko, V.I., Chernaya, N. N., and Chernyi, A. V. (1994): Gravity data inversion for a contact surface, Part III. Izvestiya Earth Physics, **29**, No. 7, pp. 613 – 621.

Stanley, J. M. and Green, R. (1976): Gravity gradients and the interpretation of the truncated plate. Geophysics, **41**, pp. 1370 - 1376.

Strakhov, V. N. (1963): Reduction of the Problem of Analytic Continuation into a Horizontal Layer to the Solution on Linear Integral Equations of the Convolution Type with Rapidly Decreasing Kernels, Bull. Izv., Academy of Sciences USSR, Geophysics, Ser., No. 8.

Strakhov, V. N. (1975): The logarithmic potential in the case of anomalous masses of variable density. Izvestiya Earth Physics, No. 2, pp. 64 – 81.

Sunkel, H. and Kraiger, G. (1983): The Prediction of Free-air Anomalies. Manuscripta Geodaetica, **8**, pp. 229 – 248.

Telford, W. M., Geldart, L. P. and Sheriff, R. E. (1990): *Applied Geophysics*, 2nd Edition, Cambridge University Press, New York.

Tikhonov, A. N. (1943): Stability of Inverse Problems, Dokl. Akad. Nauk SSSR, **39** (5), pp. 195 – 198.

Tikhonov, A. N. (1963): Resolution of ill-posed problems and the regularization methods. Dokl. Akad. Nauk SSSR, **151**, pp. 501-504 (*In Russian*).

Tikhonov, A. N. and Glasko, V. B. (1964): Approximation solution of integral equations of the first type. *Zh. Vychislit. Matem. iMatem*. Fiz., **4**, No. 3, pp. 564 – 570.

Tikhonov, A. N. and Glasko, V. B. (1965): Application of the regularization method in nonlinear problems, J. Comp. Math. Math. Phys., **5** (3), pp. 363 – 373.

Tikhonov, A. N. and Arsenin, A. Y. (1974): Methods of Solving Incorrectly Posed Problems, Nauka, **224,** Moscow.

Tkachenko, Y. F. (1975): Correlation method of determining the density of the intermediate layer. Izvestiya Earth Physics, No. 7, pp. 93 – 96.

U.S. Geological Survey and U. S. Department of Interior: *GTOPO30 Documentation* http://edcwww.cr.usgs.gov/landdaac/gtopo30/gtopo30.html

Vasco, D. W. (1989): Resolution and variance operators of gravity and gravity gradiometry. Geophysics, **54**, pp. 90 – 101.

Wells, D. (1986): *The Penguin Dictionary of Curious and Interesting Numbers*. Middlesex, England. Penguin Books, p. 59.

Wessel, P and Smith, W. H. F. (1995): *The Generic Mapping Tools (GMT) Version 3.0 Technical Reference and Cookbook*. SOEST/NOAA.

Yamamoto, A., Nozaki, K., Fukao, Y., Furumoto, M., Shichi, R., and Ezaka, T. (1982): Gravity survey in the Central Ranges, Honshu, Japan. Journal of Physics of the Earth, **30**, pp. 201-243.

Zhang, J., Zhong, B., Zhou, X. and Dai, Y. (2001): Gravity anomalies of 2-D bodies with variable density contrast. Geophysics, **66**, No. 3, pp. 809 - 813.